Chem Soc Rev

# Hierarchical Photocatalysts



| | |
|---|---|
| Journal: | *Chemical Society Reviews* |
| Manuscript ID | CS-SYN-11-2015-000838.R3 |
| Article Type: | Review Article |
| Date Submitted by the Author: | 25-Feb-2016 |
| Complete List of Authors: | Li, Xin; South China Agricultural University, College of Science;<br>Yu, Jiaguo; Wuhan University of Technology,<br>Jaroniec, Mietek; Kent State University, Department of Chemistry |
| | |

Journal Name

ARTICLE

# Hierarchical Photocatalysts

Xin Li,[a,e] Jiaguo Yu,[b,c*] Mietek Jaroniec[d*]

Received 00th January 20xx,
Accepted 00th January 20xx

DOI: 10.1039/x0xx00000x

www.rsc.org/

As a green and sustainable technology, the semiconductor-based heterogeneous photocatalysis has received much attention during the past decades because it has potential to solve both the energy and environmental problems. To achieve efficient photocatalysts, various hierarchical semiconductors have been designed and fabricated at the micro/nanometer scale in recent years. This review presents a critical appraisal of fabrication methods, growth mechanisms and applications of advanced hierarchical photocatalysts. Especially, the different synthesis strategies such as two-step templating, in-situ template-sacrificial dissolution, self-templating method, in-situ template-free assembly, chemically induced self-transformation and post–synthesis treatment are highlighted. Finally, some important applications including photocatalytic degradation of pollutants, photocatalytic $H_2$ production and photocatalytic $CO_2$ reduction are reviewed. A thorough assessment of the progress made in photocatalysis may open new opportunities in designing highly effective hierarchical photocatalysts for advanced applications ranging from thermal catalysis, separation and purification processes to solar cells.

## 1. Introduction

As a green and promising technology, heterogeneous photocatalytic reduction and oxidation reactions, based largely on semiconductors and solar energy, have recently attracted extensive interest in the fields of energy, materials, environment and chemistry.[1-7] Since the Fujishima-Honda effect of $TiO_2$ photoelectrode was first reported in 1972,[8] many achievements in the development of novel semiconductor photocatalysts for various photocatalytic applications have been made.[9-16] So far, hundreds of new semiconductor materials are currently available for diversified and multifunctional applications, including oxides of the metallic elements with $d^0$ and $d^{10}$ configurations,[2, 5, 17-20] sulfides,[21-26] (oxy)nitrides,[12, 17, 27-30] metal-free semiconductors,[31-36] plasmonic metals[37-43] and elemental photocatalysts[44-48]. However, none of these photocatalysts completely satisfies all practical requirements such as long lifetime of photogenerated electron–hole pairs, small band gap optimal for full utilization of solar light energy, relatively high safety, low cost, high efficiency and stability, which greatly hinders their practical applications.[2] Therefore, there is an urgent need to develop highly efficient and stable visible-light-driven photocatalysts by optimizing the existing synthesis strategies through coupling them with nanocarbons, adding co-catalysts, constructing proper heterojunctions, designing all-solid-state Z-schemes, and more.[2, 49-59] Typically, these engineering strategies to modify heterogeneous photocatalysts with enhanced activity can be divided into two types: structural and compositional optimizations.[51] Especially, as the photocatalytic properties of semiconductors are strongly dependent on their crystal morphologies and structural features at the nanometer level, the optimization and control of the structural properties of a given semiconductor is crucial for enhancing its photocatalytic performance. So far, numerous promising structure-engineering strategies have been proposed for the preparation of highly efficient photocatalysts with desirable structure and morphology. Among them, the self-assembly synthesis of hierarchical semiconductor nanostructures has turned out to be a feasible strategy to efficiently prevent aggregation and enhance the quantum efficiency of the specific photocatalysts due to their unique shape- and structure-dependent catalytic properties.

Since the pioneering work by Yang et al in 1998 reporting the formation of hierarchical ordered oxides with three-dimensional structures,[60] a significant progress has been made in the design and synthesis of hierarchical functional nanomaterials with controllable morphology, nanocrystallinity, composition, exposure of facets, dimensionality, microstructure, and more, for enhancing catalytic activity and selectivity.[61] In particular, the work by Zhang and Yu on the sonochemical synthesis of hierarchical porous titania spheres, which showed an enhanced activity toward photodegradation of n-pentane in air,[62] initiated a number of publications on the design and fabrication of novel inorganic semiconductor materials with hierarchical superstructures through the oriented assembly of nanosized building blocks such as nanorods, nanotubes, and nanoplates.[63-67] These so-called “hierarchical photocatalysts” are

[a] College of materials and energy, South China Agricultural University, Guangzhou, 510642, PR China.
[b] State Key Laboratory of Advanced Technology for Material Synthesis and Processing, Wuhan University of Technology, Wuhan, 430070, PR China. E-mail: **jiaguoyu@yahoo.com (Yu, J.).**
[c] Department of Physics, Faculty of Science, King Abdulaziz University, Jeddah 21589, Saudi Arabia
[d] Department of Chemistry and Biochemistry, Kent State University, Kent, OH 44242, USA. E-mail: **jaroniec@kent.edu (M. Jaroniec).**
[e] Key Laboratory of Energy Plants Resource and Utilization, Ministry of Agriculture, Key Laboratory of Biomass Energy of Guangdong Regular Higher Education Institutions, Institute of New Energy and New Materials, South China Agricultural University, Guangzhou 510642, PR China

usually referred to as the nanostructured semiconductors having multidimensional domains at different levels or multimodal pore structures. Several typical hierarchical nanostructures (such as urchin-like, brush-like, flower-like, tree-like, dendritic and branched structures) composed of different nanosized building blocks are shown in Figure 1. Generally, hierarchical porous structures of photocatalysts can be created by mimicking the existing in nature marvelous hierarchical and fractal structures such as trees and the surface structures of plant leaves (Figure 2).[68] Importantly, hierarchical photocatalysts as those shown in Figure 1 possess readily accessible and interconnected porous networks and high specific surface areas, which not only enhance the efficiency of light harvesting and adsorption of reactants, but also facilitate the transport of guest species to the binding sites. Thus, the synergetic effects of different dimensional levels and multimodal pore structures often lead to the significant enhancement of the performance of hierarchical photocatalysts. These outstanding features of hierarchical nanostructured semiconductors make them promising candidates for heterogeneous photocatalysis. To date, a large number of important papers have been published on the design of hierarchical photocatalysts with multiple porous structures and enhanced efficiency. Despite some excellent reviews devoted to the hierarchical semiconductors such as $TiO_2$, $SnO_2$ and ZnO, only a fraction of important topics referring to their preparation and applications in photocatalysis[69-74] and photoelectrochemistry [75] has been apprised. In recent years, there is a great deal of enthusiasm in exploiting hierarchical nanostructured semiconductor photocatalysts, which resulted in many significant achievements. Thus, we believe that a comprehensive and inspiring review on this subject is timely to promote further developments in this important, exciting and still emerging area of research.

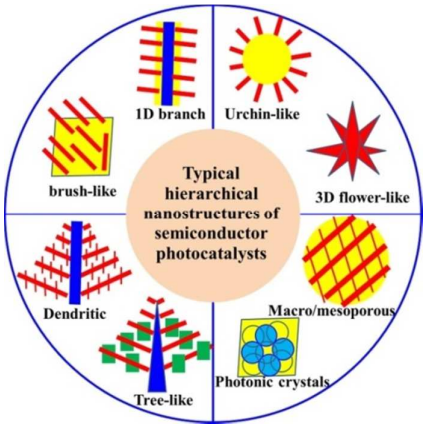


**Figure 1** Typical hierarchical structures of photocatalysts

In this review, we thoroughly summarize recent developments in the area of hierarchical nanostructured semiconductors for various photocatalytic applications. A special emphasis is directed toward better understanding of the design, fabrication, performance and applications of hierarchical semiconductor photocatalysts. The advantages of hierarchical structures are first briefly discussed in the context of heterogeneous photocatalysis. Then, the fabrication strategies and growth mechanism of hierarchical photocatalysts are presented. Also, various applications of hierarchical photocatalysts for degradation of pollutants, air purification, $H_2$ production, and $CO_2$ reduction are reviewed, and future research challenges are discussed.

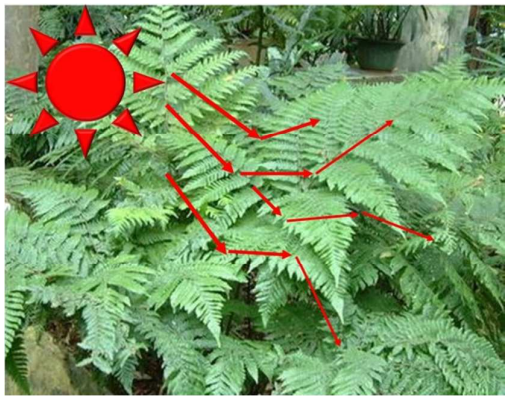

**Figure 2** Example of hierarchical structures in nature.

## 2. Fundamentals of heterogeneous photocatalysis

### 2.1 Thermodynamics of heterogeneous photocatalysis

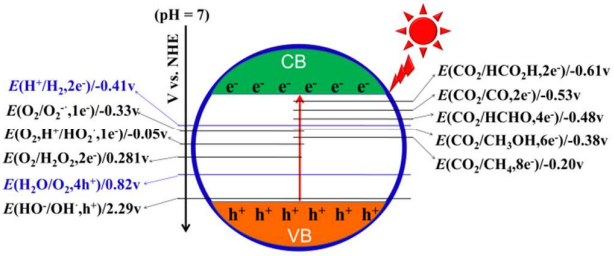


**Figure 3** Redox potentials of different species in heterogeneous photocatalysis

Fundamentals of heterogeneous photocatalysis have been widely elaborated elsewhere.[74, 76, 77] As shown in **Figure 3**, a given photocatalyst, when exposed to an appropriate light source, can be excited by the photons with energy equal to or greater than its corresponding band-gap energy, which leads to the generation of photo-induced electron/hole ($e^-/h^+$) pairs, instead of producing thermal energy through the recombination of photogenerated $e^-$ and $h^+$ in the bulk. Some charge carriers can migrate to the surface and initiate a series of chemical reactions with the adsorbed species on the surface of the catalyst, resulting for instance in the degradation of pollutants, reduction of $CO_2$ and $O_2$, evolution of $H_2$ and $O_2$, or formation of organic compounds. From thermodynamic viewpoint, the surface reduction and oxidation reactions can be driven by the photogenerated $e^-$ and $h^+$, respectively, only when their reduction and oxidation potentials lie between the conduction band (CB) and valence band (VB) potentials. The potentials of typical reactions are given in Figure 3 and Table 1. The redox potentials of metal species at different pH values in an aqueous solution must be chosen on the basis of their corresponding Pourbaix diagram, whereas, all other redox potentials shown in Table 1 exhibit the same linear pH dependence with a slope of -

0.059 V, apart from $E_0'(O_2/O_2^-)$ which is pH-independent.[78] For example, to achieve the overall water splitting over a semiconductor, its conduction band potential must be more negative than that of $H_2$ generation and its valence band potential must be more positive than that required for $O_2$ generation.[2, 5, 6] Similarly, to achieve the photocatalytic degradation of a given pollutant, the photogenerated $e^-$ and $h^+$ on the surface of a semiconductor should have suitable reduction and oxidation ability to react with the adsorbed species ($O_2$, $OH^-$, etc.) on the surface of the catalyst and generate free radicals ($O_2^{\bullet-}$, •OH, etc.), which could then act as reactive species and further degrade the adsorbed organic pollutants.[26, 79] Additionally, as shown in Figure 3 and Table 1, it is clear that the multielectron reduction reactions of $O_2$ and $CO_2$ are thermodynamically more favorable than their corresponding single-electron processes on the surface active sites of semiconductors, due to the smaller negative reduction potentials of multielectron processes.[1, 80] Interestingly, the four-electron oxidation reaction of water can be easily realized as compared with the single-electron oxidation reaction of $OH^-$ (the formation of hydroxyl radicals) in aqueous solution, due to the super-high oxidation potentials of the latter.

Thus, the thermodynamic driving forces in photocatalytic processes are strongly dependent on the relative relationships between the CB/VB potentials of the semiconductor photocatalysts used and the redox potentials of reversible target reactions. Thus, the more negative CB positions of semiconductors are beneficial for the reduction reactions, while the more positive VB positions of semiconductors are favorable for the oxidation reactions. The band positions (at pH=7 in aqueous solution) for some important semiconductor photocatalysts and their potential applications are listed in Figure 4. As depicted in Figure 4, it is clear that the ideal energy band diagram of $TiO_2$ should ensure the simultaneous formation of the holes, •OH radicals, $O_2^-$ and $H_2O_2$ at pH = 7, all of which have been proven to play an important role in the photocatalytic oxidative degradation of organic compounds.[74, 79, 81] Furthermore, $TiO_2$ itself is also relatively inexpensive, highly stable and readily available, and therefore it is commonly used as the best semiconductor material for environmental photocatalysis.[74] Importantly, the primary oxidants in the photocatalytic degradation of the intractable organic pollutants have proven to be the free •OH radicals, which are thought to be more reactive than the surface-bound analogues because of their reorganization energy.[82, 83] Accordingly, it is readily accepted that all semiconductors with sufficient positive VB potentials for producing the •OH radicals, such as $WO_3$, ZnO, $SnO_2$, $SrTiO_3$, $BiVO_4$, $Bi_2WO_6$, BiOCl and BiOBr (on the left side of Figure 4), are the promising photocatalyst candidates for the photodegradation of organic pollutants, However, the electron transfer from CB to dissolved oxygen molecule has been generally recognized as the rate-determining step in solar photocatalytic mineralization of organic pollutants.[83, 84] Thus, an enhancement of the photocatalytic activity of a photocatalyst toward degradation of pollutants can be achieved by enhancing $O_2$ reduction reactions.[84] For example, although the photogenerated electrons in $WO_3$ cannot drive the single-electron reduction reaction of $O_2$, they can efficiently promote the formation of $H_2O_2$ over $WO_3$ through the multielectron reduction of $O_2$.[80] More interestingly, the use of Pt nanoparticles as cocatalyst in the case of $WO_3$ has been found to accelerate the multielectron $O_2$ reduction, which resulted in highly efficient and durable decomposition of organic compounds.[80] On the contrary, the photocatalysts with more negative CB positions could produce the photogenerated electrons with strong reduction ability, which could efficiently enhance the $H_2$ evolution and $CO_2$ reduction. These reductive photocatalysts include $Ta_3N_5$, TaON, CdS, $C_3N_4$, SiC, ZnS, BiOCl, Si, $Bi_2S_3$ and $Cu_2O$ (on the right side of Figure 4). It is well known that the use of proper cocatalysts (or electrocatalysts) could greatly increase their photocatalytic performance toward $CO_2$ reduction or $H_2$ generation.[1, 2, 52, 74, 85-89] However, for this kind of photocatalysts, it has been demonstrated that the hole removal rate is the key efficiency-limiting step for photo-driven solar-fuel production.[90] Therefore, optimization of the hole transfer step (for instance, by loading suitable hole-transfer/hole-storage cocatalysts and by using appropriate electron donors) may offer potential opportunities for achieving higher quantum efficiency for solar-fuel generation.[33, 90-93]

Note that some of the aforementioned two kinds of photocatalysts, such as $Ta_3N_5$, TaON, CdS, $C_3N_4$, SiC, ZnS, BiOCl, $SrTiO_3$, ZnO and $TiO_2$, can be utilized as potential photocatalysts for overall water splitting because they have suitable CB and VB positions for $H_2$ and $O_2$ evolutions, respectively. Therefore, from the thermodynamic viewpoint, a perfect match of the energy levels and the redox potentials is very crucial for achieving high efficiency of photocatalytic processes. However, as can be seen from Figure 4 semiconductors with more negative CB and more positive VB levels generally possess much wider band gaps, which will significantly reduce the utilization efficiency of visible light in the renewable solar energy production (which accounts for about 43% of solar energy), thus leading to the low solar energy conversion efficiency. Hence, numerous efforts have been undertaken to fabricate new visible-light photocatalysts through different strategies such as energy-band engineering or solid-solution method.[2, 13, 30, 94, 95] However, the amounts of introduced crystal/lattice defects during narrowing the band gaps of wide-band semiconductors should be carefully controlled, because the excessive defects could act as new charge recombination centers and greatly reduce the photocatalytic activity.[2, 96] Furthermore, the introduced donor or acceptor levels could also reduce the oxidation or reduction abilities of newly fabricated visible-light photocatalysts, respectively, which can diminish their photocatalytic performance. Consequently, the obvious contradiction between the redox abilities (determined by the CB/VB levels) and absorption capacity of visible light (determined by the value of band gaps), should be carefully optimized and balanced in the development of visible-light-driven semiconductor photocatalysts.

**Table 1**. Standard redox potentials for selected species.[97]

| Reaction | $E^0$(V) vs NHE at pH=0 |
|---|---|
| **$H_2$** | |
| $2H^+ + 2e^- \rightarrow H_2(g)$ | 0 |
| **$O_2$ and $N_2$** | |
| $O_2(g) + e^- \rightarrow O_2^-$ (aq) | -0.33 |
| $O_2(g) + H_2O + 2e^- \rightarrow HO_2^-(aq) + OH^-$ | −0.0649* |
| $O_2(g) + H^+ + e^- \rightarrow HO_2^{\bullet}(aq)$ | −0.046 |

| | |
|---|---|
| $HO_2^-(aq) + H_2O + e^- \rightarrow \bullet OH + 2\,OH^-$ | 0.184* |
| $O_2^-(aq) + H_2O + e^- \rightarrow HO_2^-(aq) + OH^-$ | 0.2* |
| $O_2(g) + 2H^+ + 2e^- \rightarrow H_2O_2(aq)$ | 0.695 |
| $2H_2O(aq) + 4h^+ \rightarrow O_2(g) + 4H^+$ | 1.229 |
| $OH^- + h^+ \rightarrow \bullet OH$ | 2.69 |
| $4\,OH^-(aq) + 4h^+ \rightarrow O_2(g) + 2\,H_2O$ | 0.401 |
| $N_2(g) + 2\,H_2O + 6\,H^+ + 6\,e^- \rightarrow 2\,NH_4OH(aq)$ | 0.092 |
| $O_3(g) + 2\,H^+ + 2\,e^- \rightarrow O_2(g) + H_2O$ | 2.075 |
| **Metal-ions** | |
| $MoO_4^{2-} + 4H_2O + 6e^- \rightarrow Mo(s) + 8OH^-$ | -0.913* |
| $Co(OH)_2 + 2e^- \rightarrow Co(s) + 2\,OH^-$ | −0.733* |
| $Ni(OH)_2 + 2e^- \rightarrow Ni(s) + 2\,OH^-$ | -0.72* |
| $Cu_2O(s) + H_2O + 2\,e^- \rightarrow 2\,Cu(s) + 2\,OH^-$ | −0.365* |
| $Co^{2+} + 2e^- \rightarrow Co(s)$ | −0.277 |
| $Ni^{2+} + 2e^- \rightarrow Ni(s)$ | −0.257 |
| $Mo^{3+} + 3e^- \rightarrow Mo(s)$ | -0.2 |
| $AgI + e^- \rightarrow Ag(s) + I^-$ | -0.1522 |
| $AgBr + e^- \rightarrow Ag(s) + Br^-$ | 0.0711 |
| $AgCl + e^- \rightarrow Ag(s) + Cl^-$ | 0.2223 |
| $Sn^{4+} + 2e^- \rightarrow Sn^{2+}$ | 0.15 |
| $Cu^{2+} + e^- \rightarrow Cu^+$ | 0.159 |
| $BiOCl + 2H^+ + 3e^- \rightarrow Bi(s) + H_2O + Cl^-$ | 0.1697 |
| $Bi^{3+} + 3e^- \rightarrow Bi(s)$ | 0.308 |
| $Cu^{2+} + 2e^- \rightarrow Cu(s)$ | 0.340 |
| $Cu^+ + e^- \rightarrow Cu(s)$ | 0.520 |
| $PdCl_4^{2-} + 2e^- \rightarrow Pd(s) + 4\,Cl^-$ | 0.64 |
| $PtCl_4^{2-} + 2e^- \rightarrow Pt(s) + 4\,Cl^-$ | 0.758 |
| $Rh^{3+} + 3e^- \rightarrow Rh(s)$ | 0.76 |
| $Fe^{3+} + e^- \rightarrow Fe^{2+}$ | 0.771 |
| $Ag^+ + e^- \rightarrow Ag(s)$ | 0.7991 |
| $IrCl_6^{3-} + 3e^- \rightarrow Ir(s) + 6\,Cl^-$ | 0.86 |
| $Pd^{2+} + 2e^- \rightarrow Pd(s)$ | 0.915 |
| $[AuCl_4]^- + 3e^- \rightarrow Au(s) + 4\,Cl^-$ | 0.93 |
| $NiO_2 + 2\,H^+ + 2\,e^- \rightarrow Ni^{2+} + 2H_2O$ | 1.593 |
| **$CO_2$** | |
| $CO_2 + e^- \rightarrow CO_2^-$ | -1.9 |
| $2\,CO_2(g) + 2\,H^+ + 2\,e^- \rightarrow HOOCCOOH(aq)$ | -0.481 |
| $CO_2(g) + 2H^+ + 2e^- \rightarrow HCOOH(aq)$ | -0.199 |
| $CO_2(g) + 2\,H^+ + 2e^- \rightarrow CO(g) + H_2O$ | -0.11 |
| $CO_2(g) + 4H^+ + 4e^- \rightarrow C(s) + 2H_2O$ | 0.206 |
| $CO_2(g) + 4H^+ + 4e^- \rightarrow HCHO(aq) + H_2O$ | -0.07 |
| $CO_2(g) + 6H^+ + 6e^- \rightarrow CH_3OH(aq) + H_2O$ | 0.03 |
| $CO_2(g) + 8H^+ + 8e^- \rightarrow CH_4(g) + 2H_2O$ | 0.169 |
| $2CO_2(g) + 8H_2O + 12e^- \rightarrow C_2H_4(g) + 12OH^-$ | 0.07 |
| $2CO_2(g) + 9H_2O + 12e^- \rightarrow C_2H_5OH(aq) + 12OH^-$ | 0.08 |
| $3CO_2(g) + 13H_2O + 18e^- \rightarrow C_3H_7OH(aq) + 18OH^-$ | 0.09 |
| **Other** | |
| $N_2H_4(aq) + 4\,H_2O + 2e^- \rightarrow 2\,NH_4^+ + 4\,OH^-$ | 0.1 |
| $H_2S(g) + 2h^+ \rightarrow S(s) + 2\,H^+$ | 0.144 |
| $SO_2(aq) + 4\,H^+ + 4\,e^- \rightarrow S(s) + 2\,H_2O$ | 0.50 |
| $H_3AsO_3(aq) + H_2O + 2h^+ \rightarrow H_3AsO_4(aq) + 2\,H^+$ | 0.56 |
| $NO_2(g) + H_2O + h^+ \rightarrow NO_3^-(aq) + 2\,H^+$ | 0.80 |
| $NO(g) + 2\,H_2O(l) + 3h^+ \rightarrow NO_3^-(aq) + 4\,H^+$ | 0.957 |
| $H_2O_2(aq) + H^+ + e^- \rightarrow H_2O + OH^-$ | 1.14 |
| $Cr_2O_7^{2-} + 14\,H^+ + 6\,e^- \rightarrow 2\,Cr^{3+} + 7\,H_2O$ | 1.36 |
| $HO_2^\bullet + H^+ + e^- \rightarrow H_2O_2(aq)$ | 1.44 |
| $H_2O_2(aq) + 2\,H^+ + 2\,e^- \rightarrow 2\,H_2O$ | 1.763 |

Superscript * denotes the standard redox potentials in basic solutions (pH=14).

$E^0(pH) = E^0(pH = 0) - 0.059pH$.

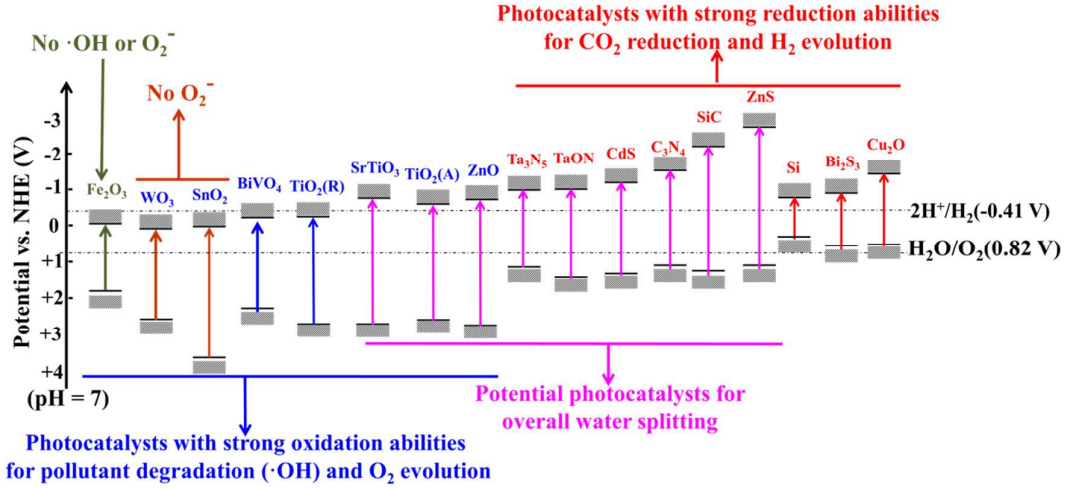


**Figure 4** Band positions and potential applications of some typical photocatalysts (at pH = 7 in aqueous solutions).

### 2.2 Kinetics of heterogeneous photocatalysis

However, the suitable thermodynamic properties (including band gaps and CB/VB levels) do not guarantee good photocatalytic efficiency. This is because the overall photocatalytic performance of semiconductor photocatalysts can be significantly influenced by many other factors including the structure at micro and nano levels, adsorption capacity, surface/interface morphology, cocatalysts, crystallinity and composition of the materials, besides their band-gap properties.[2] So far, it is well known that the complicated charge-carrier dynamics and surface reaction kinetics mainly lead to the low quantum efficiency in the multi-step processes of

heterogeneous photocatalysis.[84, 98] It is commonly accepted that as shown in Figure 5, the mechanism governing heterogeneous photocatalysis consists of four consecutive tandem steps: (1) light harvesting; (2) charge excitation/separation; (3) charge migration, transport and recombination; and (4) charge utilization (surface electrocatalytic reduction and oxidation reactions). Therefore, the overall photocatalysis efficiency is strongly dependent on the cumulative effects of these four consecutive steps, which can be expressed by eqn. 1:[2]

$$\eta_c = \eta_{abs} \times \eta_{cs} \times \eta_{cmt} \times \eta_{cu} \quad (1)$$

where $\eta_c$ is the solar energy conversion efficiency, $\eta_{abs}$ is the light absorption efficiency, $\eta_{cs}$ the charge excitation/separation efficiency, $\eta_{cmt}$ is the charge migration and transport efficiency, and $\eta_{cu}$ is the charge utilization efficiency for photocatalytic reactions.

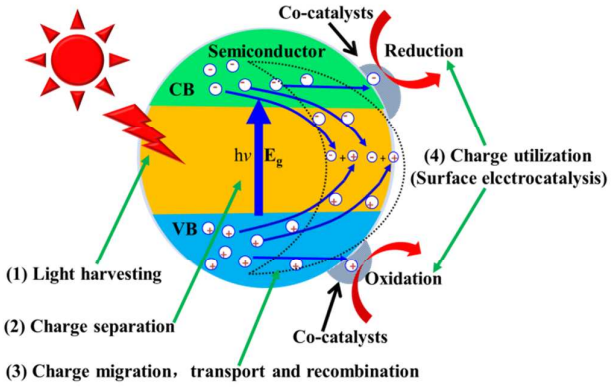


**Figure 5** Four different stages in heterogeneous photocatalysis

Clearly, a loss in the partial efficiency at each stage will add to the decrease in the overall photocatalytic efficiency. Firstly, the flat and smooth surface of photocatalysts is beneficial for the light reflection, which is not advantageous for the light harvesting or absorption. It is believed that the porous photocatalysts with hierarchical macro/mesopores or appropriate inner structures allow the multiple reflections and scattering of light inside their pore channels as well as within the interiors of cavities, which results in enhancing the light harvesting and offers more photogenerated electrons and holes to improve the catalytic activity.[32, 99, 100] Secondly, a quick recombination kinetics of photogenerated electron–hole pairs in the bulk or on the surface of a semiconductor is another major limiting factor in achieving high photocatalytic efficiency, which is one of the most important, difficult and challenging scientific issues in the heterogeneous photocatalysis.[2] Finally, the low specific surface area and significant agglomeration of nanostructured particles not only greatly decrease the surface reduction and oxidation kinetics, but also increase the reagents diffusion barriers, which are all unfavorable for the enhancement of photocatalytic efficiency. On the one hand, for the uphill reactions such as water splitting and $CO_2$ reduction, the slow surface multi-electron reaction kinetics could lead to the inevitable accumulation of photogenerated electrons and holes on the surface of photocatalysts, which would accelerate the unexpected charge carrier recombination and photocorrosion process of photocatalysts themselves, and consequently reduce their photoactivity.[1, 2] On the other hand, for the photodecomposition of organic compounds in aqueous solutions or in a gas phase, the enhanced adsorption and diffusion kinetics of reactants in a porous photocatalyst could also greatly improve the photocatalytic efficiency due to the reduced mass-transport barriers and higher chemical activation rates of the adsorbed species.[83]

All these highlighted kinetic factors in heterogeneous photocatalysis have been shown to significantly influence the overall efficiency of the existing photocatalysts. From the viewpoint of their practical use, these factors should be minimized or efficiently controlled to further enhance and optimize the photocatalytic processes. There is some consensus in the photocatalysis-related literature [52, 101-103] that as compared to the thermodynamic factors, the aforementioned kinetic factors (such as charge carrier kinetics, surface reaction kinetics, adsorption and diffusion kinetics) are considered to be more important in the design and development of highly efficient photocatalysts.

## 3. Advantages of hierarchical photocatalysts

Various technologies and methods have been proposed to deal with the challenges related to the aforementioned thermodynamic and kinetic aspects of heterogeneous photocatalysis. Among them, the fabrication of hierarchical photocatalysts at the micro/nanometer scales has been identified as a promising strategy to simultaneously solve all of the aforementioned problems at different stages of photocatalysis processes, as shown in Figure 5**.** Clearly, the properly designed hierarchical structures (including porosity and morphology) of photocatalysts can not only enhance the light harvesting and improve molecular diffusion/transport kinetics, but also increase the surface area and the amount of active sites, which accelerate the surface reaction kinetics. Additionally, the conduction and valence bands of hierarchically assembled nanomaterials can be adjusted by reducing the size of building blocks to the nanoscale level and taking advantage of the quantum size effect.[104] Some distinct advantages of hierarchical structures that lead to the enhancement of the overall photocatalytic efficiency are summarized in Figure 6 and discussed below.

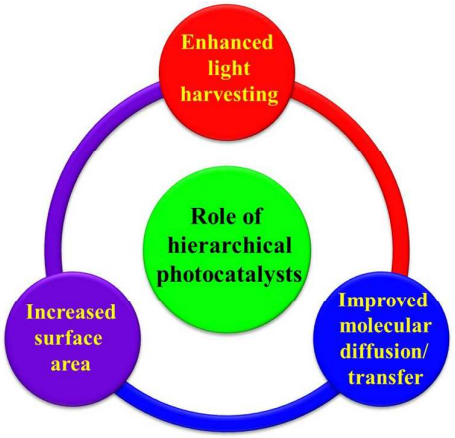


**Figure 6** Significance of hierarchical nanostructures in enhancing photocatalysis

### 3.1 Improved molecular diffusion/ transport

Design and formation of novel hierarchical morphologies and interconnected pore networks can also result in the creation of more efficient channels for the transport of reactant molecules to reactive sites present on the pore walls, which facilitate diffusion.[62, 105, 106] According to IUPAC (International Union of Pure and Applied Chemistry) pores can be classified into three categories: micropores (below 2 nm in diameter), mesopores (between 2 and 50 nm) and macropores (greater than 50 nm).[107] It is well known that the diffusion of organic molecules within microporous channels (<2 nm), such as those in zeolites, can be hindered.[108] To efficiently improve the diffusion of reactant molecules and the possibility of recycling and reuse of photocatalysts, semiconductor materials with ordered mesopores and large surface areas have been widely utilized to fabricate the advanced composite photocatalysts.[109, 110] Although mesopores improve the accessibility of molecules to/from catalytic sites, the relatively slow mass transport, small specific surface area, and reduced mesostructural order can still limit practical applications of mesoporous photocatalysts.[111] To overcome these limitations, the hierarchically ordered macro-mesoporous composite photocatalysts have been extensively fabricated by creating structures with inter- and intra-particle porosity.[68, 112-115] Importantly, the hierarchical structures with pores of different sizes feature excellent transport paths, which can not only greatly reduce the length of the mesopore channels, but also increase the accessible surface area of the composite photocatalysts.[111] Thus, in the case of hierarchical photocatalysts with properly interconnected of pores of different sizes, the reactant molecules (guest species) can easily diffuse into the reaction sites and the products can also freely move out of them (see Figure 7).[106, 116]

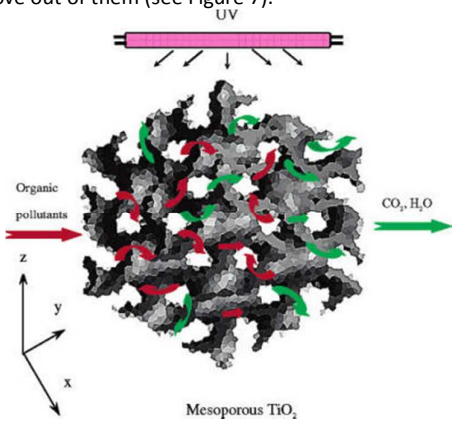


**Figure 7**. Three-dimensional mesoporous architecture in the $TiO_2$ nanocrystalline thin film with continuous and periodically porous network that offers transport routes for gaseous reactants to move in and out of the framework. Reproduced with permission from ref. 116. Copyright © 2004, American Chemical Society.

It was revealed that the diffusion and transport rates of large molecules in media featuring large mesopores (>10 nm) and macropores (>50 nm) are comparable to those in open media.[106, 108] For example, the physical adsorption mechanism of the popular methylene blue (MB) molecules (with a size of 1.43 nm×0.6 nm×0.4 nm) in micropores resembles pore filling, which is governed by stronger interactions between MB and micropore walls, resulting in the hindered transport of this dye.[117] However, the efficient transport of MB molecules to the surface binding sites can be easily achieved in the materials with hierarchical mesopores (>14 nm) and macropores (>50 nm).[114] Thus, the improved transfer and diffusion of the reactants and products molecules are beneficial for the enhancement of photocatalytic performance.

### 3.2 Enhanced light harvesting

It is known that the overall photocatalytic efficiency could be greatly enhanced through increasing the light-harvesting ability of photocatalysts. However, the improvement of light harvesting efficiency is still one of the main challenges in the design of highly active photocatalysts. So far, the efforts toward enhancing the light-harvesting ability of heterogeneous photocatalytic systems are still insufficient. One of the promising ways of improving light absorption of photocatalysts is through the design and fabrication of hierarchical macroporous or mesoporous architectures, which recently attracted a great deal of attention.[112] In general, the hierarchically structured photocatalysts with 3D morphologies can be constructed through different methods such as the self-assembly of nanosized building blocks or templating methods.[70] The hierarchically porous core-shell and hollow structures created during the formation of photocatalysts could increase the number of light traveling paths, which results in the enhancement of interaction time and absorption efficiency inside pores as compared to the nonporous photocatalysts. For example, it was shown that porous $TiO_2$ and $WO_3$ with (semi-)hollow structures exhibited a greatly enhanced photocatalytic degradation activity due to more efficient utilization of light through its multiple reflections in the hollow structures (see Figure 8A).[100, 118]

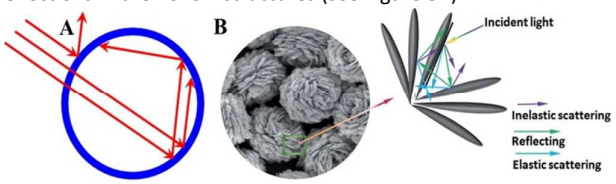


**Figure 8**. Schematic illustration of the reflecting and scattering effects in hollow (A) and hierarchical (B) microspheres. Panel B, reproduced with permission from ref. 119. Copyright © 2014, Royal Society of Chemistry.

In addition, the urchin-like hierarchical $Fe_3O_4$@$Bi_2S_3$ core-shell structures,[120] $Co_3O_4$ particles,[121] CdS@ZnO and CdS@$Al_2O_3$ heteroarrays[122] also showed significantly enhanced photocatalytic degradation and $H_2$-evolution activities, respectively. It is believed that the enhanced light absorption is due to the so-called light-scattering effects, which play the key role in enhancing the light harvesting efficiency of hierarchically structured photocatalysts (see Figure 8B).[119] For example, the transmission spectra of films (Figure 9) show clearly that a hierarchically micro-nanoporous $TiO_2$ film exhibited much higher light-collection efficiency than a nanostructured film due to the improved light scattering effects.[123] Similarly, a polished planar Si surface applied in organic-inorganic hybrid solar cells shows a significant light reflectance ranging from 15 to 30% in the solar spectrum (400–1100 nm), whereas, the reflectance of hierarchical Si surfaces is reduced to less than 10% due to a significant improvement in light trapping.[124] Obviously, the

intrinsic interconnected accessible mesopore channels and the formation of hierarchical structures are the crucial factors to promote the light-harvesting efficiency. In contrast, it was demonstrated that a drop of 20-30% in the photocatalytic activity was observed in the absence of light-penetrating and gas-diffusing macrochannels, further indicating the beneficial effects of macrochannels.[112, 114] Therefore, the fabrication of hierarchically ordered macro-/mesoporous materials has been considered as one of the most popular approaches to enhance the overall light utilization efficiency due to the improved light scattering and increased light-harvesting ability.[114]

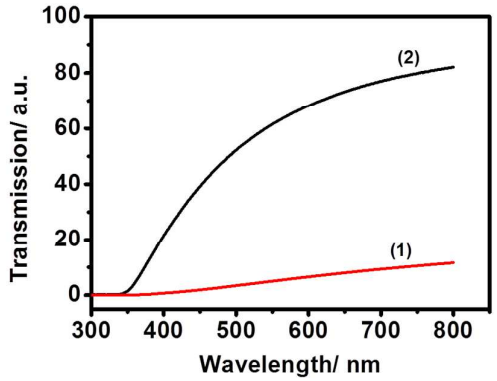


**Figure 9**. UV-Vis transmission spectra of a hierarchically micro-nanoporous $TiO_2$ film (1), and a nanostructured film (2). Reproduced with permission from ref. 123. Copyright © 2008, Elsevier Inc.

**3.3 Increased surface area**

Apart from improving light harvesting and mass transport, the enlargement of the surface area of semiconductors has been also proven to be one of the most efficient approaches for enhancing photocatalytic activity.[112, 115, 125] Although it is well known that the macro/mesoporous materials exhibit relatively small surface areas as compared to those of microporous ones,[126-129] the majority of photocatalysts with hierarchical macro/mesopores still possess the considerably high specific surface area (~50-500 $m^2/g$).[68] Interestingly, the specific surface area of some hierarchically porous carbons can reach 800-2800 $m^2/g$.[130-132] Typically, three-dimensional (3D) hierarchical nanostructures have many unique features including high surface to volume ratios, large accessible surface area, and better permeability, which could not only provide abundant active adsorption sites and photocatalytic reaction sites,[120] but also improve uniformity of the distribution of active sites in the as-prepared photocatalysts. Furthermore, it was also reported that the hierarchical photocatalysts exhibited lower apparent activation energy than the photocatalysts with destroyed macrochannels in the case of photocatalytic decomposition of acetone in air.[114] For example, the hierarchical porous $Ni(OH)_2$ and NiO nanosheets with the surface areas of 201 and 127 $m^2/g$, respectively, can be fabricated through the template-free hydrothermal reaction–precipitation route.[133] The resulting materials showed better adsorption capacities for $N_2$ and Congo red (CR) than the conventional NiO ($S_{BET}$=2.5 $m^2/g$) due to the increased surface areas (Figure 10). Similarly, it was recently demonstrated that the hierarchical γ-$Al_2O_3$ exhibited a unique hierarchical nanostructure and high surface area (≈140$m^2/g$), leading to much higher adsorption of $CO_2$ and pollutants in air and water, respectively.[134, 135] Importantly, the hierarchically macro-mesoporous Pt/γ-$Al_2O_3$ composite microspheres with high surface area also showed higher catalytic activity for oxidative decomposition of HCHO at room temperature, due to the improved diffusion of reactants and products, and the high dispersion of accessible catalytic Pt nanoparticles.[136] More interestingly, the hierarchical Pt/AlOOH nanoflakes with high specific surface area and large pore volume showed higher catalytic activity toward decomposition of HCHO at room temperature due to the presence of abundant surface hydroxyls and excellent adsorption performance of HCHO.[137] The superstructures of $TiO_2$ nanocrystals supported on the hierarchical flower-like AlOOH also exhibited the enhanced photocatalytic activity toward degradation of rhodamine B (RhB) in aqueous solution in comparison to P25 and pure $TiO_2$ powders due to their hierarchical structures with high surface area, easily accessible to light and reactants.[138] All these factors can substantially improve the surface reaction kinetics, and considerably reduce the surface recombination of charge carriers, which is crucial for achieving superior photoactivity of these hierarchical photocatalysts.

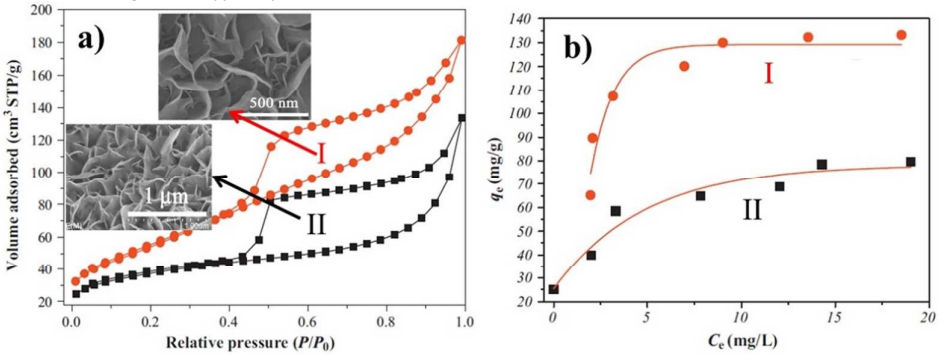


**Figure 10**. (a) Nitrogen adsorption-desorption isotherms and (b) adsorption isotherms for Congo red (CR) (T=25 °C; adsorbent dose = 200 mg/L; CR concentration = 15–50 mg/L and pH 7) of the samples I (hierarchical porous $Ni(OH)_2$ nanosheets) and II (hierarchical porous NiO nanosheets). Reproduced with permission from ref. 133. Copyright © 2011, Elsevier Inc.

Furthermore, the enhanced efficiency for collection, transfer and separation of charge carriers can also be partially achieved in the

hierarchical heterostructured nanocomposites.[139-142] In addition, the hierarchical photocatalysts fabricated by self-assembly of nanosized building blocks can avoid the agglomeration and sintering problems observed for conventional nanosized photocatalysts. Importantly, the hierarchical photocatalysts with self-supported structures generally exhibit a uniform particle size distribution in the range of micrometers, which is more beneficial for the recovery, reuse and recycling of photocatalysts from aqueous suspensions after the photocatalytic reaction than in the case of nanosized particles.[143] Considering the role of the aforementioned factors in increasing photocatalytic activity, it is reasonable to accept that the design of hierarchical nanoarchitectures is a promising strategy to develop highly efficient photocatalyts through optimization of the photocatalytic activity of the existing semiconductors. Typically, the superior photocatalytic performance of the hierarchical micro/nanostructures can be related to their unique structural features, which can suppress the aggregation of micro/nanoscale building blocks, increase specific surface area and the amount of active reaction sites, and reduce the diffusion barrier. All these advantages of hierarchical nanoarchitectures lead to their widespread applications in various fields of photocatalysis. An optimal photocatalyst should be hierarchically porous with interconnected macropores (enabling good light-harvesting, molecular diffusion and gas/liquid flow rates) and mesopores (ensuring high surface area and substrate–gas contact).[114] Various fabrication methods and growth mechanisms of hierarchical nanostructures have been proposed, which will be presented in the following section.

## 4. Strategies for fabrication of hierarchical photocatalysts

The above discussion shows that hierarchical nanostructures play a very important role in enhancing light-absorption capacity and photocatalytic efficiency. So far, a great number of hierarchical semiconductor nanostructures has been rationally designed and fabricated. Generally, the 3D hierarchical micro/nanocomposite structures are fabricated via the self-assembly of nanosized building blocks (including nanoparticles, 1D nanowires, and 2D nanosheets). For example, many interesting hierarchical semiconductor photocatalysts including branched 1D or 2D nanojunctions (Figure 11),[144-150] brush-like,[142, 151-153] 3D flower-like microspheres,[114, 154-158] hierarchical "forest-like" nanostructures (Figure 12)[159] and hierarchically photonic crystals (PCs, Figure 13)[160-169] have been developed by different groups. However, it is very difficult to directly design and fabricate various kinds of hierarchical photocatalysts with highly controlled hierarchical morphologies. Thus, it is necessary to develop a simple and low-cost method to prepare the photocatalysts with high crystallinity and hierarchical nanostructures. Some so far reported methods to prepare hierarchical semiconductor structures are summarized in Figure 14, which shows that these methods can be classified into three types: templating strategies (two-step template method and in-situ template-sacrificial dissolution), template-free strategies (self-templating strategy, in-situ template-free assembly, chemically induced self-transformation), and post-synthetic treatment.

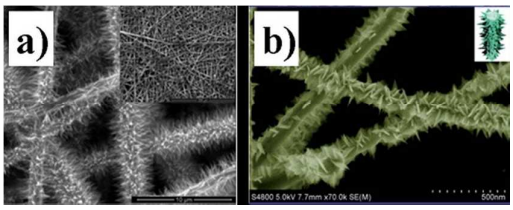


**Figure 11** (a), SEM images of ZnO nanorods hydrothermally grown on the $TiO_2$ nanofibers; (b),Typical high magnification SEM image and model (inset) of the as-grown $Cu_2O$ nanosheet–nanowires. Reproduced with permission from ref. 150 (panel a). Copyright © 2012, American Chemical Society. Reproduced with permission from ref. 147 (panel b). Copyright © 2014, Royal Society of Chemistry.

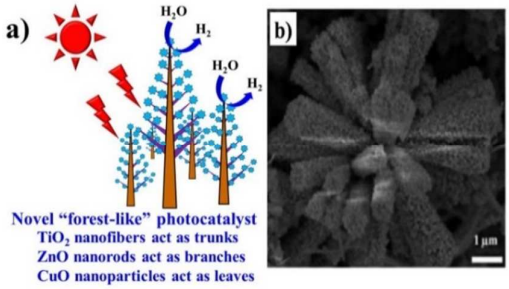


**Figure 12** a) Schematic illustration of a "forest-like" photocatalyst by nature mimicking; b) top view SEM image of hierarchical "forest-like" $TiO_2$ nanofiber/ZnO nanorods/CuO nanoparticle photocatalyst. Reproduced with permission from ref. 159. Copyright © 2012, Elsevier Inc.

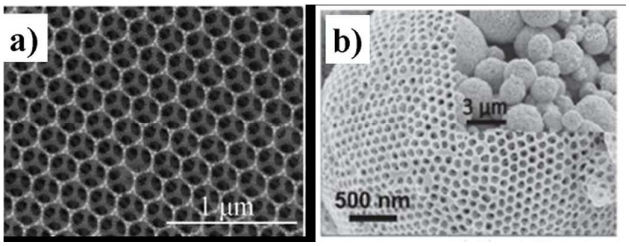


**Figure 13** a) SEM images of the $ZnGa_2O_4$ photonic crystals prepared by using polystyrene spheres as templates; b) $TiO_2$-PC spheres obtained by spray and sacrificing template methods. Reproduced with permission from refs. 169 (panel a) and 166 (panel b). Copyright © 2014 and 2013, Royal Society of Chemistry.

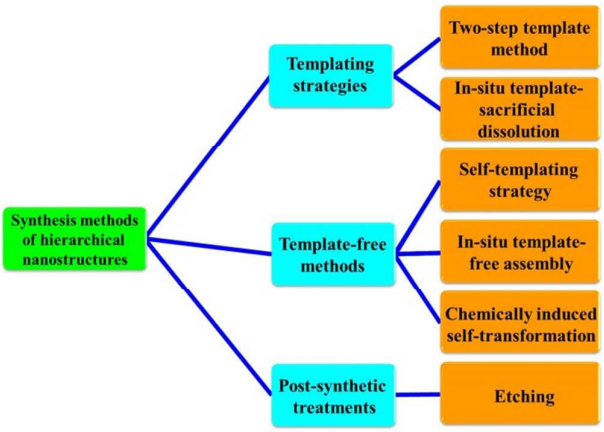


**Figure 14** Synthesis methods of hierarchical nanostructures.

### 4.1 Two-step template method

Template strategy is one of the most important and commonly used methods to synthesize hierarchical nanostructured materials owing to its distinct advantages including good reproducibility, large scale synthesis and abundant types of physical templates.[170] In general, the pre-existing nanostructured templates with various morphologies are required in the synthesis process to control the oriented growth of hierarchical nanomaterials. According to the physical properties of the employed templates, the templating synthesis can generally be sorted into three categories: hard templating (nanocasting), soft templating and bio-templating. Normally, the inorganic and organic mesostructured frameworks with relatively rigid shapes can be utilized as the so-called ''hard templates'' to fabricate 3D hierarchical macro/mesoporous materials, such as zeolites, alumina membranes, polystyrene latex (PSL),[171] metal oxides (such as $Fe_2O_3$ and $CaCO_3$), poly-(methyl methacrylate) (PMMA), ordered mesoporous carbon and silica spheres (SBA-15, MCM-41, and KIT-6).[172] For example, various hierarchical porous $TiO_2$ or ZnO spheres can be fabricated by using $SiO_2$ microspheres as templates, which exhibit greatly improved photocatalytic property due to the formation of controlled macroporosity.[62, 173-176] In comparison to the hard templates, soft templates are highly deformable and easily removable. Thus, various soft templates such as block copolymers (e.g., Pluronics P123, F127, PEG or F108), microemulsions (micelles and vesicles), ionic liquids,[177] hydrogels (sol-gel networks), surfactants (e.g., sodium dedecyl sulfate (SDS) and cetyl trimethylammonium bromide (CTAB)), and even gas bubbles,[178-180] etc., have been widely utilized in the synthesis process to reduce the interfacial energy barrier for sequential nucleation–growth,[170, 181] and create hierarchical structures. Furthermore, the nanoporous g-$C_3N_4$ photocatalysts with enhanced photocatalytic activities could be also prepared through the soft templating including P123,[182] bubbles,[183, 184] and ionic liquids.[185] In future, it is also expected that the macro/mesoporous photocatalysts with hierarchical architectures can be created through a combination of hard and soft templating methods.[71, 186] Additionally, biomaterial-based templates involving natural leaves[187] butterfly wings,[188] legume,[189] rice-husk,[190] silk fibroin[191] and cellulose[192] have been widely used to fabricate the hierarchical photocatalysts with improved photocatalytic activity. For example, a kind of legume has been chosen as a bio-template to synthesize the film of ZnAl-layered double hydroxide. A detailed strategy for bio-templated fabrication of ZnAl-LDH film and the resulting calcination product (hierarchical mixed metal oxide (MMO) framework) is shown in Figure 15. It was found that the bio-templated ZnAl-MMO framework exhibits 2.4 times higher BET specific surface area and much wider pore size distribution than the conventional ZnAl-MMO powder, which resulted in enhancing its photocatalytic performance toward decomposition of organic compounds.[189] In this aspect, the biomaterial-based templating synthesis represents a promising direction for future research in hierarchical nanomaterials since the cheap and abundant bio-templates can be obtained through green approaches. Importantly, the removal of bio-templates can also be easily realized under relatively mild conditions.[170]

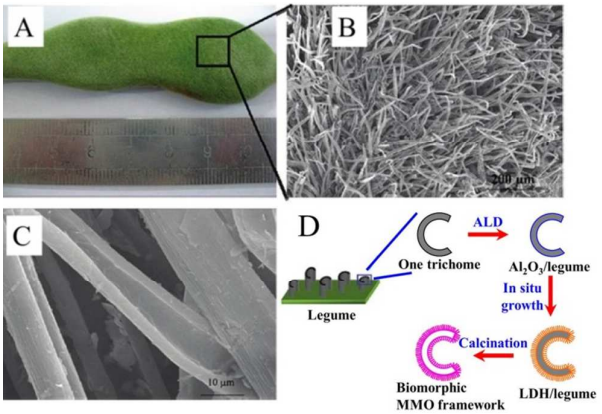


**Figure 15**. (A) Optical photograph of legume; low (B) and high (C) magnification SEM images of the tubular trichome on the surface of legume; (D) Schematic illustration of legume-templating ZnAl-layered double hydroxide and hierarchical mixed metal oxide (MMO) framework. Reproduced with permission from ref. 189. Copyright © 2009, American Chemical Society.

### 4.2 In-situ template-sacrificial dissolution

Usually hard templating includes two steps: the surface coating of the template with nanocrystals and the template removal by calcination or etching. Although this two-step method has been widely used to prepare hierarchical photocatalysts, the post-synthetic removal of the templates through high-temperature calcination or etching is generally costly, and problematic from "green" chemistry viewpoint. On the contrary, the one-step in-situ template-sacrificial dissolution method avoids these problems because it can be performed under significantly milder conditions (e.g., room temperature). For example, the fabrication of hierarchically nanoporous $TiO_2$ hollow microspheres could be carried out in pure water by using $SiO_2$ microspheres as templates and $TiF_4$ as the precursor at 60 °C.[176] As shown in Figure 16, the shells of hierarchically nanoporous $TiO_2$ hollow microspheres are composed of many small $TiO_2$ spherical particles with diameters of about 100 nm. The corresponding SEM and TEM images in Figure 16 partially confirm the presence of hierarchically nanoporous structures. It is believed that many smaller primary crystallites

aggregate and form these small spherical particles within microspheres. The inter-aggregation among these spherical particles results in the formation of larger pores with size of 10 to 110 nm.

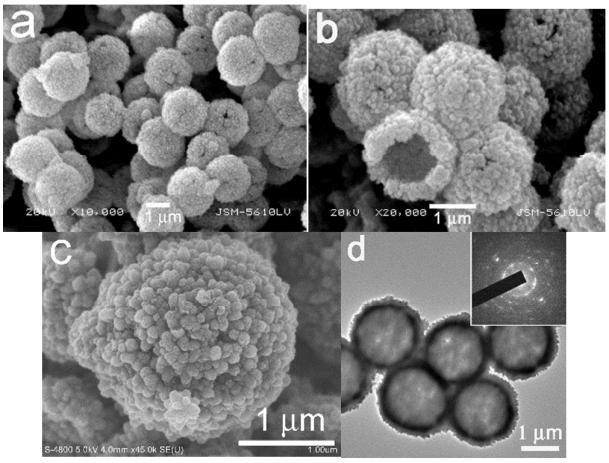


**Figure 16** (panels a and b) SEM, (c) FESEM, and (d) TEM images of hierarchically nanoporous $TiO_2$ hollow microspheres. Reproduced with permission from ref. 176. Copyright © 2008, American Chemical Society.

The formation mechanism of hollow $TiO_2$ microspheres is attributed to the following hydrolysis and dissolution reactions occurring in the reaction system (see Figure 17):

$$TiF_4 + 4H_2O \rightarrow TiO_2{\cdot}2H_2O + 4HF \quad (2)$$

$$SiO_2 + 4HF \rightarrow SiF_4 + 2H_2O \quad (3)$$

The hydrolysis of $TiF_4$ leads to the production of HF and $TiO_2$ sol. The produced HF will dissolve $SiO_2$ template to form $SiF_4$. Therefore, with increasing reaction time and continuous hydrolysis of $TiF_4$, the increasing concentration of HF results in the gradual dissolution of $SiO_2$ cores and the formation of $TiO_2$ hollow spheres with movable $SiO_2$ cores inside. Finally, the $SiO_2$ cores will completely dissolve by HF, resulting in the formation of $TiO_2$ hollow spheres.

Additional photocatalytic experiments indicate that the prepared $TiO_2$ hollow microspheres can be easily separated and re-used from the aqueous solution by sedimentation or filtration after photocatalytic reaction. Therefore, the prepared $TiO_2$ hollow spheres are advantageous in comparison to the conventional powder photocatalysts used in environmental purification. These hierarchically $TiO_2$ hollow microspheres are also useful as catalysts, catalysts supports, and materials for solar cells, separations and nanotechnology.

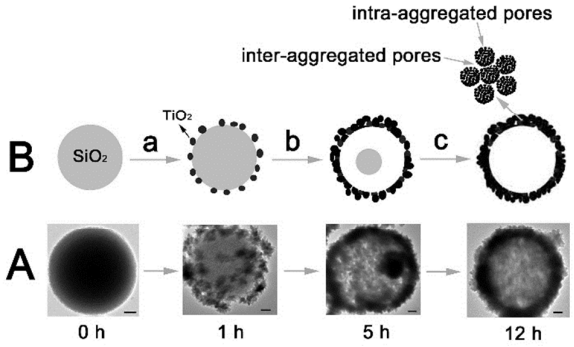


**Figure 17** Schematic illustration of the formation of hierarchically nanoporous $TiO_2$ hollow microspheres obtained through the template-directed deposition and in situ template-sacrificial dissolution. Reproduced with permission from ref. 176. Copyright © 2008, American Chemical Society.

**4.3 Self-templating strategy**

Both hard templating and in-situ sacrificial-template dissolution methods have drawbacks related to the high cost of templates, unexpected morphological changes during template removal, presence of heterogeneous impurities and tedious synthetic procedures. All these disadvantages may limit the large-scale fabrication of photocatalysts by using the aforementioned methods.[193] Thus, it is impractical to synthesize hierarchical photocatalysts in a large scale for industrial applications using these methods. Because of this, tremendous efforts have been undertaken to develop the simple, facile, low-cost, "green", and template-free routes for fabrication of hierarchical micro/nanostructures of various materials.[194, 195] Among them, the self-templating strategy is one of the most simple and effective routes to fabricate various hierarchical photocatalysts. For example, the popular CdS photocatalysts could be fabricated through a simple anion exchange by treating $Cd(OH)_2$ nanostructures with solution containing $S^{2-}$ ions.[22, 196, 197] Recently, Xiang et al. demonstrated that the hierarchical $Cd(OH)_2$ nanosheets-based assemblies could be constructed by a hydrothermal treatment of Cd $(OH)_2$ precipitate. Then, the hierarchical porous CdS nanosheet-assembled flowers could be synthesized by a simple ion-exchange strategy using $Cd(OH)_2$ nanosheet-based material and $Na_2S$ as precursors. A detailed formation mechanism is shown in Figure 18.[198] Similarly, $CdIn_2O_4$ hollow spheres with higher photocatalytic efficiency toward decomposition of Methylene Blue (MB) in aqueous solutions can be synthesized by using CdO and $In_2O_3$ nanoparticles as self-templates.[199] Furthermore, it is known that the hierarchical BiOX nanostructures can be easily fabricated. The latter have been used as self-templates to obtain various photocatalysts such as $Bi_2WO_6$ hollow microspheres,[200] $Bi_2S_3$ nanocrystals/BiOCl hybrid architectures[201] and Ag/AgBr/BiOBr hybrids[202] via a simple in-situ ion exchange. In addition, the hollow $TiO_2$ nanostructures can be fabricated by a facile fluoride-free self-templated synthesis method based on an inside-out Ostwald ripening mechanism, in the presence of $H_2O_2$.[203] In this case, $H_2O_2$ acts as a coordination agent and interface stabilizer playing versatile roles in the self-assembly of microspheres as well as in its transformation into hollow nanostructures.[203] Thus, it is expected that more and more hierarchical photocatalysts could be fabricated through the self-templating strategy in the future.

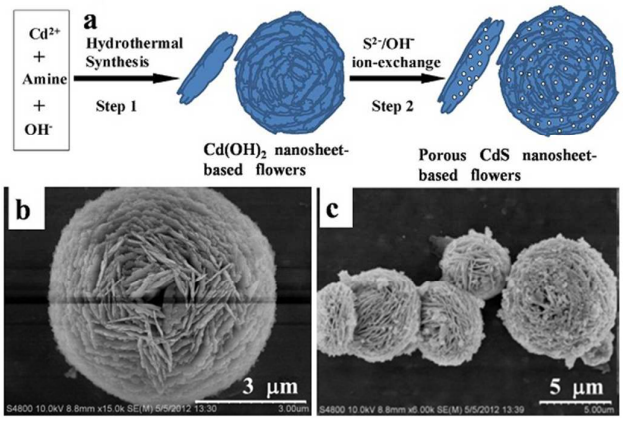


**Figure 18**. (a) A schematic illustration of the synthesis route of porous CdS nanosheet-assembled flowers; SEM images of the $Cd(OH)_2$ intermediates (b) and the as-prepared CdS products (c). Reproduced with permission from ref. 198. Copyright © 2013, Elsevier Inc.

### 4.4 In-situ template-free assembly

Another typical template-free route is the in-situ template-free assembly. For example, the hierarchically macro/mesoporpous amorphous titania can be easily fabricated at room temperature by simple dropwise addition of tetrabutyl titanate to pure water (see Figure 19).[114] The formation of hierarchically macro/mesoporpous titania is due to the spontaneous self-assembly of amorphous $TiO_2$ particles in alkoxide-water mixed solution without the presence of organic additives or templates. Calcination was shown to have a great effect on the photocatalytic activity and structure of titania. The sample calcined at 300°C exhibited the highest photocatalytic activity toward decomposition of acetone in air due to the appearance of anatase phase, large specific surface areas and its hierarchical macro-/mesoporous structures (Figure 20). The photocatalytic activity of the samples prepared at 400 and 500°C was slightly reduced due to the decreased specific surface area, but it is still higher than that of the commercial-grade Degussa P25 $TiO_2$ powder (P25). For the samples prepared at temperatures exceeding 500°C, the photocatalytic activity was obviously smaller due to the destruction of hierarchical macro/mesoporous structures and drastic decrease in the specific surface area (see Figure 20). This hierarchically macro-mesoporous network with open and accessible pores was preserved up to 500°C, indicating its relatively high thermal stability. Even for samples prepared at 800°C the macroporous channel structure was still observed.

To further investigate the positive effects of hierarchically macro/mesoporous structures on the photocatalytic performance, the hierarchically macro/mesoporous $TiO_2$ samples calcined at 300°C were ground into fine powders to destroy their hierarchically macro/mesoporous structure. Then, their photocatalytic performance was measured, indicating a decrease (about 23 %) in the photocatalytic performance of the ground $TiO_2$ sample. The above result and discussion imply that hierarchically macro/mesoporous structures indeed enhance the photocatalytic activity of titania materials. This is due to the enhanced transport of gas molecules in the catalyst. In nature, such hierarchical porous networks have been also developed to achieve rapid gas exchange over large surface area. For example, lungs of animals and gills of fish have such hierarchical network-structures, which allow for a rapid exchange of air. Therefore, it is not surprising that hierarchically macro/mesoporous structures can greatly enhance the photocatalytic performance of photocatalysts.

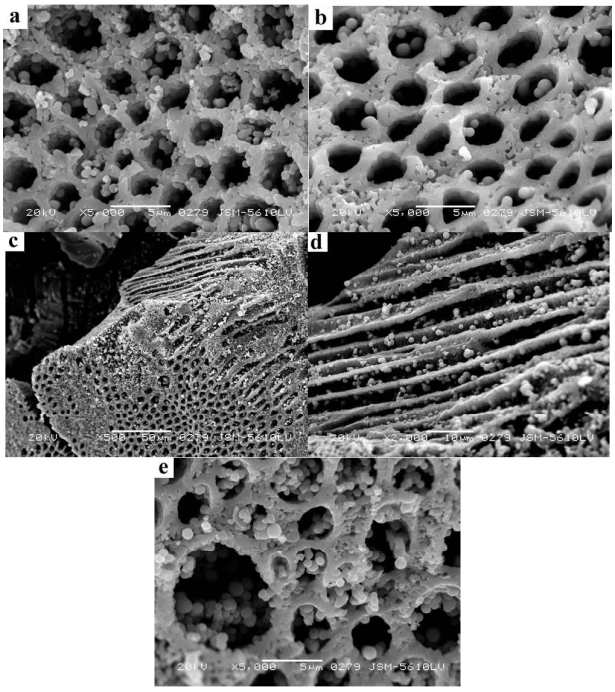


**Figure 19**. SEM images of the as-prepared (a) and calcined hierarchical macro-/mesoporous $TiO_2$ samples at (b) 300, (c,d) 500 and (e) 800°C. Reproduced with permission from ref. 114. Copyright © 2007, Wiley-VCH Verlag GmbH & Co. KGaA, Weinheim.

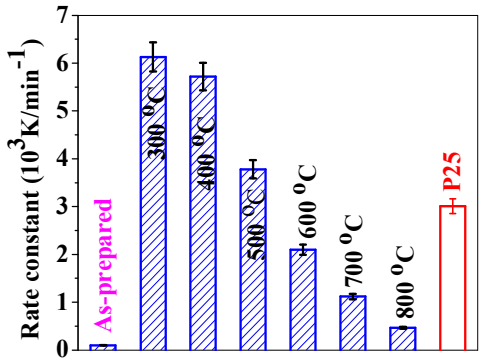


**Figure 20**. Comparison of the photocatalytic activity of P25, as-prepared and calcined hierarchical macro-/mesoporous $TiO_2$ samples at 300, 400, 500, 600, 700 and 800°C for photocatalyic decomposition of acetone in air. Reproduced with permission from ref. 114. Copyright © 2007, Wiley-VCH Verlag GmbH & Co. KGaA, Weinheim.

The formation mechanism of the hierarchically macro-mesoporous $TiO_2$ can be deduced on the basis of the SEM images shown in Figure 21. First, a direct contact between tetrabutyl titanate (TBOT)

droplets and water rapidly produces a thin semi-permeable titania membrane on the external surface of TBOT droplet (see Figures 21a and b). This membrane separates TBOT and water, and subsequent hydrolysis and condensation reactions. Then, the inward reactions proceed slowly. Meanwhile, water gradually diffuses into the interior of the TBOT droplet through the outer membrane and further reacts with TBOT until all TBOT is completely hydrolyzed. During hydrolysis and condensation reactions, the microphase-separated regions of $TiO_2$ nanoparticles and water/alcohol channels within the TBOT droplets are formed due to the hydrodynamic flow of the solvent (see Figure 21c). The key factor in the synthesis of the hierarchically macro-mesoporous $TiO_2$ is the lack of stirring.

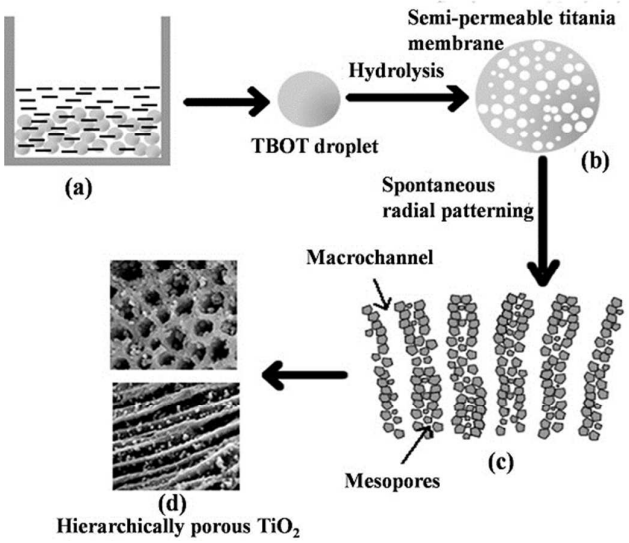


**Figure 21**. The formation mechanism of the hierarchically macro/mesoporous amorphous titania. Reproduced with permission from ref. 114. Copyright © 2007, Wiley-VCH Verlag GmbH & Co. KGaA, Weinheim.

Besides $TiO_2$, the fabrication of other hierarchical semiconductors through the in-situ template-free assembly has been also widely investigated. For example, the sea-urchin shaped $Bi_2S_3$/CdS hierarchical heterostructures composed of $Bi_2S_3$ nanorods and CdS nanoparticles grown on their surfaces (see Figure 22a) were successfully synthesized via a convenient one-pot growth rate controlled route.[204] The proposed formation mechanism as shown in Figure 22b, involves a fast formation of the initial sea-urchin shaped $Bi_2S_3$ nanoflowers, followed by the gradual growth of numerous CdS nanoparticles on $Bi_2S_3$ nanoflowers. Similarly, a 3D hierarchical rutile $TiO_2$ mesocrystalline photocatalyst with higher BET specific surface area (16 $m^2g^{-1}$) was self-assembled under microwave–hydrothermal conditions using 1D rutile nanowires with high average aspect ratio (267; defined as the length of the major axis divided by the width of the minor axis) obtained from $TiCl_3$ as the only reactant (as shown in Figure 23a).[205] Furthermore, 3D-hierarchical well-crystallized $Cu_3SnS_4$ flower-like microspheres with thin nanoplates as building blocks (as shown in Figure 23b) were successfully created through a solvothermal process, which involves aggregation, self-assembly, transformation and ripening.[206] In addition, dendritic α-$Fe_2O_3$ hierarchical structures with superior photocatalytic degradation efficiencies toward Congo red were created through a one-step facile template-free and surfactant-free hydrothermal route (see Figure 24a) [148]. The aforementioned superior photocatalytic activity was probably due to the efficiently enhanced light harvesting and exposed surface sites because of their multi-stage branch-type morphology. It is believed that these α-$Fe_2O_3$ dendritic structures form via a three step process under hydrothermal conditions (see eq. 4). In the first step $Fe(CN)_6]^{3-}$ ions are slowly converted to into $Fe^{3+}$ ions; this step may determine the growth process because of the weak dissociation tendency of $[Fe(CN)_6]^{3-}$ ions. During this growth process (see Figure 24b), the branched α-$Fe_2O_3$ nanostructures with enhanced surface area are obtained if small outgrowths are formed and continue to grow into larger branches. Next, new outgrowths can be formed on these branches and become sub-branches; such growth leads to the complex dendritic crystals as shown in Figure 24b.[148] Thus, it is highly desirable to develop a simple, low-cost, environmentally friendly aqueous solution route for a large-scale synthesis of these hierarchical micro/nanostructures at room temperature under ambient conditions, without using any template, organic solvents, additive or surfactants during the entire process.

$$[Fe(CN)_6]^{3-} \rightarrow Fe^{3-} \rightarrow FeOOH/Fe(OH)_3 \rightarrow \alpha\text{-}Fe_2O_3 \quad (4)$$

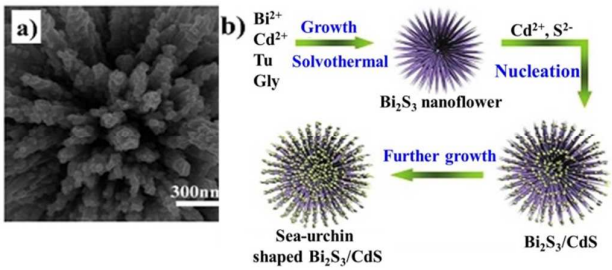


**Figure 22** (a), SEM images of the samples prepared by using molar ratio (2:1) of $Bi_2S_3$ and CdS; (b), Illustration of the morphological evolution process of the sea-urchin shaped $Bi_2S_3$/CdS hierarchical heterostructures. Reproduced with permission from ref. 204. Copyright © 2014, Royal Society of Chemistry.

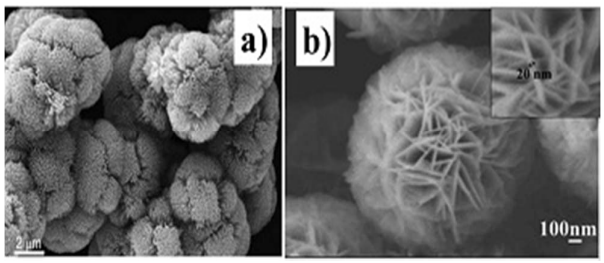


**Figure 23** (a) SEM image of the self-assembled rutile by microwave heating of $TiCl_3$ at 200 °C for 1 min; (b) SEM images of $Cu_3SnS_4$ synthesized at 200 °C for 12 hours. Reproduced with permission from refs. 205 (panel a) and 206 (panel b). Copyright © 2010 and 2013, Royal Society of Chemistry.

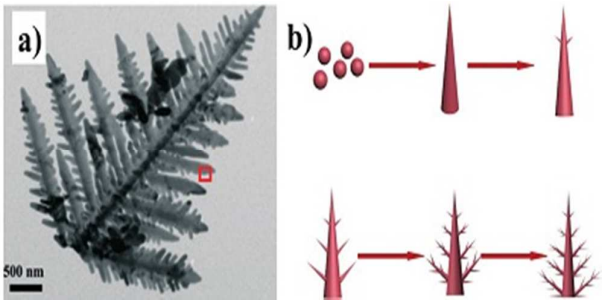


**Figure 24** (a), TEM image of a single dendritic α-$Fe_2O_3$ micro-/nano-structure; (b), Schematic illustration of growth of the as-synthesized dendritic α-$Fe_2O_3$ nanostructures. Reproduced with permission from ref. 148. Copyright © 2014, The Royal Society of Chemistry.

### 4.5 Chemically induced self-transformation

The chemical-induced self-transformation [207-211] method has been also widely applied to fabricate various hierarchically hollow microspheres, including $CaCO_3$, $TiO_2$, $SnO_2$, $Al_2O_3$ and $WO_3$.[207, 212-214] The mechanism of chemically induced self-transformation (CIST) differs from the in-situ template-free assembly, which refers to the spontaneous self-assembly of nanosized building blocks around the primary nuclei, while in CIST the hierarchical nanostructures such as hollow interiors are created via chemical etching of the primary particles. In general, the etching agents such as HF or $OH^-$ are in situ produced during the synthesis process. For example, $SnO_2$ hollow microspheres were obtained by hydrolysis of $SnF_2$ at 180 °C.[207] Clearly, the primary $SnO_2$ particles can be in-situ transformed into hollow microspheres via the fluoride-mediated self-transformation process. Also, hollow $TiO_2$ microspheres consisting of anatase nanocrystals with exposed (001) facets (ca. 20% ) were synthesized by using a slightly modified fluoride-mediated self-transformation strategy (see Figure 25).[211]

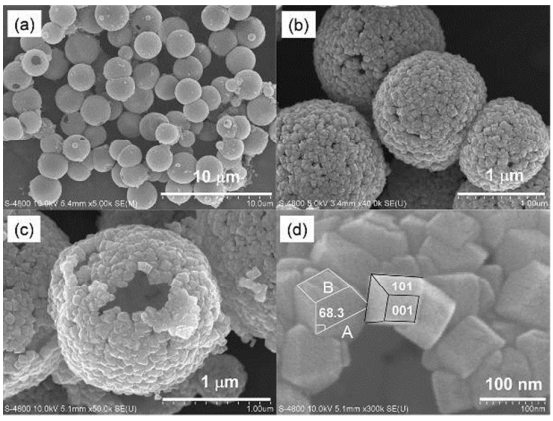


**Figure 25** SEM images of the fluoride-mediated $TiO_2$ samples: (a) overall view of $TiO_2$ microspheres; (b) image of a few microspheres showing their unique structure consisting of primary $TiO_2$ nanoparticles; (c) a single microsphere with visible hollow structure; (d) a portion of the microsphere shell composed of nanosized polyhedra with exposed (001) facets. Reproduced with permission from ref. 211. Copyright © 2010, American Chemical Society.

It was shown that the addition of ethanol can efficiently increase the percentage of exposed (001) facets and the average size of the shell-forming $TiO_2$ nanoparticles. Furthermore, the self-transformation process can be further enhanced by increasing the concentration of $H_2SO_4$.[99] The formation mechanism of the self-templated hollow spheres has been proposed based on a stepwise chemically induced self-transformation (CIST) process, as shown in Figure 26.[215] Clearly, in the fluoride mediated self-transformation process, HF plays an important role in the dissolution of interior of particles and the fabrication of hollow structures. To avoid the HF strong etching, the well-defined anatase hollow microspheres can be fabricated in the presence of urea.[216] Later, it was suggested that a combined mechanism should be considered to better understand the complex formation process of hierarchical structures.[177, 217-219]

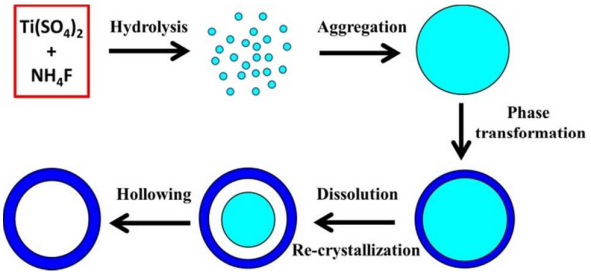


**Figure 26** Schematic illustration of the fluoride-induced self-transformation synthesis of hollow $TiO_2$ anatase microspheres.

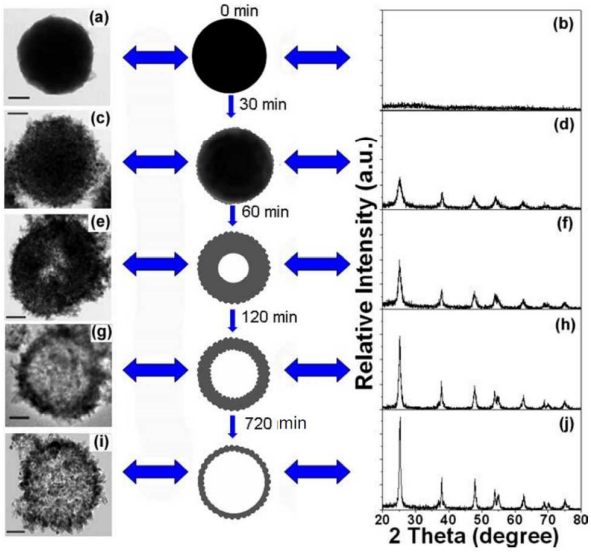


**Figure 27** Formation mechanism of anatase $TiO_2$ hollow spheres prepared by hydrothermal treatment of amorphous $TiO_2$ solid spheres in $NH_4F$ aqueous solution. The left and right panels respectively show the TEM images and the corresponding XRD patterns of the intermediate products obtained at 180 °C for different time (scale bar: 100 nm). Reproduced with permission from ref. 220. Copyright © 2010, Royal Society of Chemistry.

### 4.6 Post-synthesis treatment

The self-etching process, as an efficient strategy to fabricate hierarchical structures, recently has attracted a lot of attention. For

example, the hierarchically mesoporous F-$TiO_2$ hollow microspheres prepared by an enhanced HF etching exhibited higher photocatalytic activity toward degradation of MB than that of P25.[99] In this case the $H_2SO_4$ concentration was controlled because sulfuric acid plays an important role in the self-etching formation of the hollow and mesoporous structures. Furthermore, the photocatalysts with hierarchical structures can be formed through the selective oxidative etching[221] and chemical etching[222, 223]. It is anticipated that the surface-protected etching strategy can be further applied for producing hierarchical high-quality semiconductors for photocatalytic applications.[224, 225]

Anatase $TiO_2$ hollow spheres can be easily prepared by self-transformation of amorphous $TiO_2$ solid spheres in an $NH_4F$ aqueous solution at 180°C for 12 h (see Figure 27).[220] It was shown that $F^-$ plays an important role in the formation of $TiO_2$ hollow spheres. The $F^-$ induced hollowing of $TiO_2$ solid spheres promoted the transformation of amorphous $TiO_2$ phase to anatase nanocrystals. The formation of $TiO_2$ hollow spheres is due to localized Ostwald ripening and chemically induced self-transformation.

## 5. Applications of hierarchical photocatalysts

Based on the above analysis, it is clear that the hierarchical photocatalysts possess a lot of obvious advantages for photocatalytic applications. So far, the hierarchical photocatalysts have been applied in various photocatalytic reactions. Here, we will highlight the recent progress in the research on hierarchical photocatalysts used for photocatalytic $H_2$ production, $CO_2$ reduction and degradation of pollutants (Figure 28).

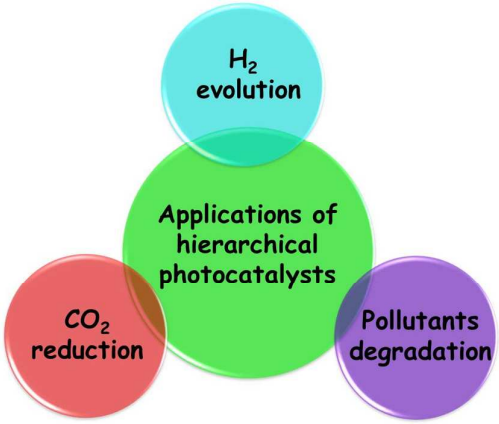


**Figure 28** Photocatalytic applications of hierarchical nanostructures.

### 5.1 Degradation of pollutants

With rapid growth of population and accelerating industrialization, the environmental contamination has become a major threat to public health all over the world. Since the first report on heterogeneous photocatalytic remediation of environmental pollutants ($CN^-$ in water) on titania by Frank and Bard in 1977,[226] the heterogeneous photocatalysis has been widely used in widespread environmental purification such as air and water purification.[4, 13-15, 83, 143, 227, 228] In particular, it was shown that some typical features such as phase structures, exposed facets, crystallinity, surface area, crystalline size and shape are critical for the enhancement of photocatalytic efficiency in the degradation of pollutants in water or air. Thus, a variety of ways for increasing the photodecomposition efficiency of pollutants over semiconductors have been exploited.[4, 79, 83, 229-234] Among them, a particular attention has been given to the formation of hierarchical photocatalysts featuring superior adsorption capacity of pollutants, light-harvesting and recycling capability (see Table 2).

#### 5.1.1. Wide band-gap $TiO_2$ for photodegardation

Among hierarchical photocatalysts shown in Table 2, titania is most often investigated due to its biological compatibility, strong oxidizing power, low cost, and long-term stability.[235] It was demonstrated that various hierarchical nanostructures or macro/mesopores in $TiO_2$ photocatalysts could increase their photo-degradation efficiency and selectivity due to the positive synergistic effect of adsorption, light absorption and charge separation.[68, 236] So far, a variety of 3D hierarchical $TiO_2$ microarchitectures with exposed facets or hollow structures have been studied as photocatalysts for photocatalytic oxidative decomposition of pollutants (formaldehyde, acetone, toluene and $NO_x$) in air at ambient conditions.[68, 114, 116, 205, 209, 220, 235-244] First, applications of hierarchical $TiO_2$ photocatalysts in the degradation of pollutants in air will be highlighted.

A trimodally hierarchical macro-/mesoporous $TiO_2$ was fabricated by a simple hydrothermal treatment of the precipitate obtained from tetrabutyl titanate in pure water (see Figure 29).[68] The prepared $TiO_2$ samples at 180 °C showed hierarchically trimodal pore-size distribution in the meso-/macroporous region, containing small intraparticle mesopores with sizes of ca. 3-7 nm, larger interparticle mesopores with sizes of ca. 20-40 nm, and macropore with sizes of ca. 0.5-3 m. Especially the sample of $TiO_2$ at 180 °C for 24 h exhibited the highest photocatalytic activity, which was about three times higher than that of Degussa P-25 (see Figure 30).

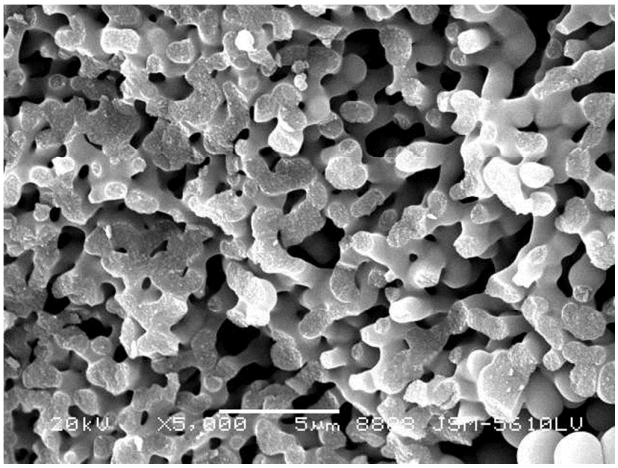


**Figure 29** SEM images of sponge-like hierarchical meso-/macroporous $TiO_2$ prepared at 180 °C for 24 (d). Reproduced with permission from ref. 68. Copyright © 2007, American Chemical Society.

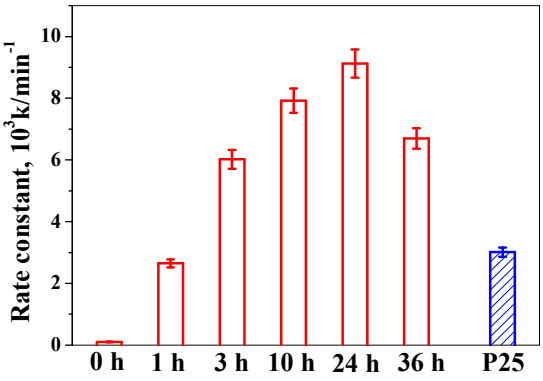


**Figure 30** Comparison of photocatalytic activity of P25 and hierarchically sponge-like meso-/macroporous $TiO_2$ prepared at 180 °C and different hydrothermal time for photocatalytic oxidation decomposition of acetone in air. Reproduced with permission from ref. 68. Copyright © 2007, American Chemical Society.

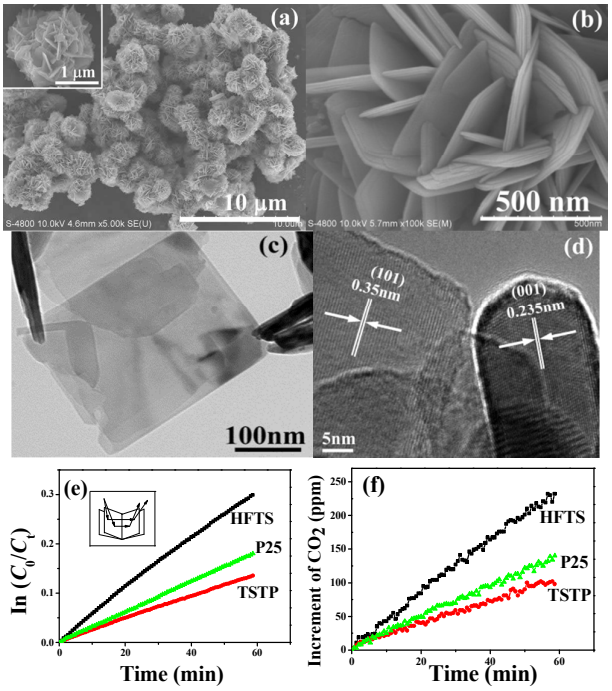


**Figure 31** SEM (a), high magnification SEM (b), TEM (c), and HRTEM (d) images of HFTS. Inset in (a) is a magnified image of an individual spherical superstructure. (e) Comparison of the photocatalytic activity of HFTS, TSTP, and P25 for photocatalytic decomposition of acetone in air. (f) Dependence of produced $CO_2$ concentration on irradiation time for HFTS, TSTP, and P25. Reproduced with permission from ref. 242. Copyright © 2011, Elsevier Inc.

Also, hierarchically flower-like $TiO_2$ superstructures (HFTS) consisting of anatase $TiO_2$ nanosheets with 87% exposed (001) facets were prepared by alcohothermal treatment of titanate nanotubes in a HF-$H_2O$-$C_2H_5OH$ mixed solution (see Figure 31).[242] The photocatalytic performance was evaluated for photocatalytic oxidative decomposition of acetone in air under UV light, indicating that the photocatalytic activity of HFTS was much higher than that of P25 and tubular shaped $TiO_2$ particles (TSTP) obtained in pure water. The enhanced photocatalytic activity is due to the combined effect of highly exposed (001) facets, hierarchically porous structure, and the increased light-harvesting capability.[242]

Apart from the photocatalytic degradation of pollutants in air, the hierarchical $TiO_2$ photocatalysts have also been widely applied in the photocatalytic oxidation of organics in water. Unfortunately, it is still a challenge to achieve high selectivity for hierarchical $TiO_2$ photocatalysts in water. Although the selective photocatalysis is of particular significance because it might provide potential opportunities for achieving the selective separation processes, selective oxidation of targeted organics from a liquid mixture,[245] $TiO_2$ as a typical photocatalyst, generally exhibits a very poor photocatalytic selectivity, due to the nonselectivity of OH radicals with strong oxidizing power.[149] Thus, it is urgent to improve the selectivity of $TiO_2$-based photocatalysts. For example, the hierarchically flower-like $TiO_2$ microsphere films were hydrothermally prepared on the Ti foil in a dilute HF aqueous solution.[149] In a typical preparation, the cleaned Ti foil was simply treated at 180 °C for 1 h in a 60 mL of 0.02 M HF aqueous solution. The prepared flower-like $TiO_2$ microspheres consisted of many $TiO_2$ nanocrystals with exposed (ca. 30%) (001) facets (see Figure 32). Interestingly, the selectivity of the $TiO_2$ film samples for photocatalytic decomposition of two azo dyes in water can be tuned by changing the exposed facets of $TiO_2$ microspheres and the etching degree of (001) facets. Furthermore, the percentage of exposed (001) facets can be slightly controlled by adjusting hydrothermal reaction time.

Generally, the photocatalytic selectivity of $TiO_2$ sample is mainly related to its adsorption selectivity towards contaminants. The adsorption selectivity of $TiO_2$ to charged species can be controlled by changing its surface charge. The isoelectric point of $TiO_2$ in water is at ca. pH 5.8. Thus, at the acidic conditions, $TiO_2$ surface with positive charge will selectively adsorb negatively charged pollutants, resulting in the selective adsorption and degradation of pollutants (Figure 33). Contrarily, the alkaline conditions are beneficial for adsorption and degradation of positively charged pollutants. Therefore, the photocatalytic selectivity of $TiO_2$ toward degradation of pollutants can be easily tuned by changing pH value of aqueous solution (Figure 34).

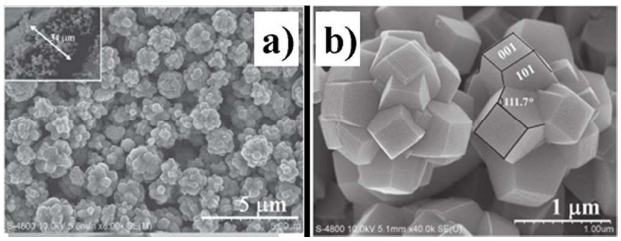


**Figure 32** SEM images (a,b) of the $TiO_2$ films composed of flower-like $TiO_2$ microspheres with exposed (001) facets prepared by hydrothermal treatment of Ti foil at 180 °C for 1 h. The inset in (A) showing the cross-sectional SEM image of the $TiO_2$ films. Reproduced with permission from ref. 149. Copyright © 2011, Royal Society of Chemistry.

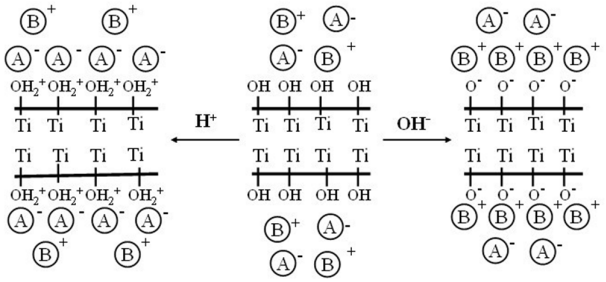


**Figure 33** Schematic illustration for the selective adsorption of pollutants on the $TiO_2$ surface. A and B represent negatively and positively charged pollutants, respectively. Reproduced with permission from ref. 149. Copyright © 2011, Royal Society of Chemistry.

Clearly, the surface chemistry of $TiO_2$ samples at the atomic level plays a key role in tuning the photocatalytic and adsorption selectivity. Another example shows that the hollow $TiO_2$ microspheres (HTS) with different surface chemistry exhibit tunable photocatalytic selectivity toward decomposition of azo dyes in water.[211] The fluorinated HTS are favorable for the photocatalytic decomposition of methyl orange (MO) in comparison to methylene blue (MB). In contrast, the surface-modified HTS by either NaOH washing or calcination at 600 °C can efficiently remove the surface-bonded fluoride species and increase the amount of surface hydroxyl groups, thus facilitate the selective degradation of MB over MO. It is believed that the surface rehydroxylation could promote the selective adsorption of MB molecules, thus leading to the decomposition of selected azo dyes. Therefore, the proposed methods for controlling hierarchical assembly, exposed facets, and surface chemistry of $TiO_2$ materials might open new avenues for designing the selective photocatalysts towards decomposition of pollutants.

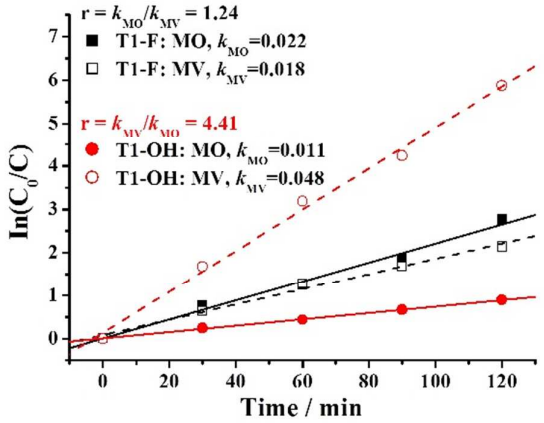


**Figure 34** Comparison of photocatalytic activity and selectivity of the $TiO_2$ films prepared at 180 °C for 1 h (T1) towards degradation of MO and MB before (T1-F) and after NaOH washing (T1-OH). The photocatalytic activity and selectivity is defined by the apparent rate constant (***k***) and the ratio (***r***) of ***k***, respectively. Reproduced with permission from ref. 149. Copyright © 2011, Royal Society of Chemistry.

**5.1.2 Visible-light photocatalysts for photodegardation**

The wide band gaps of some semiconductors including $TiO_2$ and ZnS significantly limit the efficiency of visible-light absorption. Therefore, great efforts have been undertaken to design and explore the flower-like microspherical photocatalysts with improved visible-light performance. Therefore, various elements have been doped into the wide-band-gap $TiO_2$ microspheres to enhance their visible-light activity.[246-250] So far, a number of doped $TiO_2$ with hierarchical structures and visible-light activity have been developed. For example, Fe-doped $TiO_2$ porous microspheres have been proven to exhibit excellent photodegradation activity toward MB under visible light.[251] Furthermore, a high percentage of (001) facets in the Fe-doped $TiO_2$ nanosheeet-type building blocks can promote the dissociation of the adsorbed MB molecules, thus further enhancing their photoactivity for MB degradation.[252] Apart from doping of metal cations, doping of non-metal elements has been shown to be one of the promising strategies to improve the visible-light activity of hierarchical $TiO_2$.[253] Fan and co-workers studied the influence of (N, I) co-doping effect on the photocatalytic properties of biogenic $TiO_2$ materials with hierarchical architectures under visible light.[254] It was shown that nitrogen and iodine, contained in plants, can act as self-doping agents in the synthesis of the biogenic-$TiO_2$ to induce a red shift of the band gap absorption edge, leading to a significant improvement in the photocatalytic activity of this material toward degradation of MB under visible light irradiation. Similarly, the N-F co-doping was used to efficiently enhance the photocatalytic degradation of MO over mesoporous $TiO_2$ nanobelts.[255] In addition, N-, and C-doped ZnO hierarchical photocatalysts have been found to exhibit better absorption of light in both visible and ultraviolet regions due to their smaller band gaps through generating vacant states above the Fermi level.[256] Especially, the C doping was successful in developing the potentially promising ZnO-based hierarchical photocatalysts because it causes a more efficient separation of photogenerated electron–hole pairs as compared to the N and S doping.[256] For instance, the hierarchical flower-like $Zn_5(CO_3)_2(OH)_6$ superstructures composed of porous nanosheets can be engineered through a PEG-mediated organic–inorganic interfacial cooperative self-assembly strategy.[257] The subsequent annealing in air can be used to efficiently transfer $Zn_5(CO_3)_2(OH)_6$ nanosheets into the resultant hierarchical flower-like C-doped ZnO superstructures (ZnO flowers) assembled from porous nanosheets (Figure 35A).[257] The UV-vis absorption spectra of the ZnO flower-like samples obtained at varying calcination temperatures (Figure 35B) exhibit significantly enhanced absorption in the UV and visible-light regions as compared to commercial ZnO. The corresponding pore size distributions (Figure 35C) further confirm the porous structure of ZnO flowers with both the larger mesopores (20–50 nm) and macropores (up 200 nm). The photocatalytic decomposition of the RhB dye in aqueous solutions (Figure 35D) indicates that the ZnO flowers obtained at 500 °C exhibited high activity due to the enhanced light absorption over a wide range of wavelengths.[257]

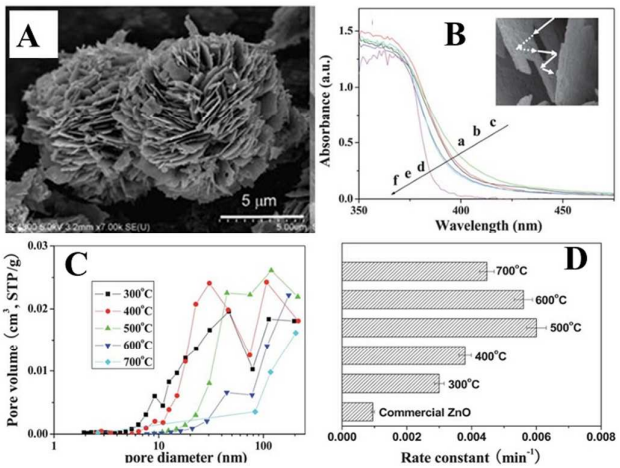


**Figure 35** (A) SEM images of the as-prepared ZnO obtained by calcination at 500 °C; (B) UV-vis absorption spectra of ZnO flower-like samples calcined at varying calcination temperatures : (a) 300, (b) 400, (c)500, (d) 600, (e) 700 °C and (f) commercial ZnO; (C) the corresponding pore size distribution curves for ZnO flowers calcined at varying calcination temperatures; (D), comparison of the apparent rate constants (*k*) for the ZnO flower-like samples calcined at various temperatures under visible-light illumination. Reproduced with permission from ref. 257. Copyright © 2011, Royal Society of Chemistry.

In addition, the increased density of the surface vacancies such as oxygen present in hierarchical photocatalysts can also efficiently promote the visible-light absorption, charge separation and photochemical redox reactions.[258-261]

Numerous highly efficient non-doped and hierarchical 3D microspheres with visible-light activity have been fabricated through the self-assembly of nanosheets/nanoplates. For example, the urchin-like CdS nanoflowers, made of CdS nanorods via a facile solvothermal synthesis in a mixed amine/water phase, exhibit high photocatalytic activity for degradation of acid fuchsine under visible light.[262] Also, the fabrication of In-containing (such as $CuInS_2$,[263] $ZnIn_2S_4$,[105, 264-269] CdS,[262] $In_2S_3$,[270, 271] $CdIn_2S_4$,[272, 273] $SnIn_4S_8$,[274] and $InVO_4$[275]) and Bi-containing hierarchical semiconductor microspheres composed of 2D nanosheets can be easily achieved due to their layered structures. Especially, the Bi-containing hierarchical semiconductors with low toxicity and cost (such as $Bi_2MoO_6$,[276] $BiVO_4$,[277-280] sensitized BiOCl,[201, 281-283] $Bi_2WO_6$,[284-288] $BiOCl_xBr_{1-x}$,[289, 290] BiOI,[291-295] BiOBr,[296-301] $BiVO_4/Bi_2O_2CO_3$,[302] C-doped and N-doped $Bi_2O_2CO_3$[303-309]) have attracted a lot of attention in the field of photocatalytic degradation due to their narrow band gaps. Recently, other 3D hierarchical microspheres obtained by the self-assembly of 0D nanoparticles,[310-314] 1D nanorods[204] or 2D nanoplates/nanosheets[315] have been also successfully synthesized and applied in the photodegradation of pollutants under visible-light irradiation. In future, more attention should be given to the engineering/modification of these Bi-containing semiconductors to further enhance their photocatalytic properties.[316-319] It is highly expected that the photoactivity of these hierarchical Bi-containing photocatalysts can be also enhanced through engineering hetrojunctions with 2D graphene and other semiconductors.[288, 320-327]

In addition, the enhanced activity has also been achieved for multifunctional composite microspheres with magnetic cores [328-330] or heterojunctions.[141, 325, 331-335] In future, it is highly desirable that the hierarchically structured microspheres can be further optimized to maximize the combined effects of the high surface area, superior scattering effect and charge separation performance. It should be also noted from Table 2 that the relationships between the hierarchical nanostructures and main active species (such as •OH radicals, $O_2^-$ and $H_2O_2$) have been ignored in many reports, which deserve more attention in future studies.

**Table 2.** Hierarchical photocatalysts for photocatalytic degradation of pollutants.

| Material | hierarchical morphology | Synthesis method | Growth mechanism | Target pollutant | Activity($k_{app}$,$10^{-3}$ $min^{-1}$) | Ref.(year) |
|---|---|---|---|---|---|---|
| **Photodegradation of gaseous pollutants** | | | | | | |
| $TiO_2$ | macro-mesoporous structure | sol–gel reactions/ calcination | Surfactant template | Ethylene(g) | 15 min/42% | [112](2005) |
| $TiO_2$ | macro-mesoporous structure | template-free sol–gel reactions | self-assembly | acetone(g) | (6.13) | [114](2007) |
| $TiO_2$ | macro/mesoporous structures | hydrothermal treatment | | Acetone(g) | (10.2) | [236](2012) |
| $TiO_2$ | worm-like macroporous | template-free hydrothermal approach | packed aggregates of particles | HCHO(g) | 60 min/ 90.6% | [244](2015) |
| BiOI/BiOCl | flower-like | room temperature template free method | self-assembly of nanoplates | NO(g) | 150 s/54.6% (200) | [336](2012) |
| **Aqueous-phase photodegradation of methyl orange (MO)** | | | | | | |
| $TiO_2$ | nanoporous hollow microspheres | low-temperature template | In-situ template-sacrificial | MO | (16.1) | [176](2008) |

| | | | | | | |
|---|---|---|---|---|---|---|
| | | method | dissolution | | | |
| $TiO_2$ | hierarchical microspheres | one step hydrothermal route | self-assembly of nanotubes | MO | 50 min/100% | [337] (2015) |
| $TiO_2$ /ZnO | hedgehogs and fan blades | solvothermal method | Ostwald ripening | MO | 30 min/ 97% (0.117) | [338](2015) |
| ZnO–$SnO_2$ | hollow spheres, hierarchical nanosheets | hydrothermal method | | MO | 30 min/100% | [339](2007) |
| $ZnIn_2S_4$ | marigold-like microspheres | hydrothermal method | Self-assembly of nanosheets | MO | 3h/100% | [266](2009) |
| $Bi_2S_3$ | flower-like morphology | reflux method | self-assembly of nanorods | MO | 97%/97%(77.6) | [340](2013) |
| BiOBr | 3-D microspherical architectures | solvothermal synthesis | self-assembly of nanosheets | MO | 5h/100% | [341](2008) |
| β-$Ag_2WO_4$ | porous hollow nanospheres | precipitation reaction | self-assembly of nanoparticles | MO | 330min/90% | [342](2013) |
| CdS | dendritic nanoarchitectures | template-free hydrothermal route | self-assembly of nanoparticles | MO | 80min/85% (34.6) | [343](2009) |
| **Aqueous-phase photodegradation of methylene blue (MB)** | | | | | | |
| F-$TiO_2$ | mesoporous hollow microspheres | hydrothermal treatment | self-etching mechanism by HF | MB | 6 h/92% | [99](2008) |
| $TiO_2$/graphene | ordered macro-mesoporous frameworks | Sol-gel template synthesis | confinement self-assembly | MB | 90 min/90% (71) | [111](2011) |
| $SnO_2$ | hierarchical nanostructures | hydrothermal process | self-assembly of nanosheets | MB | 20 min/ 99% | [344](2014) |
| $SnO_2$/a-$Fe_2O_3$ | branched nanoheterostructures | hydrothermal strategy | epitaxial growth of $SnO_2$nanorods | MB | 4h/87% | [345](2010) |
| γ-$Fe_2O_3$/ZnO | double-shelled hollow structures | Hydrothermal-hydrolysis-calcination | Growth of ZnO flakes | MB | 50 min/95.2% | [346](2012) |
| $WO_3$ | porous flower-like structures | hydrothermal treatment | self-assembly of nanoplates | MB | 60min/80% | [347](2012) |
| $ZnIn_2S_4$ | Porous submicrospheres | template-free, microwave-solvothermal approach | Self-assembly of nanofibers | MB | (7.5) | [105](2007) |
| **Aqueous-phase photodegradation of Rhodamine B (RhB)** | | | | | | |
| $TiO_2$ | hollow microspheres with exposed (001) facets | hydrothermal strategy | morphology controlling by $NH_4HF_2$ | RhB | 2 h/80% (50) | [348](2010) |
| $TiO_2$ | porous hollow microspheres/ chains | hydrothermal approach | fluoride-mediated self-transformation strategy | RhB | 90 min/90% | [216](2009) |
| Titanate/N-doped anatase | flower-like hierarchical spheres | hydrothermal approach | Self-assembly of nanosheets | RhB | 60 min/100% | [349] (2015) |
| ZnO | hollow spheres | hydrothermal strategy | Carbon sphere template | RhB | (1222) | [350](2008) |
| $TiO_2$/AlOOH | flower-like boehmite superstructures | Hydrothermal treatment | In-situ transformation of $Al(OH)_3$ microspheres | RhB | 60min/92% | [138](2009) |
| $WO_3$ | hollow shells | annealing of acid-treated precursors | | RhB | 150min/100% | [351](2008) |
| $WO_3$ | flower-like assemblies | template-free | self-assembly of | RhB | 5h/60% (175) | [315](2009) |

| | | | | | | |
|---|---|---|---|---|---|---|
| | | hydrothermal treatment | nanoplates | | | |
| $WO_3$ | sphere-like micropatterns | hydrothermal reaction | Self-assembly of nanorods | RhB | 210 min/ 84% | [352](2013) |
| $BiVO_4/Bi_2O_2CO_3$ | nanosheets-based hierarchical structure | template-free hydrothermal approach | urea-assisted hydrolysis reactions | RhB | 60 min/97% | [302](2011) |
| $Bi_2O_2CO_3$ | flower-like microspheres | two-step hydrothermal method | self-assembly of nanosheets | RhB | 75min/95% | [321](2012) |
| BiOCl | 3D microspheres | hydrothermal method | self-assembly of nanoplatelets | RhB | 80 min/100% | [353](2013) |
| $BiOCl_xBr_{1-x}$ | 3D flower-like structure | room-temperature procedure | | RB | 120 s/100% | [289](2013) |
| BiOBr | flower-like microspheres | solvothermal synthesis/ surfactant | self-assembly of nanosheets | RB | 50 min/95% (7.71) | [296](2012) |
| Ag/AgBr/BiOBr | flower-like microspheres | solvothermal method and *in-situ* ion exchange reaction | self-assembly of nanosheets | RB | 4min/93% (396) | [202](2011) |
| $Bi_2S_3$/CdS | urchin-like nanoflowers | template-free hydrothermal method | self-assembly of nanorods | RhB | 80 min/85% | [204](2014) |
| $Fe_3O_4@Bi_2S_3$ | urchin-shaped core/shell structures | solvothermal reaction ultrasound irradiation | growth of $Bi_2S_3$ nanorods | RhB | 6h/100% | [120](2012) |
| g-$C_3N_4$-BiOCl | flower-like clusters | chemical deposition–precipitation | self-assembly of BiOCl nanoplates | RhB | 60min/100% (117) | [354](2014) |
| **Aqueous-phase photodegradation of other organic and inorganic pollutants** | | | | | | |
| F-doped $TiO_2$ | nanoporous spheres | template-free hydrothermal approach | self-etching by HF | 4-chlorophenol | 6h/50% | [106](2006) |
| AgI/BiOI | hierarchical microspheres | solvothermal approach and *in-situ* ion exchange reaction | self-assembly ofnanosheets | 2,4-dichlorophenol | 60 min/ 77.7% | [355](2013) |
| NiO/TiO $^2$ | Porousflowerlike superstructures | template-free hydrothermal treatment | | p-chlorophenol | 180 min/95% | [356](2010) |
| amorphous $Fe_2O_3$ | hollow spheres | hydrothermal treatment | Self-assembly of nanoparticles | salicylic acid | 110min/75% | [357](2007) |
| **α-** $Fe_2O_3$ | hollow spheres | microwave-assisted solvothermal method | Self-assembly of nanosheets | salicylic acid | 80min/65% | [358] (2008) |
| CdS/ZnO | nanotree-like structures | hydrothermal-chemical bath method | seeded growth process | Thioanisole | 2 h/60% | [145](2014) |
| α-$Fe_2O_3$/CdS | microflowers | chemical bath method | growth of CdS nanoparticles | Cr( VI ) | 120 min/100% | [359](2013) |
| g-$C_3N_4/SnS_2$ | 3D flower-like microsphere | solvothermal method | self-assembly of $SnS_2$ nanoflakes | Cr( VI ) | 50min/100% (458.2) | [334](2014) |

### 6.2 Photocatalytic $H_2$ generation

It is generally accepted that hydrogen energy is one of the most promising green fuels. As a better alternative for classical fuels, hydrogen energy can become a promising next-generation energy carrier if it is generated via a sustainable energy.[2, 25, 360] Especially, the photocatalytic hydrogen generation from water splitting using solar energy and semiconductors has proven to be a promising strategy for solving the global energy crises and environmental pollution since the pioneering report in 1972 on the photoelctrocatalytic $H_2$ evolution over $TiO_2$.[8] In recent years, various types of heterogeneous photocatalysts have continuously emerged due to their excellent photocatalytic activity and photostability.[2, 5, 6, 361, 362] Among reported heterogeneous photocatalysts, sulfide semiconductors exhibit the highest photocatalytic $H_2$-evolution activity, especially under visible-light irradiation.[22, 23, 25, 26, 198, 363-366] Thus, some typical hierarchical sulfide photocatalysts are listed in Table 3 and will be discussed in this section.

Hierarchical single-component sulfides and their heterojunctions have been widely applied in photocatalytic $H_2$ evolution. For example, Domen et al. demonstrated that nanoporous CdS nanosheets and hollow nanorods can be prepared at room temperature via a two-step process involving the self-templating synthesis of $Cd(OH)_2$ intermediates followed by their subsequent $S^{2-}/OH^-$ ion-exchange conversion.[22] The resulting CdS photocatalysts loaded with monodisperse 3–5 nm Pt nanocrystals featured an apparent quantum yield of about 60.34% at 420 nm. Recently, Xie et al. demonstrated that the CdS-mesoporous ZnS core-shell particles exhibited a 56-fold enhancement in visible-light $H_2$-evolution rate as compared to the pure CdS.[367] Hierarchical porous CdS nanosheet-type flower-like structures were synthesized by a simple ion-exchange strategy using analogous $Cd(OH)_2$ structures and $Na_2S$ as precursors (see Figures 36A). The resulting photocatalysts exhibited a high $H_2$–production activity (468.7 μmol $h^{-1}$) with an apparent quantum efficiency (QE) of 24.7% at 420 nm, 3 times higher than

**Table 3.** Hierarchical sulfide-based photocatalysts for photocatalytic $H_2$ generation

| Material | hierarchical morphology | Synthesis method | Growth mechanism | Cocatalyst | Sacrificial agent | $R_{H2}$ (μMh$^{-1}$ g$^{-1}$)/ QE (%,420 nm) | Ref.(year) |
|---|---|---|---|---|---|---|---|
| **Single-compound photocatalysts** | | | | | | | |
| CdS | nanoporous nanosheet | precipitation and anion-exchange method | $Cd(OH)_2$ intermediates | 10 wt % Pt | 0.25 M $Na_2SO_3$ and 0.35 M $Na_2S$ | 4100/60.34 | [22](2007) |
| CdS | flower-like microspheres | hydrothermal and anion-exchange method | self-assembly of nanosheets | 0.5 wt% Pt | 10 vol% lactic acid | 9374/24.7 | [198](2013) |
| CdS | nanoporous nanosheet | precipitation and anion-exchange method | $Cd(OH)_2$ intermediates | 10 wt % Pt | 0.25 M $Na_2SO_3$ and 0.35 M $Na_2S$ | 4100/60.34 | [22](2007) |
| Cu(2 atom %)-Doped ZnS | hollow particles | anion-exchange method | chemical etching | | 0.1 M $Na_2SO_3$ and 0.1 M $Na_2S$ | 6500/ | [368](2008) |
| **Solid solution photocatalysts** | | | | | | | |
| $ZnIn_2S_4$ | flower-like microspheres | template-free hydrothermal method | aggregation of flakes | 1.0 wt % Pt | 0.25 M $Na_2SO_3$ and 0.35 M $Na_2S$ | 8420/34.3 | [265](2011) |
| $ZnIn_2S_4$ | marigold flower-like morphology | hydrothermal method | Self-assembly of nanoplates | | $H_2S$-saturated NaOH(0.25 M) | 10574/ | [369](2011) |
| $ZnIn_2S_4$ | porous submicrospheres | polyol-mediated hot-injection | self-assembly of nanosheets | 3.0 wt % Pt | 0.25 M $Na_2SO_3$ and 0.35 M $Na_2S$ | 1150/ | [264](2013) |
| $ZnIn_2S_4$ | microspheres | microwave hydrothermal method | self-assembly of nanosheets | 0.2 wt% Pt + 0.5 wt% carbon QDs | 10 v% triethanolamine | 1032.2/2.2 | [269](2014) |
| $Cd_xZn_{1-x}S$ | Volvox-like nanospheres | template-free | | | 0.25 M $Na_2SO_3$ and 0.35 M $Na_2S$ | 1766.4/ | [370](2014) |
| $Zn_{0.8}Cd_{0.2}S$ | micro-flowers | solvothermal | self-assembly | 1 wt.% Pt | 0.1 M $Na_2SO_3$ | 5000/ | [371](2013) |

| | | | | | | | |
|---|---|---|---|---|---|---|---|
| | and microspheres | | of nonorods | | and 0.1 M $Na_2S$ | | |
| **Composite photocatalysts** | | | | | | | |
| CuS(5.9%)–$Zn_xCd_{1-x}S$ | nanospheres | heating in ethylene glycol | | 1 wt% Pt | 0.1 M $Na_2SO_3$ and 0.1 M $Na_2S$ | 2464/19.1 | [372](2009) |
| $Zn_xCd_{1-x}S$/bacterial cellulose | bionanocomposite foams | Solvothermal/ ion exchange | seeded growth | | 0.05 M $Na_2SO_3$ and 0.05 M $Na_2S$ | 1450/12 | [373](2015) |
| carbon nanofiber@$ZnIn_2S_4$ | core–shell nanoarchitectures | solvothermal process | *in-situ* growth of $ZnIn_2S_4$ nanosheets | 15 wt% carbon Nanofiber | 0.25 M $Na_2SO_3$ and 0.35 M $Na_2S$ | 3166/25.35 | [374](2014) |
| $In_2S_3$/$ZnIn_2S_4$ | microflower morphology | ion-exchange route | self-assembly of nanoplates | 1 wt% Pt | 0.25 M $K_2SO_3$ and 0.35 M $Na_2S$ | 678/1.4 | [375](2013) |
| $ZnIn_2S_4$/$MoS_2$ | flower-like microspheres | solvothermal process | self-assembly of nanosheets | 15 wt% $MoS_2$ | 0.25 M $Na_2SO_3$ and 0.35 M $Na_2S$ | 975/ | [376](2014) |
| CdS/ZnS/$In_2S_3$ | microspheres | Template-free Sonochemistry synthesis | self-assembly of nanoparticles | | 1.4 M $Na_2SO_3$ and 0.1 M $Na_2S$ | 8100 40.9 | [333](2012) |
| CdS@ZnO | core-shell nanourchins | hydrothermal | self-assembly of CdS nanowires | | 0.25 M $Na_2SO_3$ and 0.35 M $Na_2S$ | 10080 15 | [122](2012) |
| CdS/g-$C_3N_4$(2 wt %) | core/shell nanowires | solvothermal and chemisorption method | | 0.6 wt %Pt | 0.25 M $Na_2SO_3$ and 0.35 M $Na_2S$ | 4152 4.3 | [377](2013) |

that of pure CdS nanoparticles (Figure 36B).[198] This study indicates that the hierarchical self-assembled porous nanosheets facilitate the separation of photo-generated electron-hole pairs, enhance light-absorption and adsorption on active sites. Interestingly, the multi-armed CdS nanorods were fabricated via a solvothermal method using dodecylamine as solvent (Figure 37a).[378] The CdS nanorods with 0.23 wt% Pt co-catalyst exhibited a high $H_2$-production rate of 1.21 $mmolh^{-1}$ with a $H_2$-production quantum efficiency (QE) of 51% at 420 nm (Figure 37b).[378] The high surface area, large pore volume and good crystallization are thought to be the key factors justifying this great performance. In addition, the CdS-based heterostructured photocatalysts with hierarchical structures (such as CdS quantum dots-$TiO_2$ /titanate nanosheets,[379, 380] CdS/graphene nanosheet-type composites[381-383] and CdS decorated 1D ZnO nanorods-2D graphene hybrids[151]) also exhibited greatly enhanced visible-light $H_2$-evolution activity due to promoted charge separation and increased surface of active sites. Especially, the hierarchical sulfide-based photocatalysts based on multiple hybrids deserve more attention.

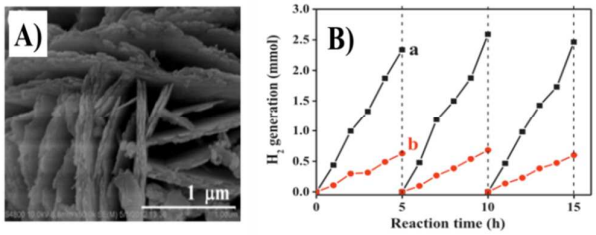


**Figure 36** (A) high- magnification SEM images of porous CdS nanosheet-type flower-like assemblies; (B) photocatalytic production of $H_2$ from aqueous lactic acid solutions over (a) the porous CdS nanosheet-type assemblies and (b) CdS nanoparticles under visible-light irradiation. Reproduced with permission from ref. 198. Copyright © 2013, Elsevier Inc.

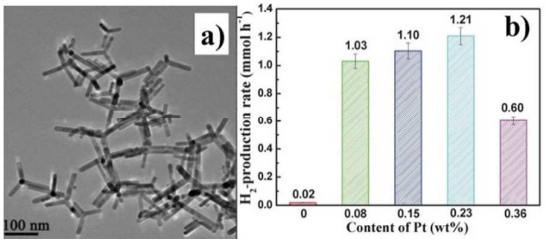


**Figure 37** (a) TEM images of the multi-armed rods (sample R140); (b) Effect of the Pt loading content on the $H_2$-production rate of the R140 sample in aqueous lactic acid solution. Reproduced with permission from ref. 378. Copyright © 2012, Royal Society of Chemistry.

Also, the hierarchical solid-solution semiconductors have been proven to be highly active $H_2$-evolution photocatalysts. For example, Zhang et al. demonstrated that the nanoporous single-crystal-like $Cd_xZn_{1-x}S$ nanosheets with hierarchical structures and adjustable composition can be obtained through a facile cation-exchange strategy of hybrid ZnS–diethylenetriamine nanosheets.[384] The results showed that the $H_2$-evolution rate of porous $Zn_{0.5}Cd_{0.5}S$ nanosheets was about 2.5 times higher than that of $Zn_{0.5}Cd_{0.5}S$

nanorods due to stronger absorption ability of photons, larger active surface area and faster charge transfer and separation. In another example, it was found that the Cu-doped ZnS hollow nano-solid-solution exhibited very high $H_2$-evolution rate under xenon lamp irradiation, which was 6 and 130 times higher than that of pure "ZnS-shell" and co-precipitated ZnS particles, respectively.[368] Importantly, the Cu doping generated high visible-light $H_2$-evolution activity. Similarly, CuS/ZnS porous nanosheet-type photocatalysts were fabricated by a simple hydrothermal and cation exchange reaction between preformed $ZnS(en)_{0.5}$ nanosheets and $Cu(NO_3)_2$ (Figures 38A and 38B).[385] The results showed that the as-prepared CuS (2 mol %)/ZnS porous nanosheets exhibited a high $H_2$-production rate of 4147 mmol$h^{-1}g^{-1}$ (Figures 37C), with a $H_2$-production quantum efficiency of 20% at 420 nm.[385]

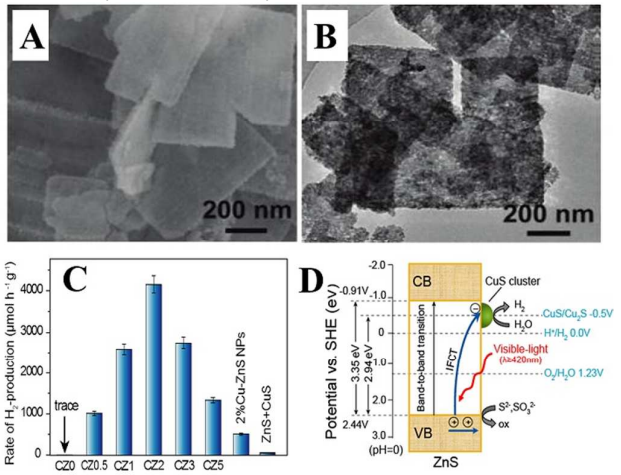


**Figure 38** (A,B) CuS/ZnS porous nanosheet-type photocatalysts fabricated by a hydrothermal and cation exchange method using pre-prepared $ZnS(en)_{0.5}$ nanosheets and $Cu(NO_3)_2$ as precursors. (C) Comparison of visible-light photocatalytic $H_2$-production rate obtained on a CuS/ZnS porous composite nanosheets and ZnS samples using $Na_2S$ and $Na_2SO_3$ as sacrificial solution. The nominal molar ratios of Cu/Zn were 0, 0.5, 1, 2, 3 and 5 mol %, and the obtained samples were labeled as CZ0 (ZnS), CZ0.5, CZ1, CZ2, CZ3 and CZ5, respectively. (D) Visible-light induced interfacial charge transfer (IFCT) mechanism from the valence band of ZnS to the CuS clusters in the CuS/ZnS system for photocatalytic $H_2$-production. Reproduced with permission from ref. 385. Copyright © 2011, American Chemical Society.

The enhanced visible-light $H_2$-evolution activity is closely associated with the synergistic effect of the photoinduced interfacial charge transfer (IFCT) from the valence band of ZnS to CuS, which in addition to the low-cost CuS/$Cu_2S$ cocatalysts is an advantage of these materials (Figures 37D). Furthermore, the Bi-doped ZnS hollow spheres showed greatly enhanced UV and visible-light photocatalytic $H_2$-production activity.[386] It seems that the promoted separation and suppressed recombination rate of photo-generated electron-hole pairs are responsible for a significant enhancement in the photoactivity due to the Bi doping. In addition, various kinds of hierarchical $ZnIn_2S_4$ microspheres[264, 265, 269, 369, 387-389] and heterojunctions[374-376, 390-392] were shown to have an improved light-absorption and charge-separation abilities, thus receiving a wide attention in photocatalytic $H_2$ evolution. For example, Li et al. demonstrated that the carbon quantum dots (CQDs) and Pt co-decorated $ZnIn_2S_4$ microspheres (ZIS MSs) can be fabricated through a facile microwave hydrothermal method followed by chemical reduction deposition (Figure 39a).[269] The resulting composite photocatalysts exhibited a high photocatalytic $H_2$ production rate of 1032.2 mmol$h^{-1}g^{-1}$ with an apparent quantum efficiency of 2.2% (420 nm) in triethanolamine aqueous solution under visible-light irradiation (Figure 39b). It is believed that the significantly improved $H_2$-evolution activity can be attributed to the synergistic effect of high crystallinity, enhanced light harvesting, high electrical conductivity of CQDs, and the vectorial electron transfer. Future efforts should be focused on the further enhancement of the photocatalytic $H_2$-evolution activity of these promising sulfide solid solutions with hierarchical structures through different engineering strategies to narrow their large band gaps by doping, to promote the charge separation by forming heterojunctions and to accelerate the surface reaction kinetics by employing proper co-catalysts.

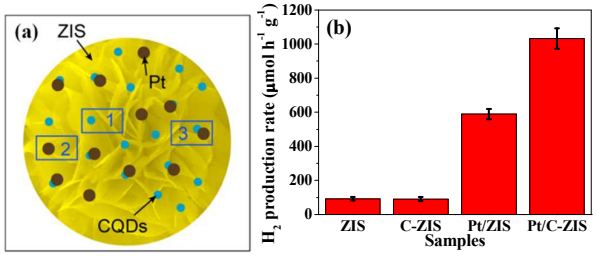


**Figure 39** (a) Possible positions of carbon quantum dots (CQDs) and platinum nanoparticles (NPs) deposited on the surface of $ZnIn_2S_4$ microspheres (ZIS MSs), (b) Comparison of the photocatalytic $H_2$ production activities of the ZIS, CZIS, Pt/ZIS, and Pt/C-ZIS samples in aqueous triethanolamine under visible-light irradiation. Reproduced with permission from ref. 269. Copyright © 2014, Wiley-VCH Verlag GmbH & Co. KGaA, Weinheim..

In addition, the formation of nanostructures composed of nanorod trunks and nanosheet branches has been also extensively achieved.[147, 150, 159, 374, 393, 394] For example, hierarchical brush-like composites of reduced graphene oxide (RGO)–$TiO_2$ nanowire arrays were fabricated via an in-situ controlled growth process and subsequent calcination.[152] It was suggested that the enhanced photocatalytic hydrogen evolution performance originated from the combined effect of the increased surface active sites, improved charge separation and enhanced light utilization efficiency. Recently, hierarchical "forest-like" $TiO_2$ nanofiber/ZnO nanorod/CuO nanoparticles photocatalyst was synthesized by a facile three-step method: electrospinning, hydrothermal and photodeposition (Figure 11).[159] The enhanced light harvesting, increased specific surface area and suppressed recombination of electrons and holes are responsible for much higher photocatalytic hydrogen generation rate. All these kinds of branched 1D or 2D nanojunctions deserve more attention in future studies. In particular, it is expected that more tree-like hierarchical nanostructures will be developed using methods with or without templates.

### 6.3 Photocatalytic $CO_2$ reduction

The depletion of fossil fuels and the increase of atmospheric $CO_2$ level accompanying their combustion have increased interest in the

capture and utilization of the most abundant greenhouse gas $CO_2$. Among various technologies, the photoconversion of $CO_2$ into useful solar fuels is thought to be one of the best solutions because it could not only reduce the atmospheric concentration of $CO_2$ and global warming, but also partly address energy demands and crisis.[1, 395, 396] Therefore, since the first demonstration of photocatalytic $CO_2$ reduction by Inoue and co-workers in 1979,[397] many rapid and significant advancements have been made during last two decades on the development of efficient and feasible photocatalysts for conversion of anthropogenic $CO_2$ into chemical or solar fuels .[1, 16, 395, 396, 398-402] Generally, the $CO_2$ photocatalytic conversion efficiency is determined by the multiple factors including charge transfer/separation efficiency, photostability, $CO_2$ adsorption and visible-light harvesting capacity, surface reaction kinetics and suppressed undesirable reaction.[1, 403-411] Fortunately, the photocatalysts with hierarchical nano/micro architectures usually display large surface area, high $CO_2$ adsorption capacity, mass transport discrepancy, and fast charge transfer and separation, allowing to achieve superior photocatalytic performance of $CO_2$ conversion to energy-bearing carbon fuels.[200] Consequently, an increasing attention has been given to the development of various hierarchical photocatalysts for photocatalytic reduction of $CO_2$.[200, 273, 412-415]

Herein, we will highlight several typical hierarchical structures widely applied in the photocatalytic reduction of $CO_2$, including the 3D hierarchical microspheres, hetero-structured nanocomposites, yolk/shell and hollow structures (see Table 4). Firstly, 3D hierarchical semiconductor microspheres such as $CdIn_2S_4$,[273] $Bi_2S_3$,[416] $Bi_2WO_6$,[200] $TiO_2$,[413] and ZnTe[417] were shown to have superior activity and selectivity toward photodriven $CO_2$ reduction due to their advanced spherical and macro/mesoporous structures. For example, a series of alkaline tantalates $MTaO_3$ (M = Li, Na, K) with hierarchical porosity were synthesized using activated carbonized tree trunks as templates.[418] It is believed that the existence of macroporous network in the tree trunk derived alkaline tantalates results in the enhanced $CO_2$ photoreduction performance, which can significantly improve light harvesting and accelerate gas diffusion. Secondly, the hierarchical hetero-structured photocatalysts[403, 404, 419-422] and nanocarbon-supported semiconductors (such as graphene/CdS nanorods,[405] graphene/$C_3N_4$,[412] graphitic carbon/$TiO_2$,[414, 423-426]) have been also employed to improve $CO_2$ adsorption and promote the charge transfer and separation, thus resulting in the enhancement of activity toward $CO_2$ photoconversion.

**Table 4.** Hierarchical photocatalysts for photocatalytic $CO_2$ reduction

| Material | hierarchical morphology | Synthesis method | Growth mechanism | Cocatalyst | Light source | Mass [g]/systems/Volume [mL] | Selected products (activity) [$\mu Mh^{-1} g^{-1}$] | Ref.(year) |
|---|---|---|---|---|---|---|---|---|
| **Gas-solid systems for $CO_2$ photoreduction** | | | | | | | | |
| Titanate Nanosheets | Yolk@Shell Microspheres | hydrothermal treatment | organic amine mediated anhydrous alcoholysis | | 300W Xe lamp, ≥ 400 nm | 0.1/ $CO_2$ and $H_2O$ vapor /200 mL | $CH_3OH$ (2.1) | [427](2015) |
| 2D $Ti_{0.9}O_2$-Graphene | hollow spheres | microwave irradiation technique | layer-by-layer assembly | | 300 W xenon lamp | 0.01/ $CO_2$ and $H_2O$ vapor /230 mL | CO(8.91), $CH_4$(1.14) | [424](2012) |
| $TiO_2$-Graphene | 2D Sandwich-Like Hybrid Nanosheets | hydrothermal approach | *In-situ* loading of $TiO_2$ nanoparticles | | 300 W xenon lamp | 0.1/ $CO_2$ and $H_2O$ vapor /230 mL | $CH_4$(8), $C_2H_6$(16.8) | [425](2013) |
| $TiO_2$-Graphene | worm-like mesoporous architecture | nanocasting route | | | 300 W xenon lamp | 0.1/ $CO_2$ and $H_2O$ vapor / 1500 mL | CO(10.06), $CH_4$(1.54) | [428](2013) |
| Graphene-g-$C_3N_4$ | sandwich-like nanostructures | impregnation-thermal reduction strategy | | | 15 W daylight bulb | $CO_2$ and $H_2O$ vapor | $CH_4$(0.587) | [412](2015) |
| $SrTiO_3$ | leaf's 3D architecture | sol-gel method/ calcination | Leaves template growth | 1 wt% Au | 300W Xe lamp, ≥ 420 nm | 0.05/ $CO_2$ and $H_2O$ vapor | CO(0.35), $CH_4$(0.23) | [429](2013) |
| $TiO_2$ | microspheres with hierarchical nanostructure | | | | 40 W Hg lamp | 0.2/ $CO_2$ and $H_2O$ vapor /230 mL | CO(2.32),$CH_4$(0.94), $H_2$(2.03) | [413](2014) |
| $NaTaO_3$ | hierarchical porous | | tree trunks as templates | 1 wt% Au | 200 W Hg–Xe lamp | 0.05/$CO_2$ and $H_2O$ vapor / 390 | CO (0.173), $CH_4$ (0.036) | [418](2015) |

| | | | | | | | |
|---|---|---|---|---|---|---|---|
| | anatomy | | | | mL | | |
| $Zn_{1.7}GeN_{1.8}O$ | sheaf-like, hyperbranched | | | 1 wt% Pt and 1 wt% $RuO_2$ | 300 W Xe lamp, > 420 nm | 0.05/$CO_2$ and $H_2O$ vapor / 390 mL | $CH_4$ (0.009) | [430](2012) |
| **Suspension systems for $CO_2$ photoreduction** | | | | | | | | |
| ZnO/ZnTe | hierarchical superstructures | hydrothermal approach | | | 300-W xenon lamp,≥420nm | 0.01/ $CO_2$ saturated water solution/ 80 mL | $CH_4$(44.56) | [431](2015) |
| $Bi_2WO_6$ | hollow microspheres | anion exchange approach | Microscale Kirkendall effect | | 300 W Xe arc lamp, ≥ 420 nm | 0.2/ $CO_2$ saturated water solution/ 100 mL | $CH_3OH$ (16.3) | [200](2012) |
| $Bi_2S_3$ | urchin-like microspheres | template-free solvothermal method | self-assembly of nanorods | | 250 W Hg lamp | 0.1/ $CO_2$saturated methanol solution/ 10 mL | HCHO(175) | [416](2013) |
| ZnTe | Hollow and mesoporous microspheres | hydrothermal approach | nucleation process/Ostwald ripening | | 300-W xenon lamp,>420 nm | 0.01/ $CO_2$ saturated water solution/ 80 mL | $CH_4$ (1.05) | [417](2015) |

Thirdly, the hollow[200, 424, 432] and yolk/shell structures[427] have been fabricated and applied in the photocatalytic reduction of $CO_2$. For example, In et al. reported that the $CH_4$ production rate over hetero-structured CuO-$TiO_{2-x}N_x$ hollow nanocubes was 2.5 times higher than that of Degussa P25 $TiO_2$ under the same experimental conditions, due to the increased absorbance below 500 nm and the formation of p-n junctions.[432] Recently, it was reported that the hierarchical amine-functionalized titanate nanosheets-based yolk@shell microspheres were synthesized via one-pot organic amine mediated anhydrous alcoholysis of titanium(IV) butoxide (Figures 40a-c). The resulting hierarchical amine-functionalized titanate nanosheets-based yolk@shell microspheres displayed highly selective photoreduction of $CO_2$ to dominant $CH_3OH$ under visible-light irradiation (Figure 40d).[427] The enhanced activity can be attributed to the strong visible light absorption, high $CO_2$ adsorption capacity and excellent light-harvesting performance. As a consequence, this study would provide some new ideas for constructing highly efficient and cost-effective $CO_2$ reduction photocatalysts by coupling the adsorptive groups into the semiconductors with multilevel interior structures. The synergistic optimization and integration of light-harvesting centers, charge transportation channels, adsorption centers and the catalytic active centers in one material play a crucial role in achieving highly functional and efficient photocatalysts for $CO_2$ reduction.[427] Recently, Yuan et al. synthesized the core–shell $TiO_2$@insulating $SiO_2$ composites via a simple sol–gel method and applied them in photoreduction of $CO_2$ with water vapor under simulated solar light irradiation.[433] The resulting hierarchical $TiO_2$@$SiO_2$ composites exhibited significantly improved photoactivity and selectivity for CO formation due to the enhanced adsorption capacity of $CO_2$ and better separation of photogenerated charge carriers. Importantly, the $SiO_2$ shell layer can also greatly inhibit the competitive $H_2$ formation on the $TiO_2$ surface. It is anticipated that the activity and selectivity of semiconductors for photoreduction of $CO_2$ to solar fuels could be finely tuned through fabricating the hierarchical silica coating layer. In addition, as can be seen from Table 4 the loading of suitable co-catalyst into hierarchical semiconductors seems to be very promising to further boost the photocatalytic activity and selectivity through improving the reaction pathways and kinetics.

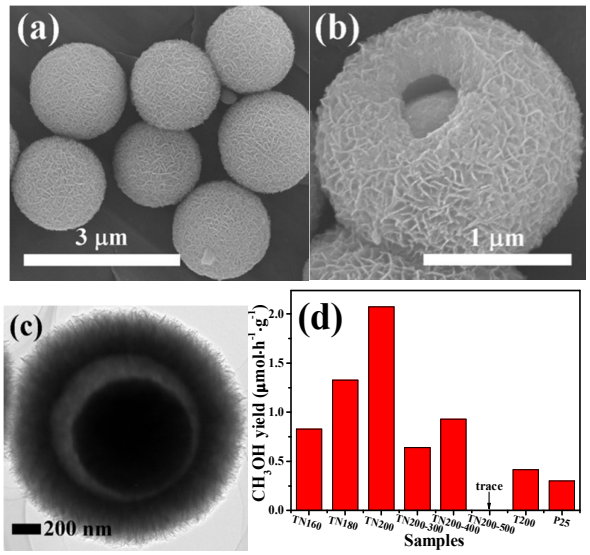


**Figure 40** FESEM (a, b) and TEM (c) of the typical sample TN200 (200 °C, alcohothermal method); (d), comparison of $CH_3OH$ generation rate for various samples. Reproduced with permission from ref. 427. Copyright © 2015, American Chemical Society.

Recently, we reported a highly efficient direct Z-scheme CdS-$WO_3$ photocatalyst by depositing CdS nanoparticles on the surface of hierarchical $WO_3$ hollow spheres used for photocatalytic $CO_2$ reduction under visible light (λ ≥ 420 nm) irradiation.[434] (see Figure 41) The prepared direct Z-scheme heterostructured CdS-$WO_3$

samples showed higher photocatalytic selectivity to $CH_4$ formation (see Figure 42a) and photocatalytic $CO_2$ reduction activity than single-phase CdS or $WO_3$ photocatalysts. The optimized 5 mol% CdS-hierarchical $WO_3$ heterostructured sample showed the highest $CH_4$ production rate of 1.02 μmol $h^{-1}$ $g^{-1}$ (see Figure 42b), exceeding the rates of $WO_3$ and CdS samples for about 100 and 10 times, respectively. The enhanced photocatalytic activity can be attributed to the Z-scheme mechanism of photocatalytic $CO_2$ reduction, which can be supported by hydroxyl radical experiments and photocurrent response analysis results. As a consequence, the as-prepared CdS-$WO_3$ hierarchical Z-scheme photocatalysts exhibit significantly enhanced activity for selective reduction of $CO_2$ to $CH_4$, due to the improved space separation of photogenerated electrons and holes. In future, more extensive efforts are needed to focus on the promising application of hierarchical Z-scheme heterostructured photocatalysts in selective photocatalytic reduction of $CO_2$. This study also highlights that the photocatalytic enhancement mechanism for $CO_2$ reduction over hierarchical photocatalysts deserves more attention.

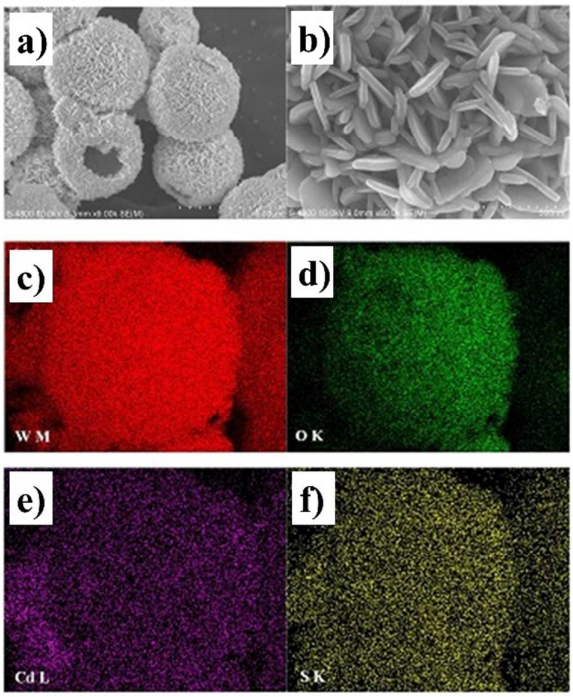


**Figure 41** SEM (a) and high-magnification SEM mages (b) of hierarchical $WO_3$ hollow spheres: EDS elemental mapping of W (c), O (d), Cd (e), and S (f) of the 5 mol% CdS-$WO_3$ sample. Reproduced with permission from ref. 434. Copyright © 2015, Wiley-VCH Verlag GmbH & Co. KGaA, Weinheim.

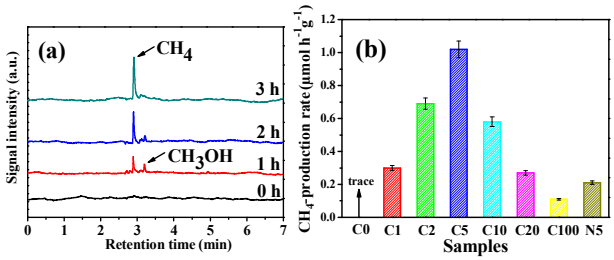


**Figure 42** (a) GC spectra of $CO_2$ reduction on the 5 mol%CdS-$WO_3$ sample at different irradiation time, (b) Comparison of the photocatalytic $CH_4$ production rate of $C_x$ ($x$=0, 1, 2, 5, 10, 20, and 100, the nominal molar ratios of CdS to ($WO_3$+CdS)), and CdS-$WO_3$ nanoparticle composite (N5) samples under visible light irradiation. Reproduced with permission from ref. 434. Copyright © 2015, Wiley-VCH Verlag GmbH & Co. KGaA, Weinheim.

## 7. Conclusions and perspectives

Although hierarchical nanostructures have been widely investigated in different fields of photocatalysis owing to their unique properties such as increased light harvesting, charge separation, mass transport and adsorption capacity, many challenges still remain in fabricating these hierarchical photocatalysts through simple and facile synthesis strategies and in better understanding their photocatalytic enhancement mechanisms. First, this review presents a systematic discussion of the thermodynamics and kinetics of heterogeneous photocatalysis, then thoroughly summarizes the design, controllable synthesis, growth mechanism and various applications of hierarchical photocatalytic nanostructures. In each section, some important achievements and typical examples coming from our group and other research teams are included and discussed.

Among various types of hierarchical nanostructured photocatalysts, the hierarchical nanostructures based on multi-dimensional hybridization of building blocks are very interesting, and deserve more attention in future. Especially, some novel hierarchical structures constructed through 2D nanosheets with exposed facets seem to be more suitable for the enhancement photocatalytic performance due to the ultrathin 2D structures and exposed high-energy facets.[149, 211] In addition, the specially designed porous mesocrystals and photonic crystal structures also hold a great potential in photocatalysis because they have been shown to exhibit high photocatalytic activity. In future, the development of mesocrystals and photonic crystal structures through simple and facile methods may open an exciting avenue to accelerate their applications in heterogeneous photocatalysis.

Although a variety of synthesis methods has been developed, it is still challenging to perform a large-scale, high-yield synthesis of hierarchical semiconductors through the biotemplating and template-free self-assembly strategies. The hierarchical structures in nature are earth-abundant, cost-effective, efficient and robust, and nature provide numerous excellent bio-templates for rational designing nature-inspired hierarchical photocatalytic nanomaterials. In future, the template-free synthesis of these high-activity photocatalysts with hierarchical porous structures and high surface areas would be desirable. Furthermore, the insufficient number of biotemplates and inadequate understanding the template-free self-assembly render the rational design of hierarchical semiconductors in desired ways and the further optimization of photocatalytic performance, which should be solved urgently in future. In this regard, more attention should be paid to the better understanding of the fundamental principles and theories of the assembly, growth, and processing of nanostructured building blocks, which is beneficial for rational controlling and designing the hierarchical photocatalysts with the multifunctional coupling. Also, there are limited reports on the functional modification of hierarchical

nanostructures. Thus, different modification strategies such as doping, forming hetero-junctions and the loading of suitable co-catalyst should be widely investigated. Especially, it is expected that the spatially separated dual co-catalysts,[2] earth-abundant metal-based (such as NiS[435] and $MoS_2$[2]) and metal-free co-catalysts (such as graphene[436] and carbon quantum dots[35]) could be loaded to the hierarchical photocatalysts to further enhance their photocatalytic performance.

It has been demonstrated that the hierarchically porous materials still hold great promise in different photocatalytic applications and may offer some exciting opportunities to construct highly efficient and stable photocatalysts. In future, it is expected that more and more non-$TiO_2$ hierarchically structured visible-light photocatalysts will be exploited and applied in various photocatalytic processes. This article shows only some typical examples of their applications in different areas of photocatalysis. There are very few reports on the applications of hierarchically structured semiconductors in $CO_2$ photoreduction and photocatalytic organic synthesis. Therefore, it is highly expected that the inexpensive hierarchically structured semiconductors with high activity will be explored and applied in photocatalytic $CO_2$ reduction and organic synthesis[145, 151, 437]. More importantly, the fundamentals of hierarchical photocatalysts, such as the effects of hierarchical nanostructures on the formation of active species (such as •OH radicals, $O_2^-$ and $H_2O_2$) and selectivity of $CO_2$ photoreduction, should be deeply investigated, which will further promote the rational design and wide applications of these multifunctional materials.

Furthermore, these hierarchically micro-meso-macrostructured photocatalysts also have great potential applications in thermal catalysis,[136, 243] adsorption separation,[133, 134, 438-441] electrochemical supercapacitors,[442] electrocatalysts,[443, 444] solar cells,[445] and purification processes. Especially, these hierarchical photocatalysts could also be used to fabricate functional inorganic membranes,[445] and be employed as a templating materials to explore new advanced materials.

In addition, the rational design and photocatalytic applications of more environmentally friendly and "green" hierarchical semiconductors are still highly expected. More efforts should be undertaken toward detailed study of hierarchical structure/function relationships and the mechanism of photocatalytic processes based on photo-generated charge transfer and separation kinetics. We hope that the present review will stimulate scientific interest in the controllable synthesis and modification of hierarchical nanostructures, as well as in their advanced environmental and energy-related applications.

## Acknowledgements

J. Yu would like to thank the 973 Program (Grant No. 2013CB632402), NSFC (21433007, 51320105001, 51372190, and 51272199), the Deanship of Scientific Research of King Abdulaziz University (No. 90-130-35-HiCi), Fundamental Research Funds for the Central Universities (WUT: 2015-III-034), Self-determined and Innovative Research Funds of SKLWUT (2015-ZD-1) and the Natural Science Foundation of Hubei Province of China (No. 2015CFA001). X. Li would like to thank Industry and Research Collaborative Innovation Major Projects of Guangzhou (201508020098), NSFC (20906034) and the State Key Laboratory of Advanced Technology for Material Synthesis and Processing (Wuhan University of Technology) (2015-KF-7) for their support.

## Notes and references

1. X. Li, J. Wen, J. Low, Y. Fang and J. Yu, *Science China Materials*, 2014, 57, 70–100.
2. X. Li, J. Yu, J. Low, Y. Fang, J. Xiao and X. Chen, *J. Mater. Chem. A*, 2015, 3, 2485-2534.
3. A. Bard and M. Fox, *Accounts. Chem. Res.*, 1995, 28, 141-145.
4. M. Hoffmann, S. Martin, W. Choi and D. Bahnemann, *Chem. Rev.*, 1995, 95, 69-96.
5. A. Kudo and Y. Miseki, *Chem. Soc. Rev.*, 2009, 38, 253-278.
6. X. Chen, S. Shen, L. Guo and S. S. Mao, *Chem. Rev.*, 2010, 110, 6503-6570.
7. X. Lang, X. Chen and J. Zhao, *Chem. Soc. Rev.*, 2014, 43, 473-486.
8. A. Fujishima and K. Honda, *Nature*, 1972, 238, 37-38.
9. K. Rajeshwar, *J. Appl. Electrochem.*, 2007, 37, 765-787.
10. K. Maeda, *J. Photoch. Photobio. C*, 2011, 12, 237-268.
11. T. Hisatomi, J. Kubota and K. Domen, *Chem. Soc. Rev.*, 2014, 43, 7520-7535.
12. Y. Moriya, T. Takata and K. Domen, *Coordin. Chem. Rev.*, 2013, 257, 1957-1969.
13. M. Pelaez, N. T. Nolan, S. C. Pillai, M. K. Seery, P. Falaras, A. G. Kontos, P. S. M. Dunlop, J. W. J. Hamilton, J. A. Byrne, K. O'Shea, M. H. Entezari and D. D. Dionysiou, *Appl. Catal. B-Environ.*, 2012, 125, 331-349.
14. A. Di Paola, E. Garcia-Lopez, G. Marci and L. Palmisano, *J. Hazard. Mater.*, 2012, 211, 3-29.
15. H. Zhang, G. Chen and D. W. Bahnemann, *J. Mater. Chem.*, 2009, 19, 5089-5121.
16. S. N. Habisreutinger, L. Schmidt-Mende and J. K. Stolarczyk, *Angewandte Chemie International Edition*, 2013, 52, 7372-7408.
17. K. Maeda and K. Domen, *J. Phys. Chem. C*, 2007, 111, 7851-7861.
18. A. Kudo, K. Ueda, H. Kato and I. Mikami, *Catal. Lett.*, 1998, 53, 229-230.
19. J. Wu, F. Duan, Y. Zheng and Y. Xie, *J. Phys. Chem. C*, 2007, 111, 12866-12871.
20. S. Zhu, T. Xu, H. Fu, J. Zhao and Y. Zhu, *Environ. Sci. Technol.*, 2007, 41, 6234-6239.
21. K. Zhang and L. Guo, *Catal. Sci. Technol.*, 2013, 3, 1672-1690.
22. N. Bao, L. Shen, T. Takata and K. Domen, *Chem. Mater.*, 2007, 20, 110-117.
23. H. Yan, J. Yang, G. Ma, G. Wu, X. Zong, Z. Lei, J. Shi and C. Li, *J. Catal.*, 2009, 266, 165-168.
24. M. Liu, D. Jing, Z. Zhou and L. Guo, *Nat. Commun.*, 2013, 4, 2278.
25. J. Yuan, J. Wen, Q. Gao, S. Chen, J. Li, X. Li and Y. Fang, *Dalton Trans.*, 2015, 44, 1680-1689.
26. Q. Li, X. Li, S. Wageh, A. A. Al-Ghamdi and J. Yu, *Adv. Energy Mater.*, 2015, 5, 1500010.
27. G. Hitoki, A. Ishikawa, T. Takata, J. N. Kondo, M. Hara and K. Domen, *Chem. Lett.*, 2002, 31, 736-737.
28. G. Hitoki, T. Takata, J. N. Kondo, M. Hara, H. Kobayashi and K. Domen, *Chem. Commun.*, 2002, 38, 1698-1699.

29. K. Maeda, T. Takata, M. Hara, N. Saito, Y. Inoue, H. Kobayashi and K. Domen, *J. Am. Chem. Soc.*, 2005, 127, 8286-8287.
30. K. Maeda, K. Teramura, D. Lu, T. Takata, N. Saito, Y. Inoue and K. Domen, *Nature*, 2006, 440, 295-295.
31. S. Cao, J. Low, J. Yu and M. Jaroniec, *Adv. Mater.*, 2015, 27, 2150-2176.
32. J. Sun, J. Zhang, M. Zhang, M. Antonietti, X. Fu and X. Wang, *Nat. Commun.*, 2012, 3, 1139.
33. X. Wang, K. Maeda, A. Thomas, K. Takanabe, G. Xin, J. Carlsson, K. Domen and M. Antonietti, *Nat. Mater.*, 2009, 8, 76-80.
34. X. Zhou, X. Li, Q. Gao, J. Yuan, J. Wen, Y. Fang, W. Liu, S. Zhang and Y. Liu, *Catal. Sci. Technol.*, 2015, 5, 2798-2806.
35. J. Liu, Y. Liu, N. Liu, Y. Han, X. Zhang, H. Huang, Y. Lifshitz, S.-T. Lee, J. Zhong and Z. Kang, *Science*, 2015, 347, 970-974.
36. X. Zhou, Q. Gao, X. Li, Y. Liu, S. Zhang, Y. Fang and J. Li, *J. Mater. Chem. A*, 2015, 3, 10999-11005.
37. Y. Sun, Z. Zhao, F. Dong and W. Zhang, *Phys. Chem. Chem. Phys.*, 2015, 17, 10383-10390.
38. X. Zhou, G. Liu, J. Yu and W. Fan, *J. Mater. Chem.*, 2012, 22, 21337-21354.
39. F. Wang, C. Li, H. Chen, R. Jiang, L.-D. Sun, Q. Li, J. Wang, J. C. Yu and C.-H. Yan, *J. Am. Chem. Soc.*, 2013, 135, 5588-5601.
40. J. Low, J. Yu, Q. Li and B. Cheng, *Phys. Chem. Chem. Phys.*, 2014, 16, 1111-1120.
41. Q. Zhang, Y. Zhou, F. Wang, F. Dong, W. Li, H. Li and G. R. Patzke, *J. Mater. Chem. A*, 2014, 2, 11065-11072.
42. F. Dong, T. Xiong, Y. Sun, Z. Zhao, Y. Zhou, X. Feng and Z. Wu, *Chem. Commun.*, 2014, 50, 10386-10389.
43. B. X. Li, T. Gu, T. Ming, J. X. Wang, P. Wang, J. F. Wang and J. C. Yu, *Acs Nano*, 2014, 8, 8152-8162.
44. W. Wang, J. C. Yu, D. Xia, P. K. Wong and Y. Li, *Environ. Sci. Technol.*, 2013, 47, 8724-8732.
45. D. Xia, Z. Shen, G. Huang, W. Wang, J. C. Yu and P. K. Wong, *Environ. Sci. Technol.*, 2015, 49, 6264-6273.
46. F. Wang, W. K. H. Ng, J. C. Yu, H. Zhu, C. Li, L. Zhang, Z. Liu and Q. Li, *Appl. Catal. B-Environ.*, 2012, 111, 409-414.
47. G. Liu, P. Niu, L. Yin and H.-M. Cheng, *J. Am. Chem. Soc.*, 2012, 134, 9070-9073.
48. G. Liu, P. Niu and H.-M. Cheng, *Chemphyschem*, 2013, 14, 885-892.
49. P. Zhou, J. Yu and M. Jaroniec, *Adv. Mater.*, 2014, 26, 4920-4935.
50. A. J. Bard, *J. Phys. Chem.*, 1982, 86, 172-177.
51. D. Zhang, G. Li, H. Li and Y. Lu, *Chem-Asian. J.*, 2013, 8, 26-40.
52. J. Ran, J. Zhang, J. Yu, M. Jaroniec and S. Z. Qiao, *Chem. Soc. Rev.*, 2014, 43, 7787-7812.
53. Q. Xiang and J. Yu, *J. Phys. Chem. Lett.*, 2013, 4, 753-759.
54. Q. Xiang, B. Cheng and J. Yu, *Angewandte Chemie International Edition*, 2015, 54, 11350-11366.
55. Q. J. Xiang, J. G. Yu and M. Jaroniec, *Chem. Soc. Rev.*, 2012, 41, 782-796.
56. Y.-P. Yuan, L.-W. Ruan, J. Barber, S. C. Joachim Loo and C. Xue, *Energy Environ. Sci.*, 2014, 7, 3934-3951.
57. F. E. Osterloh, *Chem. Soc. Rev.*, 2013, 42, 2294-2320.
58. M. Cargnello and B. T. Diroll, *Nanoscale*, 2014, 6, 97-105.
59. H. Wang, L. Zhang, Z. Chen, J. Hu, S. Li, Z. Wang, J. Liu and X. Wang, *Chem. Soc. Rev.*, 2014, 43, 5234-5244.
60. P. Yang, T. Deng, D. Zhao, P. Feng, D. Pine, B. F. Chmelka, G. M. Whitesides and G. D. Stucky, *Science*, 1998, 282, 2244-2246.
61. J. G. Yu, J. C. Yu, L. Z. Zhang, X. C. Wang and L. Wu, *Chem. Commun.*, 2004, 40, 2414-2415.
62. L. Z. Zhang and J. C. Yu, *Chem. Commun.*, 2003, 39, 2078-2079.
63. G. J. D. Soler-illia, C. Sanchez, B. Lebeau and J. Patarin, *Chem. Rev.*, 2002, 102, 4093-4138.
64. H.-B. Yao, H.-Y. Fang, X.-H. Wang and S.-H. Yu, *Chem. Soc. Rev.*, 2011, 40, 3764-3785.
65. X. Du and J. He, *Nanoscale*, 2011, 3, 3984-4002.
66. X.-Y. Yang, Y. Li, A. Lemaire, J.-G. Yu and B.-L. Su, *Pure. Appl. Chem.*, 2009, 81, 2265-2307.
67. M.-Q. Zhao, Q. Zhang, J.-Q. Huang and F. Wei, *Adv. Funct. Mater.*, 2012, 22, 675-694.
68. J. Yu, L. Zhang, B. Cheng and Y. Su, *J. Phys. Chem. C*, 2007, 111, 10582-10589.
69. Y. Li, Z.-Y. Fu and B.-L. Su, *Adv. Funct. Mater.*, 2012, 22, 4634-4667.
70. C. M. A. Parlett, K. Wilson and A. F. Lee, *Chem. Soc. Rev.*, 2013, 42, 3876-3893.
71. N. D. Petkovich and A. Stein, *Chem. Soc. Rev.*, 2013, 42, 3721-3739.
72. H. Wang and A. L. Rogach, *Chem. Mater.*, 2013, 26, 123-133.
73. P. S. Kumar, J. Sundaramurthy, S. Sundarrajan, V. J. Babu, G. Singh, S. I. Allakhverdiev and S. Ramakrishna, *Energy Environ. Sci.*, 2014, 7, 3192-3222.
74. J. Wen, X. Li, W. Liu, Y. Fang, J. Xie and Y. Xu, *Chinese. J. Catal.*, 2015, 36, 2049-2070.
75. H.-Y. Chen, Y.-F. Xu, D.-B. Kuang and C.-Y. Su, *Energy Environ. Sci.*, 2014, 7, 3887-3901.
76. A. J. Bard, *Science*, 1980, 207, 139-144.
77. A. Linsebigler, G. Lu and J. Yates Jr, *Chem. Rev.*, 1995, 95, 735-758.
78. P. M. Wood, *Biochem. J.*, 1988, 253, 287-289.
79. C. Chen, W. Ma and J. Zhao, *Chem. Soc. Rev.*, 2010, 39, 4206-4219.
80. R. Abe, H. Takami, N. Murakami and B. Ohtani, *J. Am. Chem. Soc.*, 2008, 130, 7780-+.
81. A. Fujishima, T. Rao and D. Tryk, *Journal of Photochemistry and Photobiology C: Photochemistry Reviews*, 2000, 1, 1-21.
82. T. Hirakawa and Y. Nosaka, *Langmuir*, 2002, 18, 3247-3254.
83. H. Park, Y. Park, W. Kim and W. Choi, *J. Photoch. Photobio. C*, 2013, 15, 1-20.
84. H. Tada, Q. Jin, A. Iwaszuk and M. Nolan, *J. Phys. Chem. C*, 2014, 118, 12077-12086.
85. Y. Zhong, J. Yuan, J. Wen, X. Li, Y. Xu, W. Liu, S. Zhang and Y. Fang, *Dalton Trans.*, 2015, 44, 18260-18269.
86. J. Wen, X. Li, H. Li, S. Ma, K. He, Y. Xu, Y. Fang, W. Liu and Q. Gao, *Appl. Surf. Sci.*, 2015, 358, 204-212.
87. J. Jiang, J. Yu and S. Cao, *J. Colloid. Interf. Sci.*, 2016, 461, 56-63.
88. M. S. Akple, J. Low, S. Wageh, A. A. Al-Ghamdi, J. Yu and J. Zhang, *Appl. Surf. Sci.*, 2015, 358, 196-203.
89. S. Liang, Y. Xia, S. Zhu, S. Zheng, Y. He, J. Bi, M. Liu and L. Wu, *Appl. Surf. Sci.*, 2015, 358, 304-312.
90. K. Wu, Z. Chen, H. Lv, H. Zhu, C. L. Hill and T. Lian, *J. Am. Chem. Soc.*, 2014, 136, 7708-7716.

91. G. Liu, J. Shi, F. Zhang, Z. Chen, J. Han, C. Ding, S. Chen, Z. Wang, H. Han and C. Li, *Angew. Chem. Int. Edit.*, 2014, 53, 7295-7299.
92. E. Pastor, F. M. Pesci, A. Reynal, A. D. Handoko, M. Guo, X. An, A. J. Cowan, D. R. Klug, J. R. Durrant and J. Tang, *Phys. Chem. Chem. Phys.*, 2014, 16, 5922-5926.
93. G. Liu, T. Wang, H. Zhang, X. Meng, D. Hao, K. Chang, P. Li, T. Kako and J. Ye, *Angew. Chem. Int. Edit.*, 2015, 54, 13561-13565.
94. H. Tong, S. X. Ouyang, Y. P. Bi, N. Umezawa, M. Oshikiri and J. H. Ye, *Adv. Mater.*, 2012, 24, 229-251.
95. R. Asahi, T. Morikawa, T. Ohwaki, K. Aoki and Y. Taga, *Science*, 2001, 293, 269-271.
96. H. J. Queisser and E. E. Haller, *Science*, 1998, 281, 945-950.
97. A. J. Bard, R. Parsons and J. Jordan, *Standard potentials in aqueous solution*, CRC press, 1985.
98. S. Pasternak and Y. Paz, *Chemphyschem*, 2013, 14, 2059-2070.
99. J. H. Pan, X. Zhang, A. J. Du, D. D. Sun and J. O. Leckie, *J. Am. Chem. Soc.*, 2008, 130, 11256-+.
100. H. X. Li, Z. F. Bian, J. Zhu, D. Q. Zhang, G. S. Li, Y. N. Huo, H. Li and Y. F. Lu, *J. Am. Chem. Soc.*, 2007, 129, 8406-8407.
101. C. Anderson and A. J. Bard, *J. Phys. Chem. B*, 1997, 101, 2611-2616.
102. J. Yang, D. Wang, H. Han and C. Li, *Accounts. Chem. Res.*, 2013, 46, 1900-1909.
103. G. Rothenberger, J. Moser, M. Graetzel, N. Serpone and D. K. Sharma, *J. Am. Chem. Soc.*, 1985, 107, 8054-8059.
104. A. P. Alivisatos, *Science*, 1996, 271, 933-937.
105. X. Hu, J. C. Yu, J. Gong and Q. Li, *Cryst. Growth. Des.*, 2007, 7, 2444-2448.
106. W. Ho, J. C. Yu and S. Lee, *Chem. Commun.*, 2006, 42, 1115-1117.
107. K. Sing, D. Everett, R. Haul, L. Moscou, R. Pierotti, J. Rouquerol and T. Siemieniewska, *Pure Appl. Chem*, 1985, 57, 603-619.
108. D. R. Rolison, *Science*, 2003, 299, 1698-1701.
109. W. Zhou and H. Fu, *Chemcatchem*, 2013, 5, 885-894.
110. G. Li, D. Zhang and J. C. Yu, *Chem. Mater.*, 2008, 20, 3983-3992.
111. J. Du, X. Lai, N. Yang, J. Zhai, D. Kisailus, F. Su, D. Wang and L. Jiang, *Acs Nano*, 2011, 5, 590-596.
112. X. C. Wang, J. C. Yu, C. M. Ho, Y. D. Hou and X. Z. Fu, *Langmuir*, 2005, 21, 2552-2559.
113. G. C. Xi and J. H. Ye, *Chem-Eur. J.*, 2010, 16, 8719-8725.
114. J. Yu, Y. Su and B. Cheng, *Adv. Funct. Mater.*, 2007, 17, 1984-1990.
115. Z. Y. Yuan, T. Z. Ren and B. L. Su, *Adv. Mater.*, 2003, 15, 1462-1465.
116. J. C. Yu, X. C. Wang and X. Z. Fu, *Chem. Mater.*, 2004, 16, 1523-1530.
117. C. Pelekani and V. L. Snoeyink, *carbon*, 2000, 38, 1423-1436.
118. J. Yu, H. Yu, H. Guo, M. Li and S. Mann, *Small*, 2008, 4, 87-91.
119. T. Xiong, F. Dong and Z. Wu, *Rsc. Adv.*, 2014, 4, 56307-56312.
120. S. Luo, F. Chai, L. Zhang, C. Wang, L. Li, X. Liu and Z. Su, *J. Mater. Chem.*, 2012, 22, 4832-4836.
121. R. Edla, N. Patel, M. Orlandi, N. Bazzanella, V. Bello, C. Maurizio, G. Mattei, P. Mazzoldi and A. Miotello, *Appl. Catal. B-Environ.*, 2015, 166, 475-484.
122. D. Barpuzary, Z. Khan, N. Vinothkumar, M. De and M. Qureshi, *J. Phys. Chem. C*, 2012, 116, 150-156.
123. Y. Zhao, X. Zhang, J. Zhai, J. He, L. Jiang, Z. Liu, S. Nishimoto, T. Murakami, A. Fujishima and D. Zhu, *Appl. Catal. B-Environ.*, 2008, 83, 24-29.
124. W.-R. Wei, M.-L. Tsai, S.-T. Ho, S.-H. Tai, C.-R. Ho, S.-H. Tsai, C.-W. Liu, R.-J. Chung and J.-H. He, *Nano Lett.*, 2013, 13, 3658-3663.
125. L. Zhang, W. Wang, L. Zhou and H. Xu, *Small*, 2007, 3, 1618-1625.
126. X. Li, X. Chen and Z. Li, *J. Chem. Eng. Data.*, 2010, 55, 3164-3169.
127. X. Li, Z. Li, Q. Xia and H. Xi, *Appl. Therm. Eng.*, 2007, 27, 869-876.
128. X. Li, Z. Li, Q. Xia, H. Xi and Z. Zhao, *Adsorpt. Sci. Technol.*, 2006, 24, 363-374.
129. X. Li and Z. Li, *J. Chem. Eng. Data.*, 2010, 55, 5729-5732.
130. J. Gorka and M. Jaroniec, *carbon*, 2011, 49, 154-160.
131. N. P. Wickramaratne and M. Jaroniec, *carbon*, 2013, 51, 45-51.
132. J. Choma, J. Gorka, M. Jaroniec and A. Zawislak, *Top. Catal.*, 2010, 53, 283-290.
133. B. Cheng, Y. Le, W. Cai and J. Yu, *J. Hazard. Mater.*, 2011, 185, 889-897.
134. W. Q. Cai, Y. Z. Hu, J. G. Yu, W. G. Wang, J. B. Zhou and M. Jaroniec, *Rsc. Adv.*, 2015, 5, 7066-7073.
135. W. Cai, J. Yu and M. Jaroniec, *J. Mater. Chem.*, 2010, 20, 4587-4594.
136. L. Nie, A. Meng, J. Yu and M. Jaroniec, *Sci. Rep-Uk.*, 2013, 3, 3215.
137. Z. Xu, J. Yu and M. Jaroniec, *Appl. Catal. B-Environ.*, 2015, 163, 306-312.
138. X. Yu, J. Yu, B. Cheng and M. Jaroniec, *J. Phys. Chem. C*, 2009, 113, 17527-17535.
139. F. Dong, X. Feng, Y. Zhang, C. Gao and Z. Wu, *Rsc. Adv.*, 2015, 5, 11714-11723.
140. X. Zhang, G. Ji, Y. Liu, X. Zhou, Y. Zhu, D. Shi, P. Zhang, X. Cao and B. Wang, *Phys. Chem. Chem. Phys.*, 2015, 17, 8078-8086.
141. K. Ji, J. Deng, H. Zang, J. Han, H. Arandiyan and H. Dai, *Appl. Catal. B-Environ.*, 2015, 165, 285-295.
142. M. Deo, D. Shinde, A. Yengantiwar, J. Jog, B. Hannoyer, X. Sauvage, M. More and S. Ogale, *J. Mater. Chem.*, 2012, 22, 17055-17062.
143. F. Wu, W. Liu, J. Qiu, J. Li, W. Zhou, Y. Fang, S. Zhang and X. Li, *Appl. Surf. Sci.*, 2015, 358, 425-435.
144. C. Cheng and H. J. Fan, *Nano Today*, 2012, 7, 327-343.
145. S. Liu, M.-Q. Yang, Z.-R. Tang and Y.-J. Xu, *Nanoscale*, 2014, 6, 7193-7198.
146. F.-X. Xiao, S.-F. Hung, H. B. Tao, J. Miao, H. B. Yang and B. Liu, *Nanoscale*, 2014, 6, 14950-14961.
147. Y. Zhao, W. Wang, Y. Li, Y. Zhang, Z. Yan and Z. Huo, *Nanoscale*, 2014, 6, 195-198.
148. Y. Jiao, Y. Liu, F. Qu and X. Wu, *Crystengcomm.*, 2014, 16, 575-580.
149. Q. Xiang, J. Yu and M. Jaroniec, *Chem. Commun.*, 2011, 47, 4532-4534.
150. T. J. Athauda, J. G. Neff, L. Sutherlin, U. Butt and R. R. Ozer, *Acs Appl. Mater. Inter.*, 2012, 4, 6916-6925.
151. C. Han, Z. Chen, N. Zhang, J. C. Colmenares and Y.-J. Xu, *Adv. Funct. Mater.*, 2015, 25, 221-229.
152. X. Cao, G. Tian, Y. Chen, J. Zhou, W. Zhou, C. Tian and H.

Fu, *J. Mater. Chem. A*, 2014, 2, 4366-4374.
153. R. Wang, J. Guo, D. Chen, Y.-E. Miao, J. Pan, W. W. Tjiu and T. Liu, *J. Mater. Chem.*, 2011, 21, 19375-19380.
154. J. Hou, Y. Qu, D. Krsmanovic, C. Ducati, D. Eder and R. V. Kumar, *J. Mater. Chem.*, 2010, 20, 2418-2423.
155. M. Wang, Y. Shi, Y. Tang and G. Jiang, *Mater. Lett.*, 2014, 132, 236-239.
156. H. Guo, X.-Y. Lu, Y. Pei, H. Chua, B. Wang, K. Wang, Y. Yang and Y. Liu, *Rsc. Adv.*, 2014, 4, 37431-37436.
157. Y. Qiu and X. Li, *Dalton Trans.*, 2014, 43, 14537-14541.
158. T.-W. Sun, Y.-J. Zhu, C. Qi, G.-J. Ding, F. Chen and J. Wu, *J. Colloid. Interf. Sci.*, 2016, 463, 107-117.
159. H. Bai, Z. Liu and D. D. Sun, *Int. J. Hydrogen. Energ.*, 2012, 37, 13998-14008.
160. H. Chen, S. Chen, X. Quan and Y. Zhang, *Environ. Sci. Technol.*, 2009, 44, 451-455.
161. X. F. Li, X. Z. Zhen, S. G. Meng, J. J. Xian, Y. Shao, X. Z. Fu and D. Z. Li, *Environ. Sci. Technol.*, 2013, 47, 9911-9917.
162. Y. Lu, H. Yu, S. Chen, X. Quan and H. Zhao, *Environ. Sci. Technol.*, 2012, 46, 1724-1730.
163. Z. Y. Cai, Z. G. Xiong, X. M. Lu and J. H. Teng, *J. Mater. Chem. A*, 2014, 2, 545-553.
164. T. Huo, X. Zhang, x. dong, X. Zhang, C. Ma, G. Wang, H. Ma and m. xue, *J. Mater. Chem. A*, 2014, 2, 17366-17370.
165. S. G. Meng, D. Z. Li, X. Z. Zheng, J. X. Wang, J. Chen, J. L. Fang, Y. Shao and X. Z. Fu, *J. Mater. Chem. A*, 2013, 1, 2744-2747.
166. Q. Yang, M. Li, J. Liu, W. Shen, C. Ye, X. Shi, L. Jiang and Y. Song, *J. Mater. Chem. A*, 2013, 1, 541-547.
167. X. Z. Zheng, S. G. Meng, J. Chen, J. X. Wang, J. J. Xian, Y. Shao, X. Z. Fu and D. Z. Li, *J. Phys. Chem. C*, 2013, 117, 21263-21273.
168. S. G. Meng, D. Z. Li, P. Wang, X. Z. Zheng, J. X. Wang, J. Chen, J. L. Fang and X. Z. Fu, *Rsc. Adv.*, 2013, 3, 17021-17028.
169. X. Li, X. Zhang, X. Zheng, Y. Shao, M. He, P. Wang, X. Fu and D. Li, *J. Mater. Chem. A*, 2014, 2, 15796-15802.
170. Y. Liu, J. Goebl and Y. Yin, *Chem. Soc. Rev.*, 2013, 42, 2610-2653.
171. F. Iskandar, A. B. D. Nandiyanto, K. M. Yun, C. J. Hogan, Jr., K. Okuyama and P. Biswas, *Adv. Mater.*, 2007, 19, 1408-1412.
172. D. Gu and F. Schuth, *Chem. Soc. Rev.*, 2014, 43, 313-344.
173. X. Li, X. Liu, Y. Ma, M. Li, J. Zhao, H. Xin, L. Zhang, Y. Yang, C. Li and Q. Yang, *Adv. Mater.*, 2012, 24, 1424-1428.
174. Z. Liu, H. Bai and D. Sun, *Appl. Catal. B-Environ.*, 2011, 104, 234-238.
175. S. Dilger, M. Wessig, M. R. Wagner, J. S. Reparaz, C. M. S. Torres, Q. Liang, T. Dekorsy and S. Polarz, *Cryst. Growth. Des.*, 2014, 14, 4593-4601.
176. J. Yu, W. Liu and H. Yu, *Cryst. Growth. Des.*, 2008, 8, 930-934.
177. J. Di, J. Xia, Y. Ge, L. Xu, H. Xu, M. He, Q. Zhang and H. Li, *J. Mater. Chem. A*, 2014, 2, 15864-15874.
178. C. Zhou, Y. Zhao, T. Bian, L. Shang, H. Yu, L.-Z. Wu, C.-H. Tung and T. Zhang, *Chem. Commun.*, 2013, 49, 9872-9874.
179. J. L. Pagano, T. Bansagi, Jr. and O. Steinbock, *Angew. Chem. Int. Edit.*, 2008, 47, 9900-9903.
180. J. Sun, G. Chen, J. Wu, H. Dong and G. Xiong, *Appl. Catal. B-Environ.*, 2013, 132, 304-314.
181. X. W. Lou, L. A. Archer and Z. Yang, *Adv. Mater.*, 2008, 20, 3987-4019.
182. H. Yan, *Chem. Commun.*, 2012, 48, 3430-3432.
183. J. Xia, L. Xu, J. Zhang, S. Yin, H. Li, H. Xu and J. Di, *Crystengcomm.*, 2013, 15, 10132-10141.
184. Y. Zhang, J. Liu, G. Wu and W. Chen, *Nanoscale*, 2012, 4, 5300-5303.
185. Z. Lin and X. Wang, *Chemsuschem*, 2014, 7, 1547-1550.
186. T. Kimura, N. Miyamoto, X. Meng, T. Ohji and K. Kato, *Chem-Asian. J.*, 2009, 4, 1486-1493.
187. H. Zhou, X. Li, T. Fan, F. E. Osterloh, J. Ding, E. M. Sabio, D. Zhang and Q. Guo, *Adv. Mater.*, 2010, 22, 951-956.
188. Y. Chao, Z. Shenmin, C. Zhixin, Z. Wang, G. Jiajun and Z. Di, *J. Mater. Chem. A*, 2013, 1, 8367-8378.
189. Y. F. Zhao, M. Wei, J. Lu, Z. L. Wang and X. Duan, *Acs Nano*, 2009, 3, 4009-4016.
190. D. Yang, B. Du, Y. Yan, H. Li, D. Zhang and T. Fan, *Acs Appl. Mater. Inter.*, 2014, 6, 2377-2385.
191. X. Fei, W. Li, Z. Shao, S. Seeger, D. Zhao and X. Chen, *J. Am. Chem. Soc.*, 2014, 136, 15781-15786.
192. T. Chen, Y. Wang, Y. Wang and Y. Xu, *Rsc. Adv.*, 2015, 5, 1673-1679.
193. X. W. Lou, Y. Wang, C. Yuan, J. Y. Lee and L. A. Archer, *Adv. Mater.*, 2006, 18, 2325-2329.
194. S. C. Yan, S. X. Ouyang, J. Gao, M. Yang, J. Y. Feng, X. X. Fan, L. J. Wan, Z. S. Li, J. H. Ye, Y. Zhou and Z. G. Zou, *Angew. Chem. Int. Edit.*, 2010, 49, 6400-6404.
195. Q. Zhang, W. Wang, J. Goebl and Y. Yin, *Nano Today*, 2009, 4, 494-507.
196. X. Li, T. Xia, C. Xu, J. Murowchick and X. Chen, *Catal. Today*, 2014, 225, 64-73.
197. W. Cai, J. Yu and S. Mann, *Micropor. Mesopor. Mat.*, 2009, 122, 42-47.
198. Q. Xiang, B. Cheng and J. Yu, *Appl. Catal. B-Environ.*, 2013, 138, 299-303.
199. J. Yu, B. Huang, Z. Wang, X. Qin, X. Zhang and P. Wang, *Inorg. Chem.*, 2009, 48, 10548-10552.
200. H. Cheng, B. Huang, Y. Liu, Z. Wang, X. Qin, X. Zhang and Y. Dai, *Chem. Commun.*, 2012, 48, 9729-9731.
201. H. Cheng, B. Huang, X. Qin, X. Zhang and Y. Dai, *Chem. Commun.*, 2012, 48, 97-99.
202. H. Cheng, B. Huang, P. Wang, Z. Wang, Z. Lou, J. Wang, X. Qin, X. Zhang and Y. Dai, *Chem. Commun.*, 2011, 47, 7054-7056.
203. T. Quang Duc, L. Thanh Son and H. Huu Thu, *Crystengcomm.*, 2012, 14, 4274-4278.
204. Y. Shi, Y. Chen, G. Tian, H. Fu, K. Pan, J. Zhou and H. Yan, *Dalton Trans.*, 2014, 43, 12396-12404.
205. D. Zhang, G. Li, F. Wang and J. C. Yu, *Crystengcomm.*, 2010, 12, 1759-1763.
206. F. Chen, J. Zai, M. Xu and X. Qian, *J. Mater. Chem. A*, 2013, 1, 4316-4323.
207. J. Yu, H. Guo, S. A. Davis and S. Mann, *Adv. Funct. Mater.*, 2006, 16, 2035-2041.
208. Y. Jiaguo, Y. Huogen, G. Hongtao, L. Mei and S. Mann, *Small*, 2008, 4, 87-91.
209. J. Yu, S. Liu and M. Zhou, *J. Phys. Chem. C*, 2008, 112, 2050-2057.
210. S. Liu, J. Yu and S. Mann, *J. Phys. Chem. C*, 2009, 113, 10712-10717.
211. S. Liu, J. Yu and M. Jaroniec, *J. Am. Chem. Soc.*, 2010, 132, 11914-11916.
212. J. Yu, S. Liu and H. Yu, *J. Catal.*, 2007, 249, 59-66.
213. J. Yu, J. Fan and L. Zhao, *Electrochim. Acta*, 2010, 55, 597-

602.
214. L. Si, Z. a. Huang, K. Lv, H. Ye, K. Deng and Y. Wu, *J. Alloy. Compd.*, 2014, 612, 69-73.
215. K. Lv, B. Cheng, J. Yu and G. Liu, *Phys. Chem. Chem. Phys.*, 2012, 14, 5349-5362.
216. S. Liu, J. Yu and S. Mann, *Nanotechnology*, 2009, 20, 325606.
217. L. Zhou, W. Z. Wang, H. L. Xu, S. M. Sun and M. Shang, *Chem-Eur. J.*, 2009, 15, 1776-1782.
218. L.-P. Zhu, N.-C. Bing, L.-L. Wang, H.-Y. Jin, G.-H. Liao and L.-J. Wang, *Dalton Trans.*, 2012, 41, 2959-2965.
219. P. Hu, D. Hou, Y. Wen, B. Shan, C. Chen, Y. Huang and X. Hu, *Nanoscale*, 2015, 7, 1963-1969.
220. J. G. Yu and J. Zhang, *Dalton Trans.*, 2010, 39, 5860-5867.
221. S. Sun, X. Song, C. Kong and Z. Yang, *Crystengcomm.*, 2011, 13, 6616-6620.
222. J. Cao, B. Xu, H. Lin, B. Luo and S. Chen, *Chem. Eng. J.*, 2012, 185, 91-99.
223. H. Zeng, W. Cai, P. Liu, X. Xu, H. Zhou, C. Klingshirn and H. Kalt, *Acs Nano*, 2008, 2, 1661-1670.
224. Q. Zhang, T. Zhang, J. Ge and Y. Yin, *Nano Lett.*, 2008, 8, 2867-2871.
225. J. H. Pan, X. Z. Wang, Q. Huang, C. Shen, Z. Y. Koh, Q. Wang, A. Engel and D. W. Bahnemann, *Adv. Funct. Mater.*, 2014, 24, 95-104.
226. S. N. Frank and A. J. Bard, *J. Am. Chem. Soc.*, 1977, 99, 303-304.
227. Q. Xiang, K. Lv and J. Yu, *Appl. Catal. B-Environ.*, 2010, 96, 557-564.
228. Z. Ren, Y. Guo, C.-H. Liu and P.-X. Gao, *Frontiers in chemistry*, 2013, 1, 18-18.
229. D. Chatterjee and S. Dasgupta, *J. Photoch. Photobio. C*, 2005, 6, 186-205.
230. D. Xu, B. Cheng, S. Cao and J. Yu, *Appl. Catal. B-Environ.*, 2015, 164, 380-388.
231. Y. Liu, R. Wang, Z. Yang, H. Du, Y. Jiang, C. Shen, K. Liang and A. Xu, *Chinese. J. Catal.*, 2015, 36, 2135-2144.
232. T. Xiong, H. Zhang, Y. Zhang and F. Dong, *Chinese. J. Catal.*, 2015, 36, 2155-2163.
233. C. Yu, Y. Bai, H. He, W. Fan, L. Zhu and W. Zhou, *Chinese. J. Catal.*, 2015, 36, 2178-2185.
234. X. Wang, R. Yu, K. Wang, G. Yang and H. Yu, *Chinese. J. Catal.*, 2015, 36, 2211-2218.
235. M. Zhou, J. Yu, S. Liu, P. Zhai and B. Huang, *Appl. Catal. B-Environ.*, 2009, 89, 160-166.
236. W. Wang, J. Yu, Q. Xiang and B. Cheng, *Appl. Catal. B-Environ.*, 2012, 119, 109-116.
237. J. Yu, W. Wang, B. Cheng and B.-L. Su, *J. Phys. Chem. C*, 2009, 113, 6743-6750.
238. J. Yu, L. Yue, S. Liu, B. Huang and X. Zhang, *J. Colloid. Interf. Sci.*, 2009, 334, 58-64.
239. G. Li, D. Zhang, J. C. Yu and M. K. H. Leung, *Environ. Sci. Technol.*, 2010, 44, 4276-4281.
240. J. Yu and L. Shi, *J. Mol. Catal. A-Chem.*, 2010, 326, 8-14.
241. K. Lv, Q. Xiang and J. Yu, *Appl. Catal. B-Environ.*, 2011, 104, 275-281.
242. Q. Xiang and J. Yu, *Chinese. J. Catal.*, 2011, 32, 525-531.
243. L. Nie, J. Yu and J. Fu, *Chemcatchem*, 2014, 6, 1983-1989.
244. L. Qi, W. Ho, J. Wang, P. Zhang and J. Yu, *Catal. Sci. Technol.*, 2015, 5, 2366-2377.
245. S. Liu, C. Liu, W. Wang, B. Cheng and J. Yu, *Nanoscale*, 2012, 4, 3193-3200.
246. Y. Huang, W. Ho, Z. Ai, X. Song, L. Zhang and S. Lee, *Appl. Catal. B-Environ.*, 2009, 89, 398-405.
247. J. X. Li, J. H. Xu, W. L. Dai, H. X. Li and K. N. Fan, *Appl. Catal. B-Environ.*, 2009, 85, 162-170.
248. B. Liu, L.-M. Liu, X.-F. Lang, H.-Y. Wang, X. W. Lou and E. S. Aydil, *Energy Environ. Sci.*, 2014, 7, 2592-2597.
249. S. Hoang, T. Q. Ngo, S. P. Berglund, R. R. Fullon, J. G. Ekerdt and C. B. Mullins, *Chemphyschem*, 2013, 14, 2270-2276.
250. J. Yu, Q. Li, S. Liu and M. Jaroniec, *Chem-Eur. J.*, 2013, 19, 2433-2441.
251. T. Tong, J. Zhang, B. Tian, F. Chen and D. He, *J. Hazard. Mater.*, 2008, 155, 572-579.
252. T. Liu and H. Zhang, *Rsc. Adv.*, 2013, 3, 16255-16258.
253. J.-M. Wu and B. Qi, *J. Phys. Chem. C*, 2007, 111, 666-673.
254. N. Shi, X. Li, T. Fan, H. Zhou, J. Ding, D. Zhang and H. Zhu, *Energy Environ. Sci.*, 2011, 4, 172-180.
255. Z. He, W. Que, J. Chen, X. Yin, Y. He and J. Ren, *Acs Appl. Mater. Inter.*, 2012, 4, 6815-6825.
256. W. Yu, J. Zhang and T. Peng, *Applied Catalysis B: Environmental*, 2016, 181, 220-227.
257. S. Liu, C. Li, J. Yu and Q. Xiang, *Crystengcomm.*, 2011, 13, 2533-2541.
258. Y. Wu and G. Lu, *Phys. Chem. Chem. Phys.*, 2014, 16, 4165-4175.
259. Z. Han, L. Liao, Y. Wu, H. Pan, S. Shen and J. Chen, *J. Hazard. Mater.*, 2012, 217, 100-106.
260. P. Xu, T. Xu, J. Lu, S. Gao, N. S. Hosmane, B. Huang, Y. Dai and Y. Wang, *Energy Environ. Sci.*, 2010, 3, 1128-1134.
261. H. Jiang, H. Dai, X. Meng, K. Ji, L. Zhang and J. Deng, *Appl. Catal. B-Environ.*, 2011, 105, 326-334.
262. W.-T. Yao, S.-H. Yu, S.-J. Liu, J.-P. Chen, X.-M. Liu and F.-Q. Li, *J. Phys. Chem. B*, 2006, 110, 11704-11710.
263. L. Zheng, Y. Xu, Y. Song, C. Wu, M. Zhang and Y. Xie, *Inorg. Chem.*, 2009, 48, 4003-4009.
264. L. Shang, C. Zhou, T. Bian, H. Yu, L.-Z. Wu, C.-H. Tung and T. Zhang, *J. Mater. Chem. A*, 2013, 1, 4552-4558.
265. B. Chai, T. Y. Peng, P. Zeng, X. H. Zhang and X. J. Liut, *J. Phys. Chem. C*, 2011, 115, 6149-6155.
266. Z. Chen, D. Li, W. Zhang, Y. Shao, T. Chen, M. Sun and X. Fu, *J. Phys. Chem. C*, 2009, 113, 4433-4440.
267. Y. Chen, R. Huang, D. Chen, Y. Wang, W. Liu, X. Li and Z. Li, *Acs Appl. Mater. Inter.*, 2012, 4, 2273-2279.
268. F. Li, J. Luo, G. Chen, Y. Fan, Q. Huang, Y. Luo, D. Li and Q. Meng, *Catal. Sci. Technol.*, 2014, 4, 1144-1150.
269. Q. Li, C. Cui, H. Meng and J. Yu, *Chem-Asian. J.*, 2014, 9, 1766-1770.
270. R. Wu, Y. Xu, R. Xu, Y. Huang and B. Zhang, *J. Mater. Chem. A*, 2015, 3, 1930-1934.
271. S. Rengaraj, S. Venkataraj, C.-w. Tai, Y. Kim, E. Repo and M. Sillanpaa, *Langmuir*, 2011, 27, 5534-5541.
272. W. Wang, T. W. Ng, W. K. Ho, J. Huang, S. Liang, T. An, G. Li, J. C. Yu and P. K. Wong, *Appl. Catal. B-Environ.*, 2013, 129, 482-490.
273. W. Jiang, X. Yin, F. Xin, Y. Bi, Y. Liu and X. Li, *Appl. Surf. Sci.*, 2014, 288, 138-142.
274. L. Wang, X. Li, W. Teng, Q. Zhao, Y. Shi, R. Yue and Y. Chen, *J. Hazard. Mater.*, 2013, 244, 681-688.
275. Y. Li, M. Cao and L. Feng, *Langmuir*, 2009, 25, 1705-1712.
276. G. Tian, Y. Chen, W. Zhou, K. Pan, Y. Dong, C. Tian and H. Fu, *J. Mater. Chem.*, 2011, 21, 887-892.
277. A. Zhihui and L. Shuncheng, *Appl. Surf. Sci.*, 2013, 280, 354-359.

278. K. Ji, H. Dai, J. Deng, H. Zang, H. Arandiyan, S. Xie and H. Yang, *Appl. Catal. B-Environ.*, 2015, 168, 274-282.
279. Y. Liu, H. Dai, J. Deng, L. Zhang and C. T. Au, *Nanoscale*, 2012, 4, 2317-2325.
280. D. K. Ma, S. Wang, P. Cai, J. L. Jiang, D. P. Yang and S. M. Huang, *Chem. Lett.*, 2009, 38, 962-963.
281. J. Saihua, Z. Keqing, S. Yongqian, L. Siuming, X. Haiyan, H. Yuan and G. Zhou, *Appl. Surf. Sci.*, 2014, 290, 313-319.
282. H. Lu, L. Xu, B. Wei, M. Zhang, H. Gao and W. Sun, *Appl. Surf. Sci.*, 2014, 303, 360-366.
283. C. Huang, J. Hu, S. Cong, Z. Zhao and X. Qiu, *Appl. Catal. B-Environ.*, 2015, 174, 105-112.
284. L. Zhang, W. Wang, Z. Chen, L. Zhou, H. Xu and W. Zhu, *J. Mater. Chem.*, 2007, 17, 2526-2532.
285. Y. Huang, Z. Ai, W. Ho, M. Chen and S. Lee, *J. Phys. Chem. C*, 2010, 114, 6342-6349.
286. D. Ma, S. Huang, W. Chen, S. Hu, F. Shi and K. Fan, *J. Phys. Chem. C*, 2009, 113, 4369-4374.
287. L. Zhi, C. Feitai, G. Yuanpeng, L. Yang, F. Pengfei and W. Shaojie, *J. Mater. Chem. A*, 2013, 1, 7027-7030.
288. Y. Zhou, X. Zhang, Q. Zhang, F. Dong, F. Wang and Z. Xiong, *J. Mater. Chem. A*, 2014, 2, 16623-16631.
289. H. Gnayem and Y. Sasson, *Acs Catal.*, 2013, 3, 186-191.
290. H. Gnayem and Y. Sasson, *J. Phys. Chem. C*, 2015, 119, 19201-19209.
291. X. Xiao and W.-D. Zhang, *J. Mater. Chem.*, 2010, 20, 5866-5870.
292. G. Wu, J. Wang, D. F. Thomas and A. Chen, *Langmuir*, 2008, 24, 3503-3509.
293. Z. Xi, A. Zhihui, J. Falong and Z. Lizhi, *J. Phys. Chem. C*, 2008, 112, 747-753.
294. D. K. Ma, S. M. Zhou, X. Hu, Q. R. Jiang and S. M. Huang, *Mater. Chem. Phys.*, 2013, 140, 11-15.
295. Q.-C. Liu, D.-K. Ma, Y.-Y. Hu, Y.-W. Zeng and S.-M. Huang, *Acs Appl. Mater. Inter.*, 2013, 5, 11927-11934.
296. Y. Huo, J. Zhang, M. Miao and Y. Jin, *Appl. Catal. B-Environ.*, 2012, 111, 334-341.
297. H. Cheng, B. Huang, Z. Wang, X. Qin, X. Zhang and Y. Dai, *Chem-Eur. J.*, 2011, 17, 8039-8043.
298. J. Xia, S. Yin, H. Li, H. Xu, L. Xu and Y. Xu, *Dalton Trans.*, 2011, 40, 5249-5258.
299. Y. Feng, L. Li, J. Li, J. Wang and L. Liu, *J. Hazard. Mater.*, 2011, 192, 538-544.
300. D. Zhang, M. Wen, B. Jiang, G. Li and J. C. Yu, *J. Hazard. Mater.*, 2012, 211, 104-111.
301. J. Guohua, W. Xiaohong, W. Zhen, L. Xia, X. Xiaoguang, H. Ruanbing, T. Bolin, W. Rijing, W. Sheng, W. Tao and C. Wenxing, *J. Mater. Chem. A*, 2014, 1, 2406-2410.
302. P. Madhusudan, J. Ran, J. Zhang, J. Yu and G. Liu, *Appl. Catal. B-Environ.*, 2011, 110, 286-295.
303. F. Dong, H. Liu, W.-K. Ho, M. Fu and Z. Wu, *Chem. Eng. J.*, 2013, 214, 198-207.
304. F. Dong, T. Xiong, Z. Zhao, Y. Sun and M. Fu, *Crystengcomm.*, 2013, 15, 10522-10532.
305. Q. Li, H. Liu, F. Dong and M. Fu, *J. Colloid. Interf. Sci.*, 2013, 408, 33-42.
306. F. Dong, R. Wang, X. Li and W.-K. Ho, *Appl. Surf. Sci.*, 2014, 319, 256-264.
307. F. Dong, T. Xiong, R. Wang, Y. Sun and Y. Jiang, *Dalton Trans.*, 2014, 43, 6631-6642.
308. F. Dong, Y. Sun, M. Fu, W.-K. Ho, S. C. Lee and Z. Wu, *Langmuir*, 2012, 28, 766-773.
309. T. Xiong, H. Huang, Y. Sun and F. Dong, *J. Mater. Chem. A*, 2015, 3, 6118-6127.
310. J. Cao, L. Ren, N. Li, C. Hu and M. Cao, *Chem-Eur. J.*, 2013, 19, 12619-12623.
311. L. Yuhan, Z. Fang and P. Daocheng, *J. Mater. Chem.*, 2012, 22, 22619-22623.
312. M. Kaur and C. M. Nagaraja, *Rsc. Adv.*, 2014, 4, 18257-18263.
313. C. Yu, F. Cao, X. Li, G. Li, Y. Xie, J. C. Yu, Q. Shu, Q. Fan and J. Chen, *Chem. Eng. J.*, 2013, 219, 86-95.
314. C. Yu, K. Yang, Y. Xie, Q. Fan, J. C. Yu, Q. Shu and C. Wang, *Nanoscale*, 2013, 5, 2142-2151.
315. J. Yu and L. Qi, *J. Hazard. Mater.*, 2009, 169, 221-227.
316. W. Cui, W. An, L. Liu, J. Hu and Y. Liang, *J. Hazard. Mater.*, 2014, 280, 417-427.
317. S. Dong, Y. Cui, Y. Wang, Y. Li, L. Hu, J. Sun and J. Sun, *Chem. Eng. J.*, 2014, 249, 102-110.
318. J. Di, J. Xia, S. Yin, H. Xu, L. Xu, Y. Xu, M. He and H. Li, *J. Mater. Chem. A*, 2014, 2, 5340-5351.
319. M. Shang, W. Wang, S. Sun, J. Ren, L. Zhou and L. Zhang, *J. Phys. Chem. C*, 2009, 113, 20228-20233.
320. Y. Wang, W. Wang, H. Mao, Y. Lu, J. Lu, J. Huang, Z. Ye and B. Lu, *Acs Appl. Mater. Inter.*, 2014, 6, 12698-12706.
321. P. Madhusudan, J. Yu, W. Wang, B. Cheng and G. Liu, *Dalton Trans.*, 2012, 41, 14345-14353.
322. Y. Zhang, D. Li, Y. Zhang, X. Zhou, S. Guoabc and L. Yang, *J. Mater. Chem. A*, 2014, 2, 8273-8280.
323. Z.-R. Tang, Q. Yu and Y.-J. Xu, *Rsc. Adv.*, 2014, 4, 58448-58452.
324. H. Huang, K. Liu, Y. Zhang, K. Chen, Y. Zhang and N. Tian, *Rsc. Adv.*, 2014, 4, 49386-49394.
325. X. Gao, H. B. Wu, L. Zheng, Y. Zhong, Y. Hu and X. W. Lou, *Angew. Chem. Int. Edit.*, 2014, 53, 5917-5921.
326. H.-P. Jiao, X. Yu, Z.-Q. Liu, P.-Y. Kuang and Y.-M. Zhang, *Rsc. Adv.*, 2015, 5, 16239-16249.
327. N. Zhang, M.-Q. Yang, S. Liu, Y. Sun and Y.-J. Xu, *Chem. Rev.*, 2015, 115, 10307-10377.
328. W.-F. Ma, Y. Zhang, L.-L. Li, L.-J. You, P. Zhang, Y.-T. Zhang, J.-M. Li, M. Yu, J. Guo, H.-J. Lu and C.-C. Wang, *Acs Nano*, 2012, 6, 3179-3188.
329. G. Liu, F. He, J. Zhang, L. Li, F. Li, L. Chen and Y. Huang, *Appl. Catal. B-Environ.*, 2014, 150, 515-522.
330. X. Zhang, Y. Zhu, X. Yang, Y. Zhou, Y. Yao and C. Li, *Nanoscale*, 2014, 6, 5971-5979.
331. Z. H. Ai, L. Z. Zhang, S. C. Lee and W. K. Ho, *J. Phys. Chem. C*, 2009, 113, 20896-20902.
332. B. Ma, J. Guo, W.-L. Dai and K. Fan, *Appl. Catal. B-Environ.*, 2012, 123, 193-199.
333. Z. Shen, G. Chen, Q. Wang, Y. Yu, C. Zhou and Y. Wang, *Nanoscale*, 2012, 4, 2010-2017.
334. M. Sun, Q. Yan, T. Yan, M. Li, D. Wei, Z. Wang, Q. Wei and B. Du, *Rsc. Adv.*, 2014, 4, 31019-31027.
335. C. Xing, Y. Zhang, Z. Wu, D. Jiang and M. Chen, *Dalton Trans.*, 2014, 43, 2772-2780.
336. F. Dong, Y. Sun, M. Fu, Z. Wu and S. C. Lee, *J. Hazard. Mater.*, 2012, 219, 26-34.
337. L. Wu, Y. Qiu, M. Xi, X. Li and C. Cen, *New. J. Chem.*, 2015, 39, 4766-4773.
338. R. Zha, R. Nadimicherla and X. Guo, *J. Mater. Chem. A*, 2015, 3, 6565-6574.
339. W.-W. Wang, Y.-J. Zhu and L.-X. Yang, *Adv. Funct. Mater.*, 2007, 17, 59-64.

340. F. Chen, Y. Cao and D. Jia, *J. Colloid. Interf. Sci.*, 2013, 404, 110-116.
341. J. Zhang, F. Shi, J. Lin, D. Chen, J. Gao, Z. Huang, X. Ding and C. Tang, *Chem. Mater.*, 2008, 20, 2937-2941.
342. X. Wang, C. Fu, P. Wang, H. Yu and J. Yu, *Nanotechnology*, 2013, 24, 165602.
343. D. J. Wang, D. S. Li, L. Guo, F. Fu, Z. P. Zhang and Q. T. Wei, *J. Phys. Chem. C*, 2009, 113, 5984-5990.
344. Y. Liu, Y. Jiao, Z. Zhang, F. Qu, A. Umar and X. Wu, *Acs Appl. Mater. Inter.*, 2014, 6, 2174-2184.
345. M. Niu, F. Huang, L. Cui, P. Huang, Y. Yu and Y. Wang, *Acs Nano*, 2010, 4, 681-688.
346. Y. Liu, L. Yu, Y. Hu, C. Guo, F. Zhang and X. W. Lou, *Nanoscale*, 2012, 4, 183-187.
347. Y. Qiu, G.-L. Xu, Q. Kuang, S.-G. Sun and S. Yang, *Nano Res.*, 2012, 5, 826-832.
348. J. Yu, Q. Xiang, J. Ran and S. Mann, *Crystengcomm.*, 2010, 12, 872-879.
349. Y. Qiu, L. Wu, J. Li and X. Li, *Catal. Lett.*, 2015, 145, 647-653.
350. J. Yu and X. Yu, *Environ. Sci. Technol.*, 2008, 42, 4902-4907.
351. C. Di and Y. Jinhua, *Adv. Funct. Mater.*, 2008, 18, 1922-1928.
352. S. K. Biswas and J.-O. Baeg, *Int. J. Hydrogen. Energ.*, 2013, 38, 3177-3188.
353. J. Xiong, Z. Jiao, G. Lu, W. Ren, J. Ye and Y. Bi, *Chem-Eur. J.*, 2013, 19, 9472-9475.
354. F. Chang, Y. Xie, J. Zhang, J. Chen, C. Li, J. Wang, J. Luo, B. Deng and X. Hu, *Rsc. Adv.*, 2014, 4, 28519-28528.
355. H. Cheng, W. Wang, B. Huang, Z. Wang, J. Zhan, X. Qin, X. Zhang and Y. Dai, *J. Mater. Chem. A*, 2013, 1, 7131-7136.
356. J. G. Yu, W. G. Wang and B. Cheng, *Chem-Asian. J.*, 2010, 5, 2499-2506.
357. L. L. Li, Y. Chu, Y. Liu and L. H. Dong, *J. Phys. Chem. C*, 2007, 111, 2123-2127.
358. S.-W. Cao and Y.-J. Zhu, *J. Phys. Chem. C*, 2008, 112, 6253-6257.
359. S. Zhang, W. Xu, M. Zeng, J. Li, J. Xu and X. Wang, *Dalton Trans.*, 2013, 42, 13417-13424.
360. J. Yuan, J. Wen, Y. Zhong, X. Li, Y. Fang, S. Zhang and W. Liu, *J. Mater. Chem. A*, 2015, 3, 18244-18255.
361. A. Fujishima, X. Zhang and D. A. Tryk, *Int. J. Hydrogen. Energ.*, 2007, 32, 2664-2672.
362. J. Zhang and F. Huang, *Appl. Surf. Sci.*, 2015, 358, 287-295.
363. J. Ran, J. Yu and M. Jaroniec, *Green Chem.*, 2011, 13, 2708-2713.
364. J. Jin, J. Yu, G. Liu and P. K. Wong, *J. Mater. Chem. A*, 2013, 1, 10927-10934.
365. J. Yu, Y. Yu, P. Zhou, W. Xiao and B. Cheng, *Appl. Catal. B-Environ.*, 2014, 156, 184-191.
366. H. Yu, F. Chen, F. Chen and X. Wang, *Appl. Surf. Sci.*, 2015, 358, 385-392.
367. Y. P. Xie, Z. B. Yu, G. Liu, X. L. Ma and H. M. Cheng, *Energy Environ. Sci.*, 2014, 7, 1895-1901.
368. T. Arai, S.-i. Senda, Y. Sato, H. Takahashi, K. Shinoda, B. Jeyadevan and K. Tohji, *Chem. Mater.*, 2008, 20, 1997-2000.
369. N. S. Chaudhari, A. P. Bhirud, R. S. Sonawane, L. K. Nikam, S. S. Warule, V. H. Rane and B. B. Kale, *Green Chem.*, 2011, 13, 2500-2506.
370. H. Zhou, Q. Liu, W. Liu, J. Ge, M. Lan, C. Wang, J. Geng and P. Wang, *Chem-Asian. J.*, 2014, 9, 811-818.
371. J. Wang, B. Li, J. Chen, L. Li, J. Zhao and Z. Zhu, *J. Alloy. Compd.*, 2013, 578, 571-576.
372. W. Zhang and R. Xu, *Int. J. Hydrogen. Energ.*, 2009, 34, 8495-8503.
373. P. Wang, Z. Geng, J. Gao, R. Xuan, P. Liu, Y. Wang, K. Huang, Y. Wan and Y. Xua, *J. Mater. Chem. A*, 2015, 3, 1709-1716.
374. Y. Chen, G. Tian, Z. Ren, K. Pan, Y. Shi, J. Wang and H. Fu, *Acs Appl. Mater. Inter.*, 2014, 6, 13841-13849.
375. Z. Mei, S. Ouyang, D.-M. Tang, T. Kako, D. Golberg and J. Ye, *Dalton Trans.*, 2013, 42, 2687-2690.
376. G. Tian, Y. Chen, Z. Ren, C. Tian, K. Pan, W. Zhou, J. Wang and H. Fu, *Chem-Asian. J.*, 2014, 9, 1291-1297.
377. J. Y. Zhang, Y. H. Wang, J. Jin, J. Zhang, Z. Lin, F. Huang and J. G. Yu, *Acs Appl. Mater. Inter.*, 2013, 5, 10317-10324.
378. J. G. Yu, Y. F. Yu and B. Cheng, *Rsc. Adv.*, 2012, 2, 11829-11835.
379. H. N. Kim, T. W. Kim, I. Y. Kim and S.-J. Hwang, *Adv. Funct. Mater.*, 2011, 21, 3111-3118.
380. J. Zhang, Z. Zhu, Y. Tang, K. Muellen and X. Feng, *Adv. Mater.*, 2014, 26, 734-738.
381. T. Jia, A. Kolpin, C. Ma, R. C.-T. Chan, W.-M. Kwok and S. C. E. Tsang, *Chem. Commun.*, 2014, 50, 1185-1188.
382. K. Chang, Z. Mei, T. Wang, Q. Kang, S. Ouyang and J. Ye, *Acs Nano*, 2014, 8, 7078-7087.
383. Q. Li, B. Guo, J. Yu, J. Ran, B. Zhang, H. Yan and J. R. Gong, *J. Am. Chem. Soc.*, 2011, 133, 10878-10884.
384. Y. Yu, J. Zhang, X. Wu, W. Zhao and B. Zhang, *Angew. Chem. Int. Edit.*, 2012, 51, 897-900.
385. J. Zhang, J. Yu, Y. Zhang, Q. Li and J. R. Gong, *Nano Lett.*, 2011, 11, 4774-4779.
386. W. He, J. Cui, Y. Yue, X. Zhang, X. Xia, H. Liu and S. Lui, *J. Colloid. Interf. Sci.*, 2011, 354, 109-115.
387. J. Shen, J. Zai, Y. Yuan and X. Qian, *Int. J. Hydrogen. Energ.*, 2012, 37, 16986-16993.
388. G. Wang, G. Chen, Y. Yu, X. Zhou and Y. Teng, *Rsc. Adv.*, 2013, 3, 18579-18586.
389. N. S. Chaudhari, S. S. Warule and B. B. Kale, *Rsc. Adv.*, 2014, 4, 12182-12187.
390. J. Zhou, G. H. Tian, Y. J. Chen, X. Y. Meng, Y. H. Shi, X. R. Cao, K. Pan and H. G. Fu, *Chem. Commun.*, 2013, 49, 2237-2239.
391. Q. Liu, H. Lu, Z. Shi, F. Wu, J. Guo, K. Deng and L. Li, *Acs Appl. Mater. Inter.*, 2014, 6, 17200-17207.
392. L. Wei, Y. Chen, Y. Lin, H. Wu, R. Yuan and Z. Li, *Appl. Catal. B-Environ.*, 2014, 144, 521-527.
393. Z. Zhang, C. Shao, X. Li, Y. Sun, M. Zhang, J. Mu, P. Zhang, Z. Guo and Y. Liu, *Nanoscale*, 2013, 5, 606-618.
394. L. Chenxing, M. Zhijun, D. Guoping and Q. Jianrong, *Appl. Surf. Sci.*, 2014, 314, 481-489.
395. L. Yuan and Y.-J. Xu, *Appl. Surf. Sci.*, 2015, 342, 154-167.
396. M. Marszewski, S. Cao, J. Yu and M. Jaroniec, *Mater Horiz*, 2015, 2, 261-278.
397. T. Inoue, A. Fujishima, S. Konishi and K. Honda, *Nature*, 1979, 277, 637-638.
398. W. Tu, Y. Zhou and Z. Zou, *Adv. Mater.*, 2014, 26, 4607-4626.
399. P. D. Tran, L. H. Wong, J. Barber and J. S. C. Loo, *Energy Environ. Sci.*, 2012, 5, 5902-5918.
400. K. Wang, Q. Li, B. Liu, B. Cheng, W. Ho and J. Yu, *Appl. Catal. B-Environ.*, 2015, 176–177, 44-52.
401. Q. Xu, J. Yu, J. Zhang, J. Zhang and G. Liu, *Chem. Commun.*,

2015, 51, 7950-7953.
402. S. Ye, R. Wang, M.-Z. Wu and Y.-P. Yuan, *Appl. Surf. Sci.*, 2015, 358, 15-27.
403. H. Li, Y. Lei, Y. Huang, Y. Fang, Y. Xu, L. Zhu and X. Li, *J. Nat. Gas. Chem.*, 2011, 20, 145-150.
404. X. Li, J. Chen, H. Li, J. Li, Y. Xu, Y. Liu and J. Zhou, *J. Nat. Gas. Chem.*, 2011, 20, 413-417.
405. J. Yu, J. Jin, B. Cheng and M. Jaroniec, *J. Mater. Chem. A*, 2014, 2, 3407-3416.
406. J. Yu, J. Low, W. Xiao, P. Zhou and M. Jaroniec, *J. Am. Chem. Soc.*, 2014, 136, 8839-8842.
407. J. Low, J. Yu and W. Ho, *J. Phys. Chem. Lett.*, 2015, 6, 4244-4251.
408. J. Low, B. Cheng, J. Yu and M. Jaroniec, *Energy Storage Materials*, 2016, 3, 24-35.
409. W. Zhang, F. Dong and W. Zhang, *Appl. Surf. Sci.*, 2015, 358, 75-83.
410. M. S. Akple, J. Low, Z. Qin, S. Wageh, A. A. Al-Ghamdi, J. Yu and S. Liu, *Chinese. J. Catal.*, 2015, 36, 2127-2134.
411. Y. Li, W. Zhang, X. Shen, P. Peng, L. Xiong and Y. Yu, *Chinese. J. Catal.*, 2015, 36, 2229-2236.
412. W.-J. Ong, L.-L. Tan, S.-P. Chai and S.-T. Yong, *Chem. Commun.*, 2015, 51, 858-861.
413. B. Fang, A. Bonakdarpour, K. Reilly, Y. Xing, F. Taghipour and D. P. Wilkinson, *Acs Appl. Mater. Inter.*, 2014, 6, 15488-15498.
414. W.-J. Ong, L.-L. Tan, S.-P. Chai, S.-T. Yong and A. R. Mohamed, *Nano Res.*, 2014, 7, 1528-1547.
415. S. Zhang, L. Li, S. Zhao, Z. Sun, M. Hong and J. Luo, *J. Mater. Chem. A*, 2015, 3, 15764-15768.
416. J. Chen, S. Qin, G. Song, T. Xiang, F. Xin and X. Yin, *Dalton Trans.*, 2013, 42, 15133-15138.
417. M. F. Ehsan, M. N. Ashiq and T. He, *Rsc. Adv.*, 2015, 5, 6186-6194.
418. H. Zhou, P. Li, J. Guo, R. Yan, T. Fan, D. Zhang and J. Ye, *Nanoscale*, 2015, 7, 113-120.
419. S.-W. Cao, X.-F. Liu, Y.-P. Yuan, Z.-Y. Zhang, Y.-S. Liao, J. Fang, S. C. J. Loo, T. C. Sum and C. Xue, *Appl. Catal. B-Environ.*, 2014, 147, 940-946.
420. Y. Wang, B. Li, C. Zhang, L. Cui, S. Kang, X. Li and L. Zhou, *Appl. Catal. B-Environ.*, 2013, 130, 277-284.
421. X. Li, H. Liu, D. Luo, J. Li, Y. Huang, H. Li, Y. Fang, Y. Xu and L. Zhu, *Chem. Eng. J.*, 2012, 180, 151-158.
422. G. Xi, S. Ouyang and J. Ye, *Chem-Eur. J.*, 2011, 17, 9057-9061.
423. C. Zhang, Q. Zhang, S. Kang, B. Li, X. Li and Y. Wang, *Ecs. Solid. State. Lett.*, 2013, 2, M49-M52.
424. W. Tu, Y. Zhou, Q. Liu, Z. Tian, J. Gao, X. Chen, H. Zhang, J. Liu and Z. Zou, *Adv. Funct. Mater.*, 2012, 22, 1215-1221.
425. W. Tu, Y. Zhou, Q. Liu, S. Yan, S. Bao, X. Wang, M. Xiao and Z. Zou, *Adv. Funct. Mater.*, 2013, 23, 1743-1749.
426. M. M. Gui, S. P. Chai, B. Q. Xu and A. R. Mohamed, *Sol. Energ. Mat. Sol. C.*, 2014, 122, 183-189.
427. S. Liu, J. Xia and J. Yu, *Acs Appl. Mater. Inter.*, 2015, 7, 8166-8175.
428. Y. Wang, Y. Chen, Y. Zuo, F. Wang, J. Yao, B. Li, S. Kang, X. Li and L. Cui, *Catal. Sci. Technol.*, 2013, 3, 3286-3291.
429. H. Zhou, J. J. Guo, P. Li, T. X. Fan, D. Zhang and J. H. Ye, *Sci. Rep-Uk.*, 2013, 3, 1667.
430. Q. Liu, Y. Zhou, Z. Tian, X. Chen, J. Gao and Z. Zou, *J. Mater. Chem.*, 2012, 22, 2033-2038.
431. M. F. Ehsan and T. He, *Appl. Catal. B-Environ.*, 2015, 166, 345-352.
432. S.-I. In, D. D. Vaughn, II and R. E. Schaak, *Angew. Chem. Int. Edit.*, 2012, 51, 3915-3918.
433. L. Yuan, C. Han, M. Pagliaro and Y.-J. Xu, *J. Phys. Chem. C*, 2016, 120, 265-273.
434. J. Jin, J. Yu, D. Guo, C. Cui and W. Ho, *Small*, 2015, 11, 5262-5271.
435. Y. Xu and R. Xu, *Appl. Surf. Sci.*, 2015, 351, 779-793.
436. X. An and J. C. Yu, *Rsc. Adv.*, 2011, 1, 1426-1434.
437. X. Li, B. Weng, N. Zhang and Y.-J. Xu, *Rsc. Adv.*, 2014, 4, 64484-64493.
438. R. Chen, J. Yu and W. Xiao, *J. Mater. Chem. A*, 2013, 1, 11682-11690.
439. J. R. Ge, K. J. Deng, W. Q. Cai, J. G. Yu, X. Q. Liu and J. B. Zhou, *J. Colloid. Interf. Sci.*, 2013, 401, 34-39.
440. Y. Le, D. Guo, B. Cheng and J. Yu, *Appl. Surf. Sci.*, 2013, 274, 110-116.
441. W. W. Wang, J. B. Zhou, Z. Zhang, J. G. Yu and W. Q. Cai, *Chem. Eng. J.*, 2013, 233, 168-175.
442. C. Sheng, D. Jingjing, M. Jaroniec and Q. Shi Zhang, *J. Mater. Chem. A*, 2013, 1, 9409-9413.
443. J. Duan, S. Chen, M. Jaroniec and S. Z. Qiao, *Acs Nano*, 2015, 9, 931-940.
444. M. Zhong, E. K. Kim, J. P. McGann, S.-E. Chun, J. F. Whitacre, M. Jaroniec, K. Matyjaszewski and T. Kowalewski, *J. Am. Chem. Soc.*, 2012, 134, 14846-14857.
445. J. G. Yu, Q. L. Li, J. J. Fan and B. Cheng, *Chem. Commun.*, 2011, 47, 9161-9163.

**Xin Li** received his BS and PhD degrees in Chemical Engineering from Zhengzhou University in 2002 and South China University of Technology in 2007, respectively. Then, he joined South China Agricultural University as a faculty member, and became an associate professor of Applied Chemistry in 2011. During 2012-2013, he worked as a visiting scholar at the electrochemistry Center, the University of Texas at Austin, U.S.A. His research interests include photocatalysis, photoelectrochemistry, adsorption and the development of photocatalysts, related materials and devices.

**Jiaguo Yu** received his BS and MS in chemistry from Central China Normal University and Xi'an Jiaotong University, respectively, and his PhD in Materials Science in 2000 from the Wuhan University of Technology. In 2000, he became a Professor of the Wuhan University of Technology. He was a post-doctoral fellow at the Chinese University of Hong Kong from 2001 to 2004, visiting scientist from 2005 to 2006 at the University of Bristol, and visiting scholar from 2007 to 2008 at the University of Texas, Austin. His research interests include semiconductors, photocatalysis, photocatalytic hydrogen production, solar fuels, dye-sensitized solar cells, adsorption, $CO_2$ capture, graphene and related topics.

**Mietek Jaroniec** received his MS and PhD from M. Curie-Sklodowska University, Poland, in 1972 and 1976, respectively. Since 1991 he is a Professor of Chemistry at Kent State University, Kent, Ohio (USA). Before joining Kent State he was a Professor of Chemistry at M. Curie-Sklodowska University, Poland. His research interests revolve primarily around interdisciplinary topics of interfacial chemistry, and chemistry of materials, including physical adsorption at the gas/solid and liquid/solid interfaces, adsorbents, and catalysts. At Kent State he has established a vigorous research program in the area of ordered nanoporous materials such as ordered mesoporous silicas, organosilicas, inorganic oxides and carbons, focusing on their synthesis and environmental and energy-related applications.

## TOC Graphics

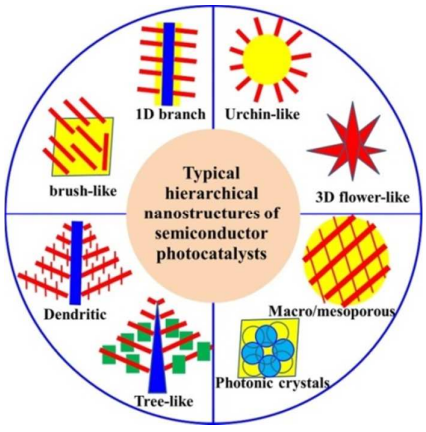


The design, fabrication, performance and applications of hierarchical semiconductor photocatalysts are thoroughly reviewed and apprised.